

MESOSCALE ANALYSES AND MODELS FOR THE TEXAS HIPLEX AREA



LP-188

TEXAS DEPARTMENT OF WATER RESOURCES

MAY 1983



MESOSCALE ANALYSES AND MODELS FOR THE TEXAS HIPLEX AREA

BY

James R. Scoggins

James P. McGuirk

Dusan Djuric

Department of Meteorology
Texas A&M University
College Station, Texas 77843

LP-188

Texas Department of Water Resources

May 1983

TEXAS DEPARTMENT OF WATER RESOURCES

Charles E. Nemir, Executive Director

TEXAS WATER DEVELOPMENT BOARD

Louis A. Beecherl Jr., Chairman
Glen E. Roney
W. O. Bankston

George W. McCleskey, Vice Chairman
Lonnie A. "Bo" Pilgrim
Louie Welch

TEXAS WATER COMMISSION

Felix McDonald, Chairman

Lee B. M. Biggart, Commissioner
John D. Stover, Commissioner

Authorization for use or reproduction of any original material contained in this publication, i.e., not obtained from other sources, is freely granted. The Department would appreciate acknowledgement.

Published and distributed
by the
Texas Department of Water Resources
Post Office Box 13087
Austin, Texas 78711

ACKNOWLEDGMENTS

The authors are indebted to several people for their contributions to the conduct of the research and the preparation of this report. Mr. Tsu-Cheng Shen met the challenge of performing all computations using computer programs developed by others as well as some he prepared; Mr. Scott Humphrey and Ms. Pamela Tabor worked diligently for long hours to prepare the figures, and Pamela assisted by Mrs. Susan Spears in the latter stages, prepared the manuscript. The work could not have been completed without their excellent support. We appreciate it most sincerely.



ABSTRACT

The principal components of this report include a brief review of previous modeling efforts in mesometeorology, the mesoscale analysis for eleven days during 1979 and 1980 on which data were available from seven rawinsonde stations, and the presentation of preliminary mesoscale environmental models for the Texas HIPLEX area for several classifications of convective activity.

This is the first time mesoscale variability above the surface for the Texas HIPLEX area could be evaluated. Both the analysis of individual case studies and the models developed from all available mesoscale results reflect large variability both temporally and spatially. The models consist of average profiles and profiles of the standard deviation of temperature, dewpoint temperature, mixing ratio, wind speed, wind direction, horizontal moisture divergence, vertical motion, and vertical moisture flux for the classifications of no convection, isolated convection, clusters, lines, and widespread convection.

The models demonstrate the complex nature of the mesoscale environment of convective storms. It appears that vertical motion is the most important factor in the formation of convective activity in the Texas HIPLEX area.



TABLE OF CONTENTS

	Page
ACKNOWLEDGEMENTS	iii
ABSTRACT	v
1. INTRODUCTION	1
2. STATUS OF PREVIOUS TEXAS HIPLEX MESOSCALE RESEARCH	2
3. A BRIEF REVIEW OF RESEARCH ON MESOSCALE METEOROLOGY	4
3.1 Prediction and Simulation Models.	4
3.2 Observational Studies	6
3.3 Supporting Studies for Mesoscale Modeling	7
3.4 Presentation of Results	9
4. MESOSCALE ANALYSES FOR SELECTED DAYS DURING 1979 and 1980	19
4.1 Days Analyzed	19
4.2 Approach.	19
5. CLASSIFICATION OF CONVECTIVE ACTIVITY	21
6. PRELIMINARY MESOSCALE ENVIRONMENTAL MODELS FOR THE TEXAS HIPLEX AREA	29
6.1 Model Construction Procedure	29
6.2 Basic Data Models	30
6.3 Kinematic Models	47
6.4 Comparison of Models of Vertical Motion	60
7. SUMMARY AND RECOMMENDATIONS	65
8. REFERENCES.	67
APPENDIX A.	Microfiche in Pocket

TABLES

5.1 No-Convection Cases (listed by date, and stratified by GMT time: N15 = No-Convection, 1500 GMT, etc.)	23
5.2 Isolated Convection Cases (listed by date and GMT time and stratified by intensity).	24
5.3 Clustered Convection (listed by date and GMT time and stratified by intensity)	26

TABLE OF CONTENTS Continued

Page

TABLES

5.4	Line Convection (listed by date and GMT time)	27
5.5	Classification of each time versus echo characteristics for the mesoscale analyses presented in Appendix A	28
6.1	Composite averages of the average and standard deviation of each variable for each convective classification. The averages were computed from similar data presented in the Appendix for each date and time. The average is on the left and the standard deviation on the right of the diagonal	53

FIGURES

3.1	Several variables after 4 h 30 min of development in the simulation model of Fritsch and Chappell (1980)	11
3.2	850 mb analyses for 12 April 1980. Heights (m) are heavy solid contours; totals index is analyzed in light solid contours; isotherms ($^{\circ}\text{C}$) are dashed; and selected wind observations (full barb = 5 m s^{-1}) are shown for (b) 1200 GMT. (From Maddox and Doswell, 1982).	12
3.3	Divergence ($\times 10^{-5} \text{ s}^{-1}$) for the total 20 kPa wind at 0600 GMT 25 April 1975. Contour interval is 2.5. (From Maddox <u>et al.</u> , 1981. The outline of the cloud from the satellite photo is added).	12
3.4	Accumulated precipitation (mm) from 0000 to 0600 GMT 25 April 1975. (From Maddox <u>et al.</u> , 1981).	12
3.5	Low-level horizontal wind at (c) 1222:30, (d) 1226:30. Lowest level of complete data is shown for each time. Reflectivity is shaded for $Z \geq 40 \text{ dBZ}$. All distances are from CP-3. (From Carbone, 1982)	13
3.6	A variety of kinematic structures seen in the squall line to emphasize the spectrum of results obtained. Major features (such as prefrontal updraft, subsidence updraft, outflow, and low-level convergence) are highly two-dimensional. (From Carbone, 1982)	13
3.7	Observed variables in a thunderstorm (from Ray <u>et al.</u> , 1981)	14

TABLE OF CONTENTS Continued

Page

FIGURES

3.8 The (a) observed and (b) modeled storm development on 3 April 1964. Observed reflectivities > 12 dBZ at 0° and modeled rainwater contents $> 0.5 \text{ g kg}^{-1}$ at $z = 0.4 \text{ km}$ are enclosed by alternating solid and dashed contours about every 30 min. Maxima in these fields are connected by solid lines. The storms are labeled and at several times the contoured regions are stippled for better visualization of the storm development. Labels for the modeled storms are the same as the corresponding observed storms except for the inclusion of M. The scale shown in (a) applies in (b). (From Wilhelmson and Klemp, 1981) 15

3.9 Distribution of precipitation within the modeled and observed storms as viewed from the southeast. The contoured surfaces represent the 0.5 g kg^{-1} rainwater surface in the model and the 35 dBZ reflectivity surfaces in the observed storm. The x-y base plane corresponds to the 29 km x 29 km domains and the vertical axis extends to 14 km. (From Klemp et al., 1981) 15

3.10 The predicted winds at 4 m at about 1500 LST over the Chesapeake Bay for August 9, 1975. Model simulation performed by W. Snow using the University of Virginia Mesoscale Model. Scale bar in m sec^{-1} . (From Pielke, 1981) 17

3.11 Predicted wind field from Experiment 3 (SB) applying at the lowest model layer ($\approx 80 \text{ m}$ above the surface) for LAT. (From Warner et al., 1978. LAT is local apparent time.) . 17

3.12 The vertical cross section of potential temperature along a coastline at 1800 LST for a 6 m sec^{-1} onshore synoptic wind. Initial input was for a typical summer day over south Florida. (From Mahrer and Pielke, 1978.) 17

3.13 Cross-section analyses of potential temperature (K) and the component of the geostrophic wind normal to the cross section (m s^{-1}) along BB' at 0000 GMT 22 February 1971. (a) As in Fig. 3.14a except for rawinsonde observations at Denver, CO (DEN); Amarillo, TX (AMA); Dallas-Fort Worth, TX (DFW); Shreveport, LA (SHV); Lake Charles, LA (LCH); and Valparaiso, FL (VPS). Wind analysis not included because of missing data. (b) As in Fig. 3.14b except analysis based on 12 h model forecast and $\Delta s = 75 \text{ km}$. (From Keyser et al., 1978.) 18

TABLE OF CONTENTS Continued

Page

FIGURES

3.14 Schematic which illustrates the behavior of pressure and vorticity for (a) change with height and (b) a case where the wind shear vector veers with height. The corresponding hodographs for environmental flow at low (L) to mid (M) levels are inset to the left. Horizontal pressure gradients parallel to the sheer vector are labeled at each level along with the preferred locations of positive (+) and negative (-) vorticity. The orientations of the resulting vertical pressure gradient forces between low and mid levels are indicated by the black arrows. 18

6.1 Profiles of temperature and dewpoint temperature for the no-convection classification. Standard deviation bars are for 1500 GMT. N15 = no-convection at 1500 GMT, etc. 31

6.2 Profiles of mixing ratio for the no-convection classification. N15 = no convection at 1500 GMT, etc. 33

6.3 Profiles of wind speed for the no-convection classification. N15 = no convection at 1500 GMT, etc. 34

6.4 Profiles of wind direction (from which wind is blowing) for the no-convection classification. N15 = no convection at 1500 GMT, etc. 35

6.5 Profiles of temperature and dewpoint temperature for the isolated convection classification. Standard deviation bars are for the I1 profile. 36

6.6 Profiles of mixing ratio for the isolated convection classification 37

6.7 Profiles of wind speed for the isolated convection classification 37

6.8 Profiles of wind direction (from which wind is blowing) for the isolated convection classification 39

6.9 Profiles of temperature and dewpoint temperature for the cluster classification. Standard deviation bars are for the C1 profile 39

6.10 Profiles of mixing ratio for the cluster classification . 40

6.11 Profiles of wind speed for the cluster classification. . . 41

TABLE OF CONTENTS Continued

Page

FIGURES

6.12	Profiles of wind direction (from which wind is blowing) for the cluster classification	41
6.13	Profiles of temperature and dewpoint temperature for the cluster classification. Standard deviation bars are for the C small profile.	43
6.14	Profiles of wind speed for the cluster classification. . .	43
6.15	Profiles of wind direction (from which the wind is blowing) for the cluster classification	44
6.16	Profiles of temperature and dewpoint temperature preceding the development of big convective clusters.	45
6.17	Profiles of temperature and dewpoint temperature for the line classification.	46
6.18	Profile of wind speed for the line classification.	48
6.19	Profile of wind direction (from which the wind is blowing) for the line classification.	48
6.21	Profiles and standard deviation of vertical motion for the no-convection classification based on 1978 data.	49
6.22	Profiles and standard deviation of vertical motion for the isolated convection classification based on 1978 data.	49
6.23	Profiles and standard deviation of vertical motion for the small clusters classification based on 1978 data	50
6.24	Profiles of vertical motion for big clusters during 1978 season.	50
6.25	Composite average and standard deviation profiles when no echoes were present	54
6.26	Composite average and standard deviation profiles when isolated cells were present.	55
6.27	Composite average and standard deviation profiles when clusters of convective cells were present.	56
6.28	Composite average and standard deviation profiles when widespread echoes were present	57
6.29	Comparison of composite average profiles for various categories of convective activity.	58
6.30	Comparison of vertical motion models	62

MESOSCALE ANALYSES AND MODELS FOR THE
TEXAS HIPLEX AREA

by

James R. Scoggins

James P. McGuirk

Dusan Djuric

Department of Meteorology

Texas A&M University

1. INTRODUCTION

Mesoscale data were collected in the Texas HIPLEX area during the five years 1976-1980 (Scoggins and Wilson, 1976; Scoggins, 1977; Reynolds et al., 1979; Williams et al., 1980; and Sienkiewicz and Gerhard, 1981). During the first three years upper air data were collected at four stations, and during the last two years upper air data were collected at seven stations. With the four-station network it was possible to examine the vertical distribution of variables only over the network as a whole, but with the seven stations it was possible to also examine spatial variations across the HIPLEX area. The composite data set consists of data for approximately 100 days spread approximately equally over the five years. Data are adequate for perhaps two thirds of these cases for analysis of mesoscale conditions over the area. Therefore, the data sample in terms of size appears to be adequate, but, because of the networks used, the sample size for determining spatial variations is still quite small.

With the analyses contained in this report, the mesoscale analysis is now virtually complete for all days for which adequate data are available. Some additional analysis could still be performed especially for single soundings or when conditions of spatial variations are not desired.

One of the original goals of the HIPLEX research was to accumulate a data sample of adequate size from which mesoscale environmental models for various convective activity categories could be developed. The analysis is now essentially complete and the first preliminary models have been developed. These models which are presented in this report, represent the mesoscale environment accompanying convective activity as classified into different categories. While the sample size (approximately 100 days) of mesoscale measurements is quite large, sample sizes for some convective categories (those associated with the most vigorous convection) are inadequate from a statistical point of view.

2. STATUS OF PREVIOUS TEXAS HIPLEX MESOSCALE RESEARCH

Because of the large variability of the mesoscale environment accompanying convective activity, a rather large data sample is required in order to describe the statistics of the environment. The data sample is adequate for some purposes, but inadequate for certain convective categories. Mesoscale analyses of various forms for the Texas HIPLEX area have been conducted by Scoggins *et al.* (1978), Scoggins *et al.* (1979), Sienkiewicz *et al.* (1980), Gerhard and Scoggins (1981), and Williams and Scoggins (1980). In addition, other studies using Texas HIPLEX data have been conducted (Haragan 1978; Jurica and Chao, 1981; and others). Results from these diverse studies indicate the incredibly complex nature of the problem of developing a rainfall enhancement strategy.

Because of the spacing of the mesoscale stations, both in space and in time, initiation mechanisms for convective activity could not be evaluated (Scoggins *et al.*, 1982). This is not a serious shortcoming, however, in the analysis of mesoscale systems inasmuch as convective activity is already present before any seeding operations take place. The models presented in this report apply to categories of convective activity after the activity has formed. In no way are the models related to initiation mechanisms or forecasting.

Convective activity and its mesoscale environment must be treated as a system. This is necessary because of the interactions and feedback mechanisms between convective clouds and their environment. The environment not only has an effect on the cloud in terms of its development and growth, i.e., energy source, but it also affects the precipitation mechanisms through the alteration of cloud microphysics. At the same time, the convective cloud, through its small-scale, high amplitude motions, significantly modifies the environment.

The seeding hypothesis is based on the assumptions that seeding with silver iodide enhances condensation and the release of latent heat, thereby increasing the bouyancy which leads to an increased vertical motion and, by continuity, to increased convergence into the cloud. Once this process has been initiated the cloud not only grows vertically thereby processing more water and increasing rain on the ground, but also spreads horizontally in areal extent as a result of cell development resulting from storm outflow. The hypothesized chain of events are not too different from those presented

by Woodley et al. (1982) for the Florida Area Cumulus Experiment (FACE). This chain of events is assumed to vary somewhat with the nature of the convective activity. In the Texas HIPLEX area, when silver iodide is introduced into a convective complex in the region where the cloud water is present and the temperature is -4°C to -10°C , the following chain of events is assumed to occur.

1. Production of greater than or equal to 100 per liter ice crystal concentration in the supercooled clouds from -4°C to -10°C .
2. Substantial glaciation of a cloud with associated release of latent heat and increase of bouyancy.
3. Increase in height of turrets.
4. Increased mesoscale moisture flux into the cloud and condensation within the cloud.
5. Conversion of extra condensate to precipitation.
6. Fall of precipitation through cloud base.
7. Increased sub-cloud convergence, more vigorous downdrafts, and interaction among them.
8. Increase in mesoscale vertical transport of moisture in the mid troposphere.
9. Changes in the characteristics of radar echoes and new cell development, such as intensity, height, and areal extent.
10. Changes in precipitation patterns.

Three of the steps in the chain of events are related directly to mesoscale environmental conditions. These are events four, seven, and eight. The development of mesoscale environmental models provides a means for establishing environmental conditions in the absence of seeding. These models will form the basis for performing theoretical calculations for determining seeding effects. At this point in the study no attempt has been made to identify or define response variables. Woodley et al. (1982) used as their primary response variables rain volumes in the total target area and in a floating target area. The specification of response variables must await the integration of results from the various aspects of all investigations for the Texas HIPLEX area.

3. A BRIEF REVIEW OF RESEARCH ON MESOSCALE METEOROLOGY

The purpose of this section is to present a brief review of the current status of research on mesoscale meteorology, and to examine procedures used by various investigators to present results of mesoscale studies. There is no easy way to present, in a compact form, all the various results and processes represented by the wide range of mesoscale studies. Yet, the problem of developing a method for rainfall enhancement requires the integration of results from a myriad of studies. It is hoped that this brief review will assist in this problem.

3.1 Prediction and Simulation Models

It is practical to distinguish between prediction and simulation models since they differ in the important problem of initialization. The prediction models are designed to start out from an observed state of the atmosphere, whereas the simulation models use a schematic state. With this exception, the dynamics is the same in both models. Often, the same model is used for simulation in some cases and for prediction in other cases.

Models can be classified by the scale of phenomena for which they are designed. There are considerable differences in equations needed for differing length scales. A systematic review of terms in the equations appropriate for various scales is given by Wippermann (1981). Generally accepted terminology of scales (Orlanski, 1975) is tabulated here:

<u>Category</u>	<u>Typical Horizontal Scales</u>	<u>Typical Horizontal Grid Size</u>
meso- α	250-2500 km	100 km
meso- β	25-250 km	10 km
meso- γ	2.5-25 km	1 km

The larger scales (alpha and beta) are typically computed with hydrostatic equations, whereas, for the gamma scale, various nonhydrostatic equations are needed (anelastic, compressible, or quasi-hydrostatic; the latter recently proposed by Orlanski (1981)). As an exception, the alpha-scale model by Ross and Orlanski (1982) used anelastic equations.

With exception of the limited fine mesh (LFM) model of the National Meteorological Center (NMC), no mesoscale model has achieved an operational status, i.e., that it can be applied with observed initial conditions for a period before the forecast time elapses. Although some mesoscale models can be used operationally, current methods for collecting and processing observations have inhibited their utilization. Also, the LFM model of the NMC

does not use mesoscale data, relying only on observations from stations which are designed to show synoptic and larger scale phenomena.

The following table, based on the STORM project (UCAR, 1982) contains the models that were active in 1981.

<u>Meso-Alpha Scale Models</u>					
Institution	Spatial dimensions	Horiz. grid size (km)	Domain size (km) ²	Emphasis	Basic reference
GFDL	2, 3	50	(2500) ²	Tropical cyclones Fronts	Ross and Orlanski, 1982
Drexel	2, 3	40	(2000) ²	Predicition with real data	Perkey, 1976
Navy	3	60	(3000) ²	Tropical cyclones	unpublished
NMC	3	60	(3000) ²	Tropical cyclones mesoscale prediction	Hovermale & Livezey, 1977
Penn State/ NCAR	2, 3	50-100	(2000) ²	Precipitation	Anthes & Warner, 1978
<u>Meso-Beta Scale Models</u>					
CSU	2, 3	10	(400) ²	Breezes	Pielke, 1981
ERL/ OWRM	3	5-20	(200-800) ²	Convection Orographic influences	Nickerson, 1979
NHRL	2, 3	20	(3000) ²	Tropical cyclones	Rosenthal, 1978
Penn State/ NCAR	2, 3	5-50	(200-2000) ²	Various	Anthes & Warner, 1978
SUNTA	2	18.5	(400) ²	Coastal front	Ballentine, 1980

The references in the last column are not the most recent; they are, rather, the basic references which best describe the model in question. Numerous other papers have been published with further results obtained with these models.

There is a number of other models on the alpha-scale which are not mentioned by the STORM Project (UCAR, 1982), mostly because development of these models has been stopped. These are the models by Friend et al. (1977), Bleck (1978), Uccellini et al. (1979) and Fritsch and Chappell (1980). On the beta-scale there is an interesting model by Tapp and White (1976), which appears to be the only non-hydrostatic model that is used on this scale. The TAMU model (Scoggins et al., 1982) should be classified

among these meso-beta scale models.

There are many active models on the meso-gamma scale. These are all non-hydrostatic. Their emphasis is on vertical development of clouds and/or on cloud microphysics. Only a few emphasize the local storm development, squall-lines, or tornadoes. Principal authors in meso-gamma scale modeling are Orville, Cotton, Soong, Wilhelmson, Schlesinger, Takahashi, Murray, Klemp, Tripoli, Lipps, Das, Eskridge, Proctor, and others. Most of the references to their work can be found in UCAR (1982). They are not listed here for practical reasons; our interest is on beta and smaller alpha scales.

3.2 Observational Studies

The interest of numerous researchers in recent years has turned toward mesoscale processes in the atmosphere. Large-scale processes have already been adequately described in the literature. A variety of mesoscale studies has appeared, but convective storms and phenomena associated with these (fronts, jets) have attracted the most attention. Other phenomena are being studied (rain bands in cyclones, ice storms, smog in Southern California, winter lake-effect snowstorms, gravity waves, and tropical cyclones), but this review primarily concerns convective storms.

It is convenient to classify the observational studies of convective storms into three groups, after their primary emphasis:

- 1) Establishment of descriptive models;
- 2) Development of properties of continuous fields in the domain of convective storms; and
- 3) Verification or representation of numerical simulation of particular events.

Studies of the first group endeavor to establish descriptive, conceptual models. These efforts have been centered at the University of Washington (typical references: Herzegh and Hobbs, 1981; Hobbs and Persson, 1982); NCAR (Zipser, 1977; Shapiro, 1981; Carbone, 1982); the University of Chicago (Fujita and Wakimoto, 1981); SUNYA (Bosart, 1981); NOAA's ERL (Maddox, 1980a) and NSSFC (Doswell, 1980; Maddox and Doswell, 1982); NSSL and CIMMS in Oklahoma (Koch and McCarthy, 1982; McCarthy and Koch, 1982); Texas A&M University (Henry and Thompson, 1978; Holliday and Thompson, 1979; Henry, 1979); and others.

Numerical analyses, using special observing networks, normally comprise the second group. These studies have been carried out by Scoggins and

collaborators at Texas A&M University (Wilson and Scoggins, 1976; Fuelberg and Scoggins, 1978 and 1980) and by Maddox and collaborators at NOAA (Maddox and Doswell, 1982; Maddox et al., 1981). Studies of thermodynamic properties of the environment should probably also be classified in this group (Zawadski et al., 1981).

Mesoscale analysis of individual cases, conducted to verify the success of numerical models in simulating the same event, comprise the third group. In addition, considerable analyses has been performed on a case study basis by developers of numerical models, primarily for the purpose of assisting development. Examples are analysis by Cotton and collaborators (Cotton et al., 1982; and Knupp and Cotton, 1982 and 1982a); and for larger meso-gamma scale events by Ray et al. (1981) and Klemp et al. (1981).

3.3 Supporting Studies for Mesoscale Modeling

While models consist mainly of equations and their numerical treatment, there are a number of scientific fields which yield important results for use in the models. There are specialists in each of these fields whose experience can be well used in modeling. It may be worth considering that each modeling group acquires one specialist for each of these fields, otherwise the modelers themselves will have to conquer each of these fields, one by one. These special fields are enumerated next, without claim that the list is definitive.

1. Numerical analysis yields grid point values based on irregularly spaced observations. Most methods of numerical analysis are based on iterative correction of an initial guess, a technique introduced first by Bergthorsson and Döös (1955), and elaborated further by Barnes (1964) and Maddox (1980). Optimum interpolation is an attractive alternative to the iterative correction. This was introduced by Gandin (1963, also described by Morel, 1973), and adapted for utilization of pressure gradients by Bleck (1975). Optimum interpolation is used in the NCAR-Drexel model (Chang et al., 1981).

2. Initialization consists of adaptation of meteorological fields such that the unwanted (and not observed) possible modes of motion are suppressed in the initial conditions in numerical models. Initialization in mesoscale models is more important than in synoptic- or large-scale numerical weather prediction, because the whole period of interest may be only 12 hours or less, and in this time, the waves in the process of geostrophic adjustment

may be rather vigorous. These waves may be easily mistaken for mesoscale flow. Of course, a significant part of mesoscale events consists of gravity oscillations, which trigger new convective cells. Also, it is possible that gravity waves cause the formation of tropical cloud clusters through the mechanism of "trapez instability," as suggested by Orlanski (1973), and Sun and Orlanski, (1981) and (1981a). However, until we learn how to handle natural gravity waves, we are forced to assume that some kind of balance exists in our initial conditions such that gravity waves are excluded. A quasi-geostrophic balance is out of the question on the mesoscale. So far, most widely used is the initialization method of nudging, whereby the fast-moving gravity waves are damped and the solution is forced toward the observed state initially (Anthes, 1974; Hoke and Anthes, 1976).

3. Parameterization of subgrid-scale processes refers almost exclusively to turbulent transfer in the boundary layer and to mixing by convective clouds. Radiation is generally not considered in mesoscale models even though the temperature distribution is very sensitive to the radiation regime in convective clouds (Stephens and Webster, 1981); an exception is the model of sea and land breezes by Mahrer and Pielke (1977).

Parameterization of turbulent fluxes is of essential importance for all scales of modeling and it is the main topic of micrometeorology. Numerous books treat this subject. For mesoscale modeling, it is practical to follow the shorter treatments of the subject given by Blackadar (1979) and Pielke (1981). Practical application of the second-order closure theory is fairly uniform, with various sophisticated forms of the exchange coefficients. In this way, formally, the first- and second-order theories are similar.

Parameterization of convective clouds is less uniformly treated. There is a variety of methods in use. There is even some uncertainty in the whole field, as expressed by Rosenthal (1979) for parameterization of cumulus convection in hurricanes: "The experienced numerical experimenter can pick and choose closures that will provide almost any desired result." Since the variety of methods is great, it is of use to study the review by Pielke (1981, pp. 250-253) before the decision is made which method of parameterization to use.

4. Numerical integration is also a science by itself. On the mesoscale, usually the same methods are used as in large-scale numerical weather

prediction. Good reviews of numerical methods are presented by Mesinger and Arakawa (1976), and Haltiner and Williams (1980). Specific problems of mesoscale modeling are usually related to a limited area of computation. With a small grid size, it is not practically possible to expand the domain too far. Therefore, the treatment of boundaries becomes crucial. An expanding grid near the boundaries may be used for simulation purposes, but it does not promise correct environmental influence on the smaller domain of mesoscale prediction. Nesting of smaller domains into the large-scale numerical weather prediction seems to be a necessary procedure for prediction models. The "porous sponge" method of Perkey and Kreitzberg (1976) is a viable way to treat one-way nesting.

3.4 Presentation of Results

Graphical presentation of results is far from being standardized in the literature. However, there are some similarities in presentation, as shown below. When the same elements are presented by various authors, it is no wonder that some similarities appear.

Most presentations include a synoptic presentation of wind including the vertical component. The popularity of wind undoubtedly stems from the specialty of most researchers who are "dynamicists." The vertical component is always computed by the kinematic method (using the continuity equation). Doppler radar may be used sometime in the future for direct observations of the vertical component.

Radar echoes are the next most used element in presentation of results. The radar echo (Doppler) is also often used to evaluate the wind in observational studies. Unfortunately, there is no radar echo as such in numerical models. Therefore, for the sake of comparison, the liquid water concentration is displayed.

Synoptic presentation of various quantities is by far the most widely used method. The time variation of particular elements is used only rarely.

All presentations (of observations and computed results alike) are complicated by the amount of data that need presentation. Quite typical for projects of this kind are the large volumes with HIPLEX data (Scoggins et al., 1979; Sienkiewicz et al., 1980; also other reports in this series). Other observational projects also possess similar voluminous technical reports. However, the situation is rather similar in numerical modeling. Even a small model may have 400 grid points in a horizontal plane and 20 levels. At all points there may be about 10 important variables. It is highly

impractical to present everything, especially when the outprint is available at numerous times. Therefore, it is left to the good judgement of the investigators to select typical results.

As an example of the multitude of variables, Figure 3.1 contains several frames from the paper by Fritsch and Chappell (1980). The variable presented and the surface shown are indicated on top of each frame. It may be seen that the sample of results is very small, compared to the possible number of such frames for other levels, times, or vertical sections. This example is also interesting since these frames are remarkably similar to the frames in the HIPLEX reports (Scoggins et al., 1979; Sienkiewicz et al., 1980). It may be that the art of presentation of results is approaching a standard.

Figures 3.2-3.4 serve as examples of analyses of observed fields. These examples are on a meso-alpha scale; examples on meso-beta scale could not be found in recent literature. The original figure captions were retained in the illustrations wherever this was possible.

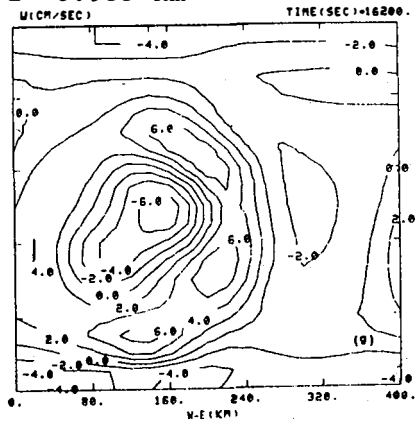
Several frames from an observational meso-gamma scale study (Carbone, 1982) are shown in Figures 3.5 and 3.6. Here the wind is evaluated from a set of three Doppler radars in California. The vertical component of motion was evaluated from the continuity equation. Some parts of the space contain no data; these regions are not reached by multiple radar beams. It may be noted that a grid size ≤ 1 km was used, which makes this analysis much more detailed than those for the HIPLEX area.

Convective storms analyzed at the NSSL in Norman, Oklahoma, by Ray et al., 1981 are shown in Figure 3.7. The wind, vertical motion, and reflectivity come from a set of four Doppler radars, supplemented by numerous other observations. In frame g (upper right), the tornado damage path is stippled. In the same frame a gust front is indicated by a thick curved line.

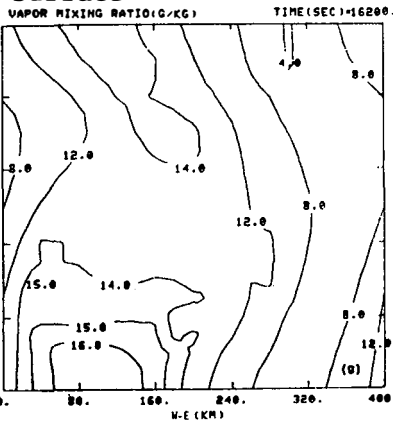
A numerical simulation that attracted great attention is the one by Wilhelmson and Klemp (1981), with their sophisticated, compressible, meso-gamma scale model (Figure 3.8). They compared their results with an observed splitting thunderstorm, as observed by radar. In order to make the comparison between the model and observations, they presented the rainwater content in the modeled cloud. In this way they obtained an element that is comparable to the radar reflectivity.

A similar comparison of modeling results with observations is shown by Klemp et al. (1981) in Figure 3.9. Here again the rainwater is compared

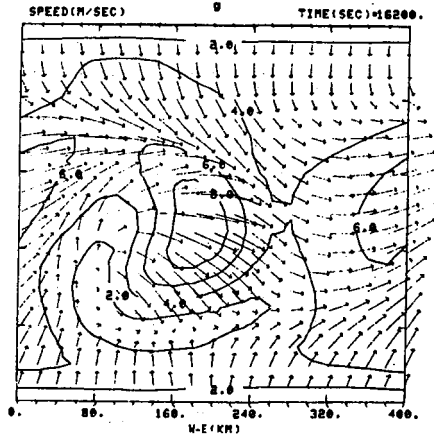
vertical motion
z = 0.988 km



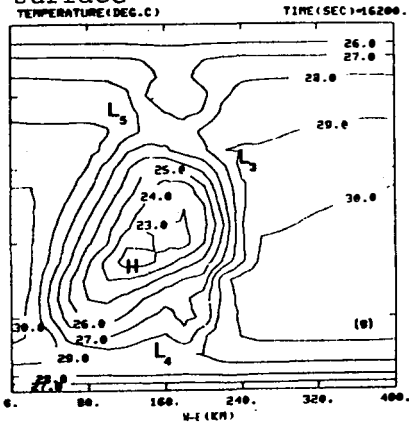
mixing ratio
surface



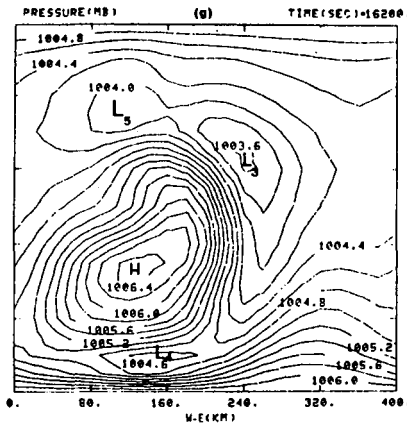
wind
surface



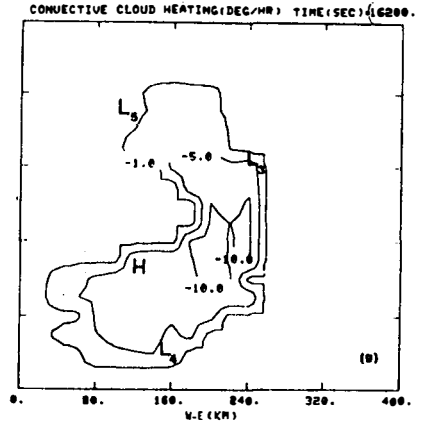
temperature
surface



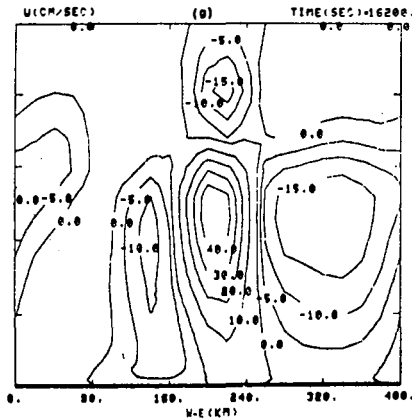
pressure
surface



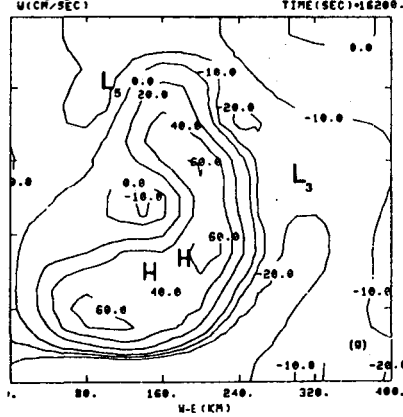
moist downdraft cooling
surface



vertical motion
E-W vertical section



vertical motion
z=9.16 km



temperature
z=9.16 km

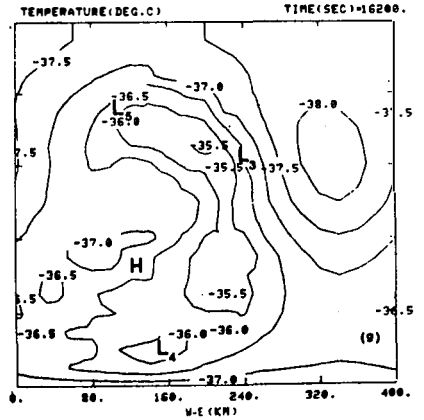


Fig. 3.1. Several variables after 4 h 30 min of development in the simulation model of Fritsch and Chappell (1980).

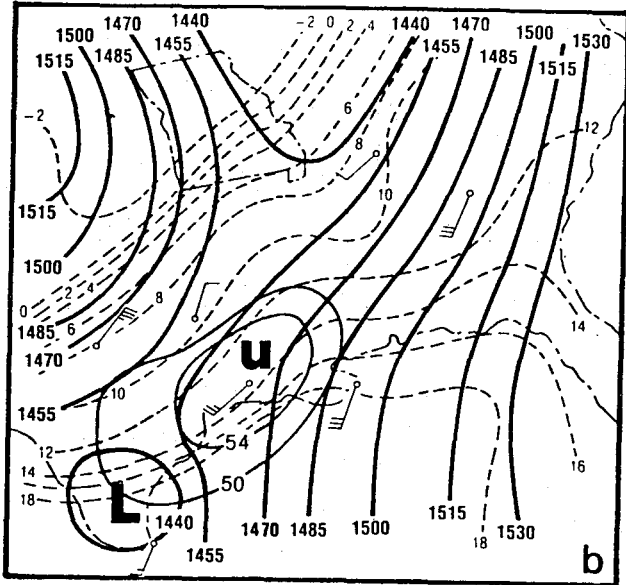


Fig. 3.2. 850 mb analyses for 12 April 1980. Heights (m) are heavy solid contours; Totals index is analyzed in light solid contours; isotherms ($^{\circ}\text{C}$) are dashed; and selected wind observations (full barb = 5 m s^{-1}) are shown for (b) 1200 GMT. (From Maddox and Doswell, 1982).

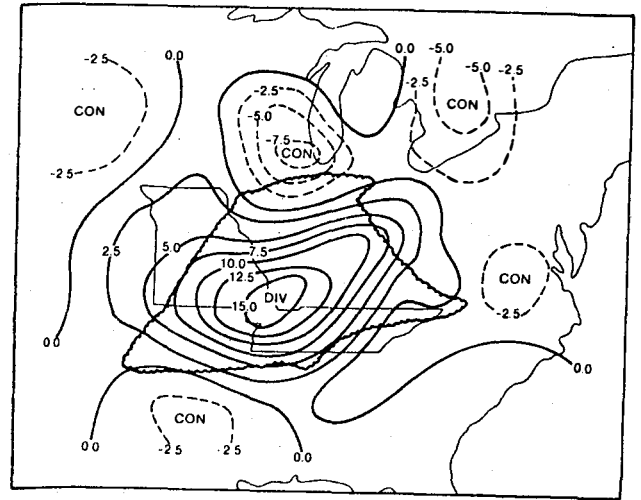


Fig. 3.3. Divergence ($\times 10^{-5} \text{ s}^{-1}$) for the total 20 kPa wind at 0600 GMT 25 April 1975. Contour interval is 2.5. (From Maddox *et al.*, 1981. The outline of the cloud from the satellite photo is added.)

JOURNAL OF THE ATMOSPHERIC SCIENCES

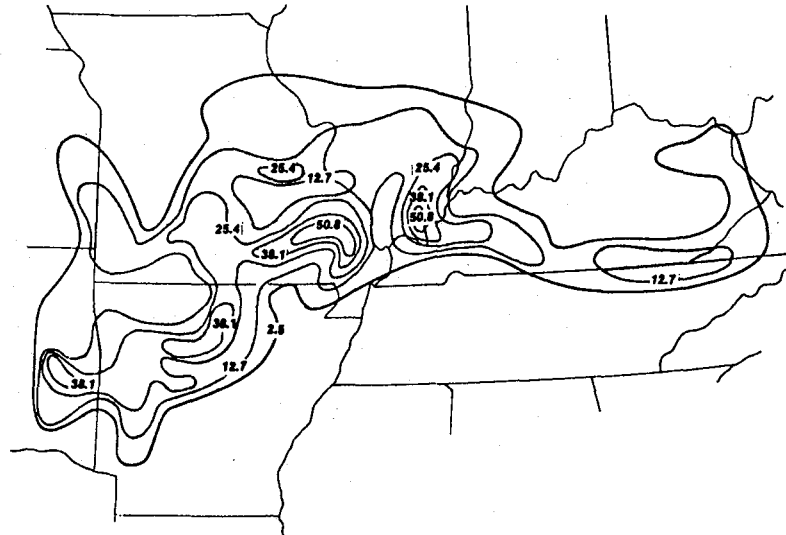


Fig. 3.4. Accumulated precipitation (mm) from 0000 to 0600 GMT 25 April 1975. (From Maddox *et al.*, 1981).

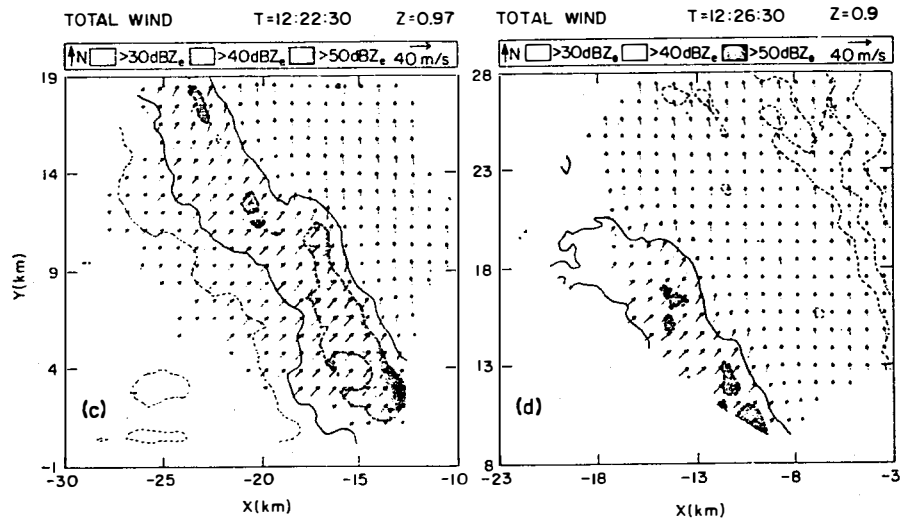


Fig. 3.5. Low-level horizontal wind at (c) 1222:30, (d) 1226:30. Lowest level of complete data is shown for each time. Reflectivity is shaded for $Z \geq 40$ dBZ. All distances are from CP-3. (From Carbone, 1982).

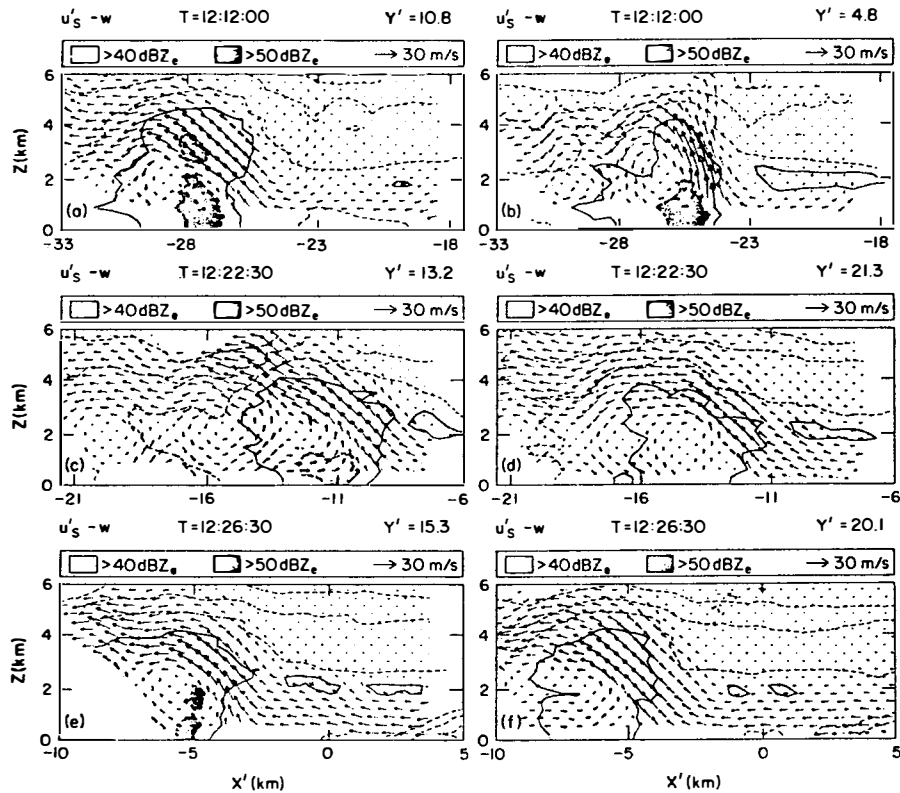
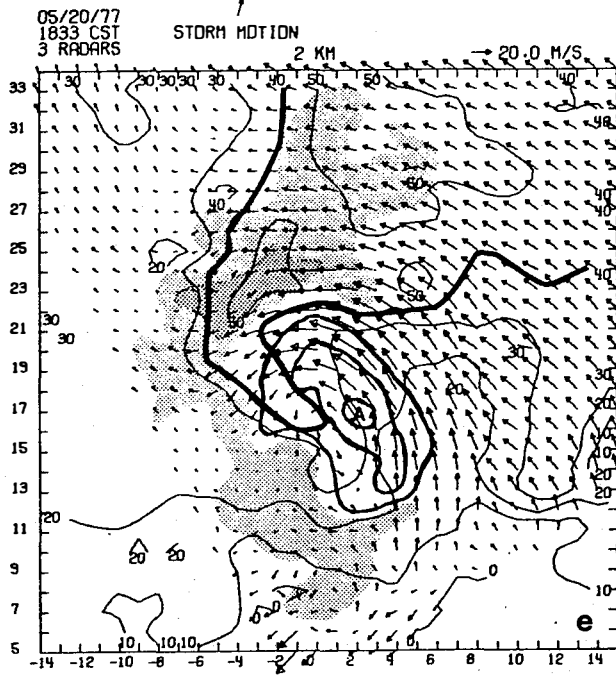
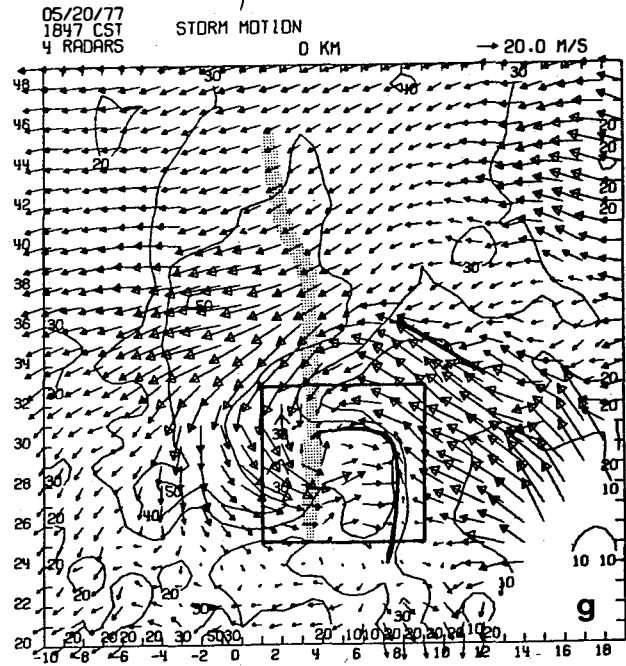


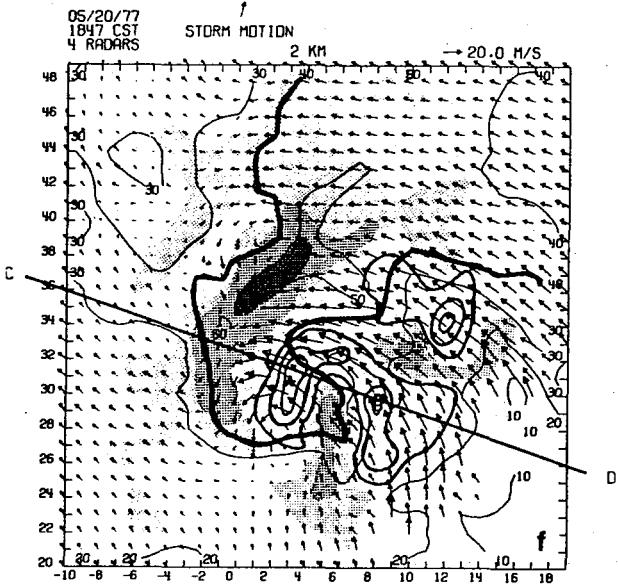
Fig. 3.6. A variety of kinematic structures seen in the squall line to emphasize the spectrum of results obtained. Major features (such as prefrontal updraft, subsidence updraft, outflow, and low-level convergence) are highly two-dimensional. (From Carbone, 1982).



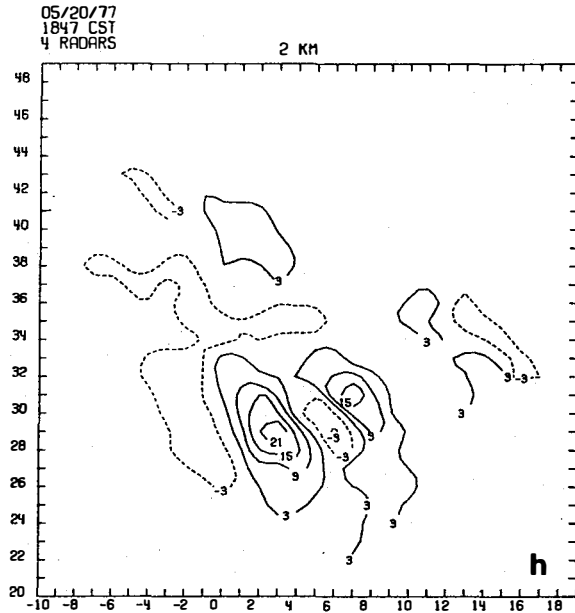
Horizontal Flow Field/Reflectivity (dBZ), 2 km.



Horizontal Flow Field/Reflectivity (dBZ), surface.



Horizontal Flow Field/Reflectivity (dBZ), 2 km. Updraft: medium lines
downdraft: stippled.



Vorticity X 10^3 , 2 km.

Fig. 3.7. Observed variables in a thunderstorm (from Ray et al., 1981).

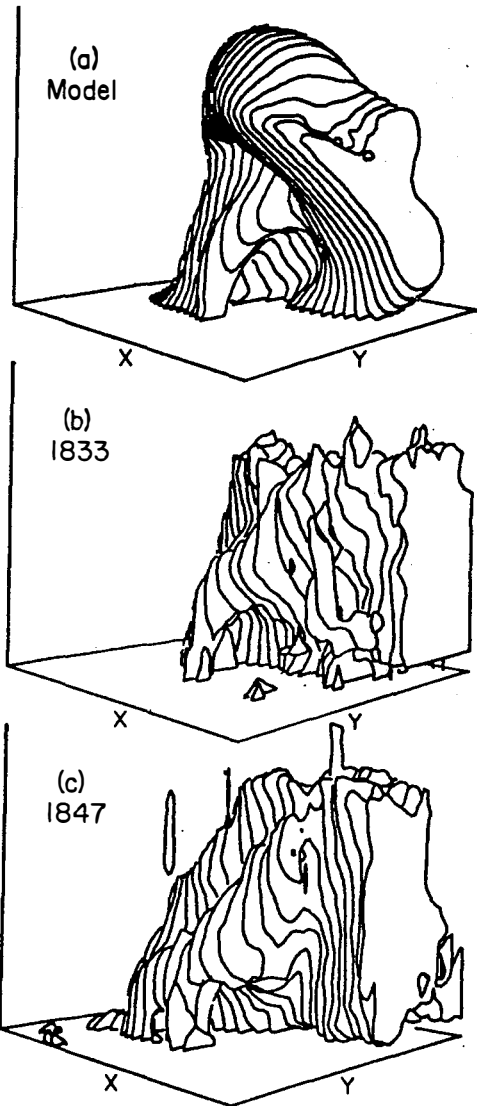
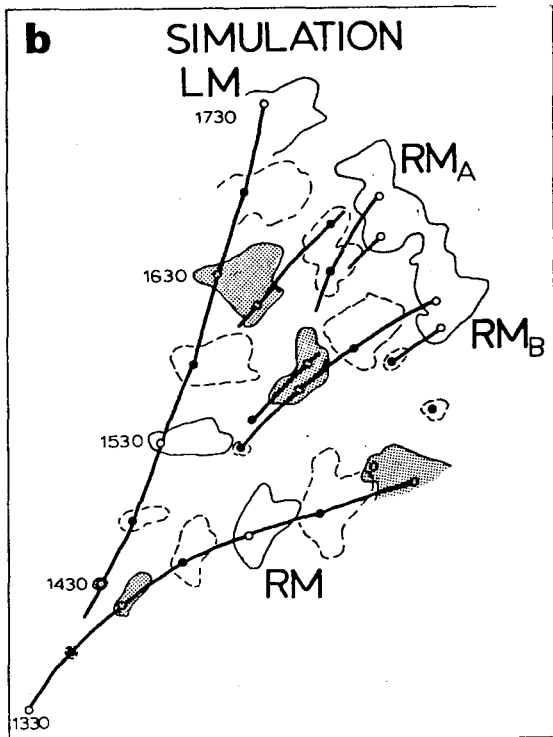
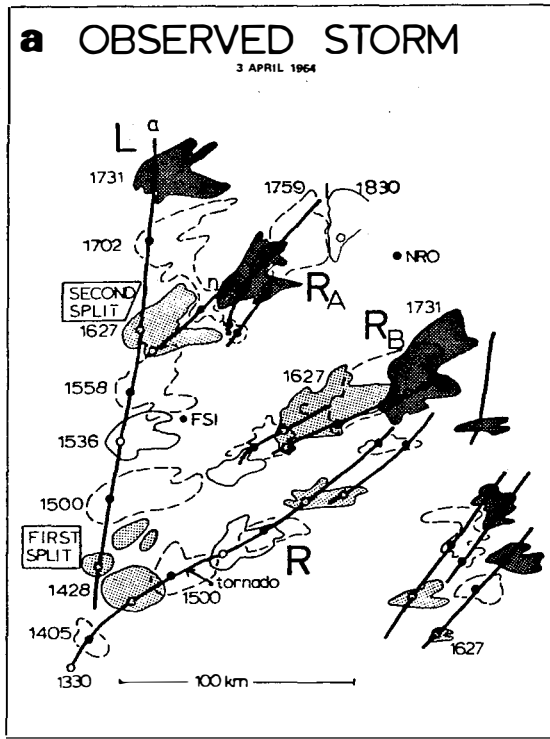


Fig. 3.9. Distribution of precipitation within the modeled and observed storms as viewed from the southeast. The contoured surfaces represent the 0.5 g kg^{-1} rainwater surface in the model and the 35 dBZ reflectivity surfaces in the observed storm. The x-y base plane corresponds to the $29 \text{ km} \times 29 \text{ km}$ domains and the vertical axis extends to 14 km. (From Klemp et al., 1981).

Fig. 3.8. The (a) observed and (b) modeled storm development on 3 April 1964. Observed reflectivities $> 12 \text{ dBZ}$ at 0° and modeled rainwater contents $> 0.5 \text{ g kg}^{-1}$ at $z = 0.4 \text{ km}$ are enclosed by alternating solid and dashed contours about every 30 min. Maxima in these fields are connected by solid lines. The storms are labeled and at several times the contoured regions are stippled for better visualization of the storm development. Labels for the modeled storms are the same as the corresponding observed storms except for the inclusion of M. The scale shown in (a) applies in (b). (From Wilhelmson and Klemp, 1981).

to the radar reflectivity. The three-dimensional presentation makes use of NCAR computer routines which are available for such complicated projects. In the figure, we see a number of vertical sections, where the front ones partially obscure the rear ones, giving a strong three-dimensional effect. This is the case of the Del City storm in which a rain-free vault was observed inside the cloud. It is quite remarkable that the model simulated this vault, in spite of starting with a rather arbitrary warm bubble in the initial conditions. Only the environmental sounding was patterned after the observed sounding near the storm.

Similar to the HIPLEX reports are the results of meso-beta scale computations of the sea breeze by Pielke (1981) and Warner et al. (1978). Putting them side-by-side in Figures 3.10 and 3.11, we can see the similarity between the two. Both of them show the afternoon convergence near the Delaware-Virginia border.

The vertical distribution of potential temperature in the sea- and land-breeze model by Mahrer and Pielke (1978) is shown in Figure 3.12. In this figure we see that the unstable stratification can be handled in non-hydrostatic models.

A more detailed vertical section is illustrated in Figure 3.13 by Keyser et al. (1978). It shows a frontal zone (Figure 3.13a) and a 12-h prediction for the same zone (Figure 3.13b). The capability of representation of fronts with horizontal resolution of 75 km is demonstrated.

Conceptual models, on the basis of observations and computations, may represent the ultimate goal of science. One such model is shown in Figure 3.14, from Rotunno and Klemp (1982). This example stresses various shears around a convective cloud.

It is evident that many methods of presentation are used to present results from model and observational mesoscale studies. In each case only representative results are shown which illustrate the nature of the processes investigated.

It is also evident that no single presentation will simultaneously depict all the important features of a mesoscale system. More importantly, it should be noted that these presentations normally depict a single scale; the picture becomes even more complicated when interests lies within the scale interaction of two or more scales, as in the five year HIPLEX experiment.

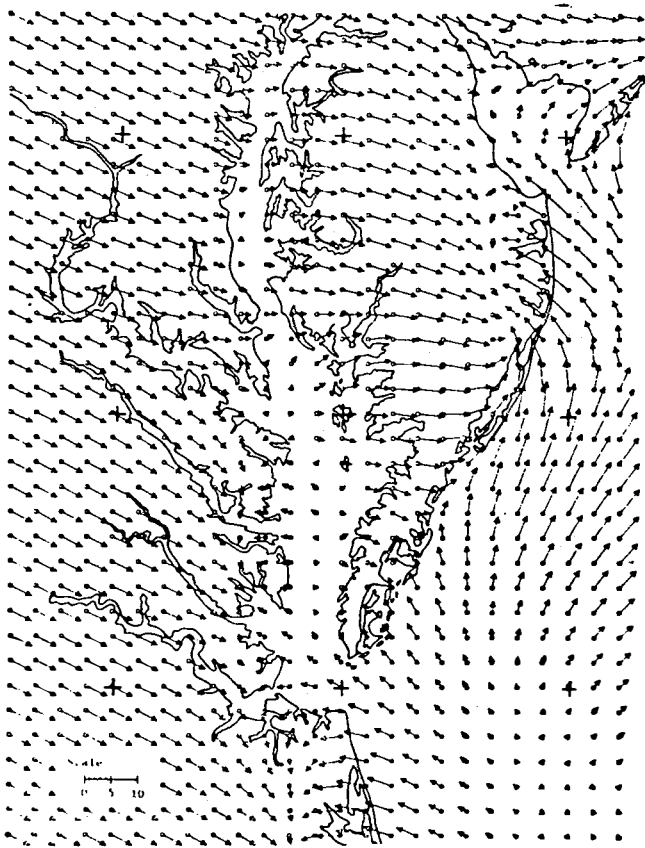
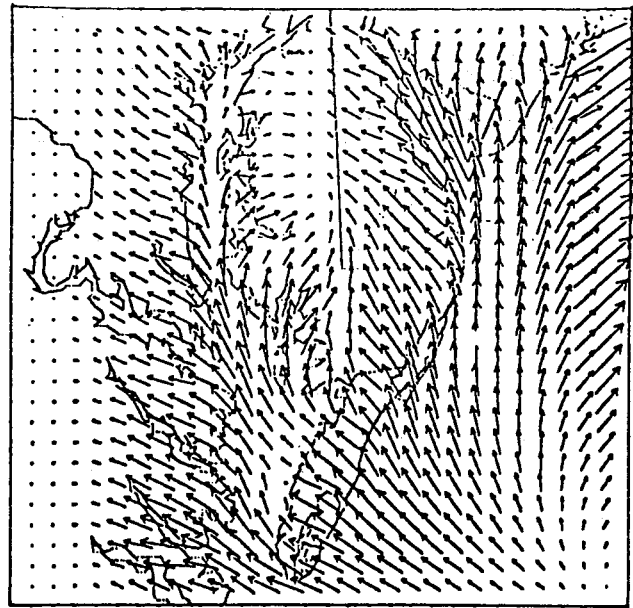


Fig. 3.10. The predicted winds at 4 m at about 1500 LST over the Chesapeake Bay for August 9, 1975. Model simulation performed by W. Snow using the University of Virginia Mesoscale Model. Scale bar in m sec^{-1} . (From Pielke, 1981.)



(c)

Fig. 3.11. Predicted wind field from Experiment 3 (SB) applying at the lowest model layer (≈ 80 m above the surface) for LAT. (From Warner *et al.*, 1978. LAT is local apparent time.)

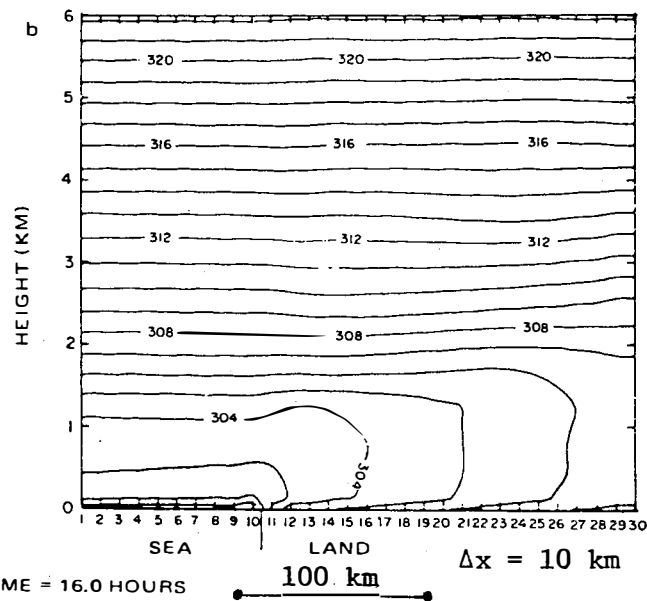


Fig. 3.12. The vertical cross section of potential temperature along a coastline at 1800 LST for a 6 m sec^{-1} onshore synoptic wind. Initial input was for a typical summer day over south Florida. (From Mahrer and Pielke, 1978.)

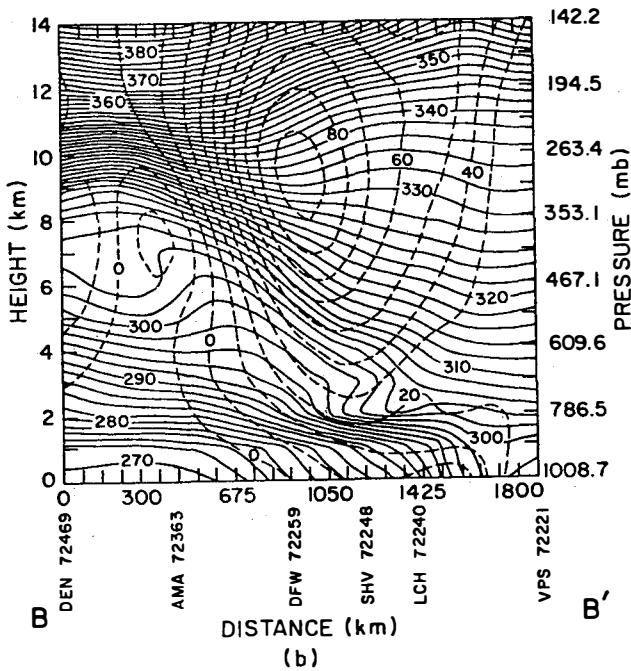
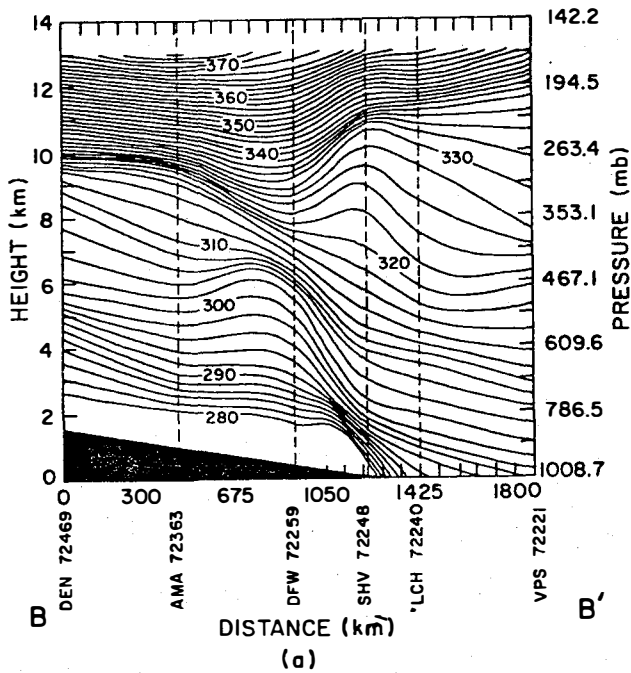
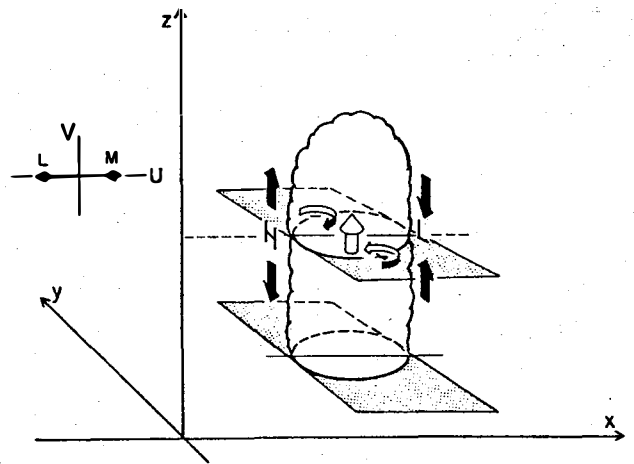


Fig. 3.13. Cross-section analyses of potential temperature (K) and the component of the geostrophic wind normal to the cross section ($m s^{-1}$) along BB' at 0000 GMT 22 February 1971.

(a) Rawinsonde observations at Denver, CO (DEN); Amarillo, TX (AMA); Dallas-Fort Worth, TX (DFW); Shreveport, LA (SHV); Lake Charles, LA (LCH); and Valparaiso, FL (VPS). Wind analysis not included because of missing data. (b) Analysis based on 12 h model forecast and $\Delta s = 75$ km. (From Keyser et al., 1978.)

(a) STRAIGHT HODOGRAPH



(b) CURVED HODOGRAPH

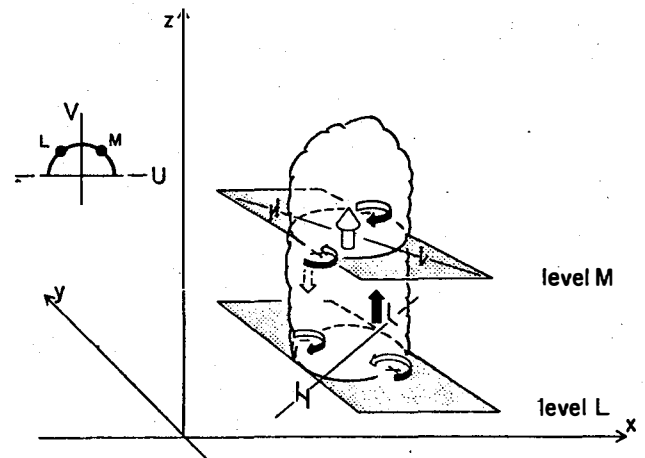


Fig. 3.14. Schematic which illustrates the behavior of pressure and vorticity for (a) a case where the wind shear vector does not change with height and (b) a case where the wind shear vector veers with height. The corresponding hodographs for environmental flow at low (L) to mid (M) levels are inset to the left. Horizontal pressure gradients parallel to the shear vector are labeled at each level along with the preferred locations of positive (+) and negative (-) vorticity. The orientations of the resulting vertical pressure gradient forces between low and mid levels are indicated by the black arrows. (From Rotunno and Klemp, 1982.)

4.0 MESOSCALE ANALYSES FOR SELECTED DAYS DURING 1979 AND 1980.

4.1 Days Analyzed

The case studies considered in this section are for 1979 and 1980 when data from seven rawinsonde stations were available. As during previous years each day and to some extent each observation time, is treated as a case study. Sounding times were 1500, 1800, 2100, 0000, and 0300 GMT on each day. The days for which analyses are presented in this report include the following:

<u>1979</u>	<u>1980</u>
May 21, 26, 27, 28	June 2, 19, 20
June 8, 9	
July 16, 18	

4.2 Approach

For each date and time the basic rawinsonde data were gridded on constant pressure surfaces using the Barnes technique and a grid interval of approximately 16 km. The parameters that were gridded included temperature, mixing ratio, u- and v- wind components, and geopotential height. Other variables were calculated from these basic data and gridded, also using the Barnes technique. Calculated variables included velocity divergence, moisture divergence, vertical motion, and vertical moisture flux. These variables were computed at 50-mb intervals from 850 mb to 200 mb. Vertical motion was computed by the kinematic method.

The analysis procedure was to subdivide the entire HIPLEX area into subareas, based on the type of convective activity present in each subarea. Contour charts of the above variables were examined and prominent mesoscale systems identified as a basis for this subdivision. The approach was to identify areas, then average each variable over a selected number of grid points within each area, and then plot profiles of each variable as a function of pressure. This provided a means of establishing the variation in the parameters across the mesoscale network and as a function of height relative to the convective activity. The areas selected were based primarily on conditions below 700 mb since the mesoscale systems, and particularly those related to moisture, are better defined in the lower regions of the atmosphere.

The profiles for each of the six variables listed above, determined by averaging over selected grid points, were plotted on the same figure

for each date and time. These figures were then used to extract average values of each variable and the near maximum deviation of the variable about its average at 800, 700, 500, and 300 mb. Tables of these numbers were prepared to show the variation across the mesoscale network as a function of date, time, and type of convective activity. The deviation from the mean is assumed to represent the standard deviation or a close approximation thereto. The interpretation of the deviation is somewhat uncertain because of the limited sample size in each case. However, once the data have been aggregated and composite profiles prepared for a relatively large sample of data, it is believed that the deviations so defined approach the standard deviation.

All contoured charts, profiles, averaging areas, and data tabulations described above for each time and each date are presented in Appendix A. These analyses and those presented in previous reports (See Section 2) for other years form the mesoscale data base from which the mesoscale models presented in Section 6 were developed.

5. CLASSIFICATION OF CONVECTIVE ACTIVITY

In an effort to organize the data describing the convective response of the Texas HIPLEX area, all sounding periods for the 1978, 1979, and 1980 seasons were classified into four convective groupings. The classification scheme was based solely on radar activity, with the primary source being digitized radar echo maps which stratified radar echoes according to three cloud-top (echo-top) height thresholds:

1. Echo heights less than 6.1 km (20,000 ft).
2. Echo heights between 6.1 km and 9.1 km (30,000 ft).
3. Echo heights greater than 9.1 km (30,000 ft).

Each radar map at each sounding time was assigned one of four classifications:

1. No convection
2. Isolated convection
3. Convective clusters
4. Lines of convective cells

Unless echoes were present which exceeded an elevation of 6.1 km, the sounding time was classified as "no convection." As soon as level two or level three echoes were present, the sounding time was classified as isolated convection, unless three or more separate level two or level three echoes appeared within the HIPLEX area or any two echoes were separated by less than two storm diameters. In these latter cases, or when the deep convection of a single echo covered an excessively large area, the convection was classified as a convective cluster. Finally, if the radar echoes assumed a line configuration, the cluster would be classified as a line. Classification was also aided by the availability of microfilm of actual PPI radar scope images at 5-minute intervals for a number of days. The classification into the four basic convective groupings could be carried out objectively.

In addition to the basic four convective classifications, the first three classes contained additional stratifications into several sub-classes. Some subjectivity entered into these stratifications. The radar film was used to accurately classify into sub-classes where the film was available. On the remaining data, experience gained from use of radar scope data was valuable. Nevertheless, it is probable that a small number of subclasses have been misclassified: for example, with only hourly radar maps it is possible to misinterpret developing convection as dissipating convection

in some marginal cases.

The no-convection cases were stratified into five sub-classifications according to the sounding time (1500, 1800, 2100, 0000, and 0300 GMT). The isolated cells were subclassified according to the intensity of development into developing, mature, and dissipating cases. For the days in which actual radar film was present, this stratification could be accurately performed; on all other days, the classification was made on a subjective basis using radar charts which preceded and followed the sounding time by one hour, and on the basis of experience gained from stratifying the cases for which radar film was available.

The convective clusters were stratified several different ways because of their importance as rain producers in the Texas HIPLEX area. Since most of the precipitation is associated with large clusters, attention should be focused on what it takes to generate large clusters. First, the clusters were stratified with the same classifications used for isolated cells i.e., developing, mature, and dissipating. Secondly, the storms were classified according to whether the clusters were large or small. This classification was almost entirely subjective. It turned out that about 60% of the small cluster cases also were classified as dissipating systems, with the majority of the remaining small clusters as developing clusters. Finally, a small number of the large clusters were collected into a grouping, called "huge" clusters, for want of a better word. In an effort to isolate precursor signals, a set of 1500 GMT soundings also was collected for days which experienced large clusters.

Table 5.1 lists the days and sounding times of all the non-convective cases. In all, there were 130 different sounding times during the three HIPLEX periods when no convection was present. These cases are collected from 41 different days in which periods of no convection were observed. On the other hand, no convection was observed at all five sounding times on only nine of the fifty-nine days for which sounding data were available. In other words, only 15% of the days for which HIPLEX data is available experienced no convection. At 2100 GMT, predictably, the incidence of no convection was smallest.

Table 5.2 lists the days and sounding times of all cases of isolated convection. This classification comprises 69 individual sounding times spanning 36 different days. On 50% of the days in which isolated convection

Table 5.1 No-Convection Cases (listed by date, and stratified by GMT time:
 N15 = No-Convection, 1500 GMT, etc.)

<u>CASE N15</u>	<u>CASE N18</u>	<u>CASE N21</u>	<u>CASE N00</u>	<u>CASE N03</u>
* 78/6/1	78/6/1	78/6/1	78/6/2	78/6/2
78/6/5	78/6/4	78/6/2	78/6/5	78/6/8
78/6/14	78/6/13	78/6/4	78/6/15	78/6/14
78/6/27	78/6/14	78/6/6	78/6/28	78/6/15
78/6/28	78/6/27	78/6/14	78/7/18	78/6/28
78/6/29	78/6/28	78/6/27	78/7/22	78/7/18
78/7/17	78/7/17	78/7/17	78/7/26	78/7/22
78/7/21	78/7/21	78/7/21	79/5/22	78/7/24
78/7/22	78/7/25	78/7/25	79/5/27	78/7/26
78/7/25	79/5/25	79/5/25	79/5/29	79/5/22
79/5/25	79/5/26	79/5/26	79/6/10	79/5/26
79/5/26	79/5/27	79/5/27	79/6/22	79/5/27
79/5/28	79/6/21	79/6/21	79/7/3	79/5/28
79/6/5	79/7/2	79/6/24	79/7/7	79/6/6
79/6/8	79/7/3	79/7/2	79/7/8	79/6/10
79/6/21	79/7/4	79/7/14	79/7/15	79/6/22
79/6/24	79/7/7	80/5/28	79/7/17	79/6/25
79/7/2	79/7/14	80/6/2	80/5/27	79/7/7
79/7/3	79/7/16	80/6/10	80/5/30	79/7/8
79/7/6	80/5/28	80/6/18	80/6/3	79/7/15
79/7/14	80/5/29		80/6/11	79/7/17
79/7/16	80/6/9		80/6/23	80/5/15
79/7/17	80/6/17		80/6/30	80/5/27
80/5/26	80/6/20			80/5/28
80/5/27	80/6/21			80/5/30
80/5/28	80/6/22			80/6/10
80/5/29				80/6/23
80/6/2				80/6/30
80/6/10				
80/6/17				
80/6/18				
80/6/20				
80/6/21				
80/6/22				

* YEAR/MONTH/DATE

Table 5.2 Isolated Convection Cases (listed by date and GMT time and stratified by intensity)

<u>CASE I1</u> (developing)	<u>CASE I2</u> (mature)	<u>CASE I3</u> (dissipating)
* 78/6/5/03	78/6/5/18	78/6/8/00
78/6/5/18	78/6/29/00	78/6/29/03
78/6/7/21	78/6/29/21	78/6/30/00
78/6/28/21	78/7/1/18	78/7/23/15
78/6/29/18	78/7/24/18	79/5/28/21
79/5/2/00	79/5/28/18	79/6/6/00
79/5/29/03	79/6/2/03	79/6/25/00
79/6/2/00	79/6/5/21	79/7/5/00
79/6/5/18	79/6/8/21	80/5/15/15
79/6/8/18	79/7/4/21	80/6/1/21
79/6/9/15	79/7/6/03	80/6/2/03
79/6/24/18	80/5/15/21	80/6/9/03
79/7/3/21	80/5/26/21	80/6/9/21
79/7/5/03	80/5/29/03	80/6/10/00
79/7/6/00	80/6/1/18	80/6/18/03
79/7/7/15	80/6/18/00	80/6/18/18
79/7/16/21	80/6/19/03	
80/5/26/18	80/6/20/21	
80/5/27/18	80/6/21/03	
80/5/27/21	80/6/22/03	
80/5/29/00		
80/5/29/21		
80/6/1/15		
80/6/2/18		
80/6/8/15		
80/6/9/15		
80/6/10/18		
80/6/17/21		
80/6/19/00		
80/6/19/15		
80/6/19/21		
80/6/21/21		
80/6/22/21		

* YEAR/MONTH/DATE/GMT

was observed, more vigorous convection--either clusters or lines--also was observed at different sounding times. Nearly 80% of the developing convection occurred in the 1500-2100 GMT time interval; most of the mature isolated convection (62%) occurred at 1800 and 2100 GMT. Sixty-two percent of the dissipating convection occurred at 0000 and 0300 GMT.

Table 5.3 lists days and sounding times when clustered convection was present. There were 61 individual observations of clusters occurring on 26 different days. Twenty-four of the 61 cluster cases were classified as large clusters and 9 of these 24 were classified as huge. Large clusters occurred on 17 days while huge clusters occurred on only 8 of the 59 HIPLEX days. Over 70% of the large cluster cases occurred at 2100 and 0000 GMT, which are also the preferred times of huge clusters. Clustered convection was relatively infrequent at 1500 GMT (only five observations), and clustered convection occurred at 0000 GMT about twice as frequently as at any other time period. Clusters occurring at 0300 GMT were weak, with no observations of large convection, and all but one of the cases in the dissipating stage.

Finally, Table 5.4 lists the ten cases of line convection. These cases span seven different days.

The mesoscale analyses described in Section 4 and presented in Appendix A were also examined for each time and classified into the four categories except where there were no lines observed. Also, a classification of wide-spread activity was added to account for cases that did not fall into any of the other categories. The classification of each date and time is presented in Table 5.5. These data were classified separately from those in Tables 5.1-5.4 because of the different analysis approach used for the various data sets. These differences relate to both the use of additional rawinsondes in the analysis and considerations of more than radar echoes in the classification (See Section 6).

Table 5.3 Clustered Convection (listed by date and GMT time and stratified by intensity)

<u>CASE C1</u> (developing)	<u>CASE C2</u> (mature)	<u>CASE C3</u> (dissipating)
+ 78/6/2/15*	78/6/6/00*	78/6/2/18
78/6/30/15	78/6/6/15	79/7/18/18*
78/7/22/18	78/6/13/21	78/6/3/03
78/7/23/18	78/6/30/18*	78/6/6/03
79/6/1/15*	78/6/30/21*	78/6/6/18
79/6/4/18	78/7/1/00*	78/6/14/00
79/6/9/00*	78/7/1/21	78/7/2/00
79/7/6/18*	78/7/22/21**	78/7/2/03
79/7/17/18	78/7/23/21*	78/7/23/00
79/7/18/21*	78/7/24/21*	78/7/23/03
79/7/19/00*	79/5/28/00**	78/7/24/00
80/5/16/00	79/6/1/18**	78/7/25/00
80/6/2/00	79/6/4/21	79/6/1/21*
80/6/21/00	79/7/3/03	79/6/5/00*
	79/7/17/21**	79/6/5/03
	79/7/18/00	79/6/9/03
	80/5/28/00*	79/7/5/18
	80/6/8/18*	79/7/5/21**
	80/6/20/00*	79/7/18/03
	80/6/22/00	79/7/18/15
		79/7/18/18*
		79/7/19/03
		80/6/8/21*
		80/6/9/00
		80/6/11/03
		80/6/19/18
		80/6/20/03

- + YEAR/MONTH/DATE/GMT
- * Also classified as large convection
- ** Large convection also classified as huge convection

Table 5.4 Line Convection (listed by date and GMT time)

CASE L
* 78/6/7/00
78/6/7/03
78/6/30/03
79/5/21/18
79/5/21/21
79/5/27/15
79/7/4/00
79/7/4/03
79/7/7/21
80/5/15/18

* YEAR/MONTH/DATE/GMT

Table 5.5 Classification of each time versus echo characteristics for the mesoscale analyses presented in Appendix A.

Widespread Echoes		Isolated Cells		Clustered Cells		No Cells	
Date	Time	Date	Time	Date	Time	Date	Time
5/21/79	2100	5/21/79	1800	5/21/79	1500	5/22/79	0000
5/22/79	0300	5/28/79	1800	5/27/79	1500 ²	5/26/79	1500
5/29/79	0300	6/9/79	0000	5/28/79	0000	5/26/79	1800
7/18/79	1500	6/9/79	0300	6/8/79	2100	5/26/79	2100
7/18/79	1800	7/19/79	0300	7/18/79	2100	5/27/79	0000
7/19/79	0000	6/20/80	2100 ¹	6/20/79	0000	5/27/79	0300
6/19/80	1800	6/21/80	0000			5/27/79	1800
6/19/80	2100					5/27/79	2100
6/20/80	0300					5/28/79	0300
6/21/80	0300					5/28/79	1500
						5/28/79	2100
						5/29/79	0000
						6/8/79	1500
						6/8/79	1800
						6/9/79	1500
						6/9/79	1800
						6/9/79	2100
						6/10/79	0000
						6/10/79	0300
						7/16/79	1500
						7/17/79	0000
						7/17/79	0300
						6/2/80	1500
						6/2/80	1800
						6/2/80	2100
						6/3/80	0000
						6/20/80	1500
						6/20/80	1800

¹Vertical Velocity and Vertical Moisture Flux not used in computing average.

²Moisture Divergence not used in computing average.

6. PRELIMINARY MESOSCALE ENVIRONMENTAL MODELS FOR THE TEXAS HIPLEX AREA

6.1 Model Construction Procedure

There are two types of mesoscale environmental models presented, viz, basic data models and kinematic models. The basic data models are based on sounding data, while the kinematic models are based on computed parameters. In each type of model, the method of specification is vertical profiles of selected parameters and their standard deviation for each convective classification. The standard deviations of average values of variables for the entire HIPLEX area as well as for averages for smaller areas were estimated for convective categories.

Each of the models contains vertical profiles of temperature, dewpoint temperature, mixing ratio, wind speed, and wind direction. These vertical profiles were obtained by averaging over all the classifications and stratifications described in Section 5. The data sets prior to 1979 consisted of four soundings at given sounding times. The data sets for 1979 and 1980 consisted of seven sounding stations. For a given day and a given sounding time each variable was average across all available stations for constant pressure surfaces between 850 and 150 mb at 50-mb increments.

Once the data had been classified, the vertical profiles were averaged for each of the classifications. The mean vertical distribution of variables averaged over each case of a given classification--for example, line convection--are then presented as an atmospheric model for that type of convection. The standard deviations calculated from the individual cases with respect to the mean are also displayed as a part of the model. Thus the standard deviations are computed in the time domain and do not represent areal variability (This is considered in Section 4 and 6.3). They represent the expected variability of the atmosphere at a given sounding time with respect to the average model.

The models described in the next section summarize the mean environmental conditions and expected deviations from these conditions when certain specified types of convective activity are present. Most of the classifications possess at least twenty individual cases and may be considered representative. Nevertheless, there are certain restrictions which must be mentioned. On a given day, several different convective classes may be observed over the HIPLEX area; thus one model normally does not represent the environmental

state for a given day.

Because of the coarse vertical resolution (50 mb) and the tendency of the atmosphere to form large vertical gradients (dry layers, shear zones, inversions) the models may be unrepresentative of the atmosphere's fine structure in the vertical. There is generally an inversion or stable layer capping the moist boundary layer. Since the elevation and strength of this layer is highly variable, the averaging procedure completely eliminates it from the model. This particular feature, as well as others like it, may be crucial in determining the existence and intensity of certain types of convection. At any rate, this fine structure is not considered in the model.

Surface pressure is somewhat variable in the HIPLEX region, as is the height of the planetary boundary layer. Thus, some of the cases within a classification sample the boundary layer conditions which extend above 850 mb, and others do not sample shallow boundary layers. It is best to assume that the models do not convey information regarding surface environmental conditions.

In this particular analysis, most of the soundings do not pass through thunderstorm regions, even when extensive convection is present. Thus it is assumed that the models essentially represent the mesoscale convective environment. Also, except for a single classification of precursors to large clustered convection the models do not sample antecedent conditions. The models, therefore, represent some composite of causative and resultant effects; it is likely that some of the most significant intermodel differences are a result, and not a contributory cause, of the convection.

6.2 Basic Data Models

No Convection: Temperature and dewpoint soundings for the no convection cases are shown in Figure 6.1. Data for all five sounding times are shown in this figure. Where less than five lines appear, the missing lines are identical with the 1500 GMT sounding. For all cases and at all locations, deviations in model soundings are small compared to the standard deviation within a given model. Nevertheless, certain of the differences are likely to be physically realistic. The 5°C difference in 850-mb temperature between 1500 GMT and 0000 GMT is clearly associated with the diurnal solar cycle. On the average, the diurnal heating becomes less significant than day-to-day variations at 800 mb, although individual soundings show that the diurnal

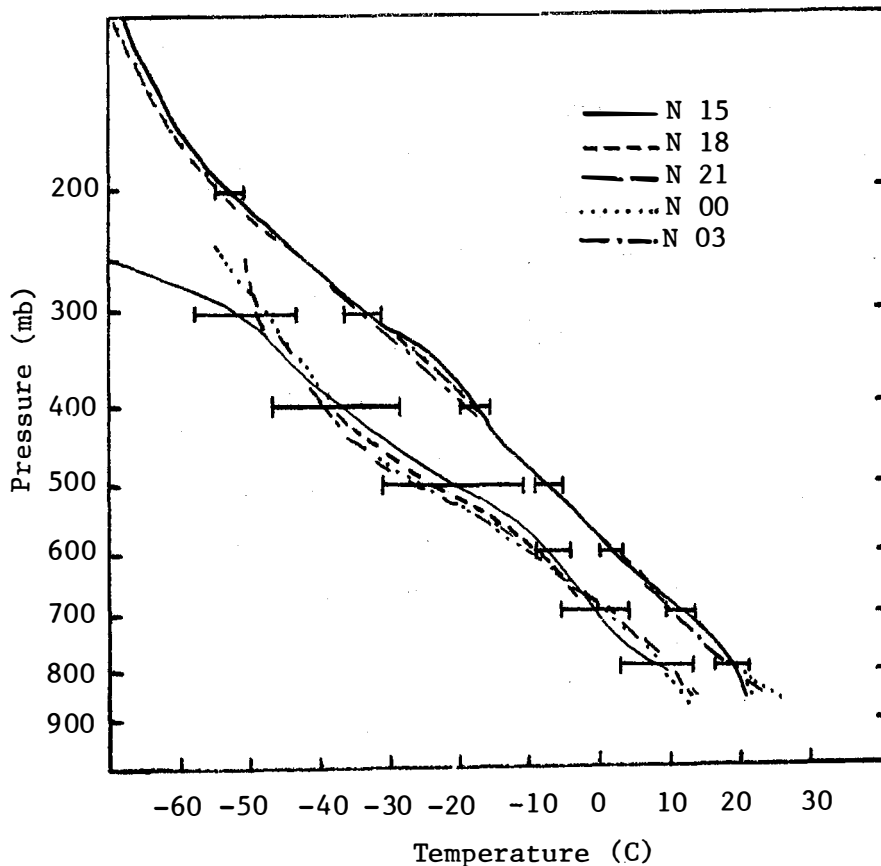


Fig. 6.1. Profiles of temperature and dewpoint temperature for the no-convection classification. Standard deviation bars are for 1500 GMT. N 15 = no-convection at 1500 GMT, etc.

variation often penetrates to 700 mb. Another region of temperature variation appears between 300 and 400 mb. There is no obvious reason for the 4°C scatter among differing cases (there is no significant convection at this level for these cases); this variation is likely to be associated with random variability.

The variation among the dewpoint temperatures are larger than those of temperature and also probably are associated with physical causes and not random variation. The 850-mb dewpoints at 1500 and 1800 GMT are larger than values later in the day. In spite of the absence of convection, fair weather cumulus and unsaturated turbulent transport carry moisture aloft and dry out the planetary boundary layer during the day. This vertical transport is reflected in larger dewpoints between 800 and 700 mb at the latter

sounding periods. A second drying region appears between about 650 and 350 mb, with dewpoint temperatures decreasing about 5°C throughout the day. This drying is most probably associated with the strong subsidence which usually accompanies the no-convection cases.

The mixing ratios for the no-convection models are shown in Figure 6.2. These curves show the same behavior as the dewpoint curves. Below 850 mb and above 650 mb the absolute moisture content decreases between 1500 and 0300 GMT; between these layers the moisture content increases. The absolute change at 850 mb is about 1.5 g kg^{-1} .

The wind speeds, regardless of direction, are shown in Figure 6.3. In general for all the no convection cases, the wind averages about 6 m s^{-1} at 850 mb, decreases to a minimum of about 3 m s^{-1} in the vicinity of 700 mb, and increases to about 17 m s^{-1} at jetstream level (200 mb). With the possible exception of the decrease of wind throughout the day at 850 mb, differences between curves are most likely due to random variation.

Wind directions appear in Figure 6.4. Directions were averaged without respect to wind speed; standard deviations were not computed. Large systematic differences occur throughout the day. In the midlayers, between 400 and 700 mb, the wind direction changes anticyclonically, with the largest change of 45 degrees at about 550 to 600 mb. Below 700 mb, the wind turns cyclonically, from 20 degrees west of south to 20 degrees east of south. Although plausible physical mechanisms could be hypothesized for these changes, well-established explanations have not yet been developed. The large variation in direction at 100 mb is a consequence of the light winds, rather than significant variation.

Isolated Convection. Temperature and dewpoint soundings for the three models of isolated convection (developing, mature, and dissipating) are shown in Figure 6.5. The differences between the three models are slight with the only systematic difference being that developing convection seems to be associated with a drier atmosphere below 600 mb, and a wetter atmosphere above 600 mb. Since there is a tendency for echo development to be related to time of day, this difference may simply be a mirroring of diurnal differences shown in the no-convection case. The only difference between the isolated convection models and the 1500 GMT no-convection model is that above 500 mb, the no-convection model possesses dewpoints a few degrees lower than isolated convection cases. The increased moisture content of

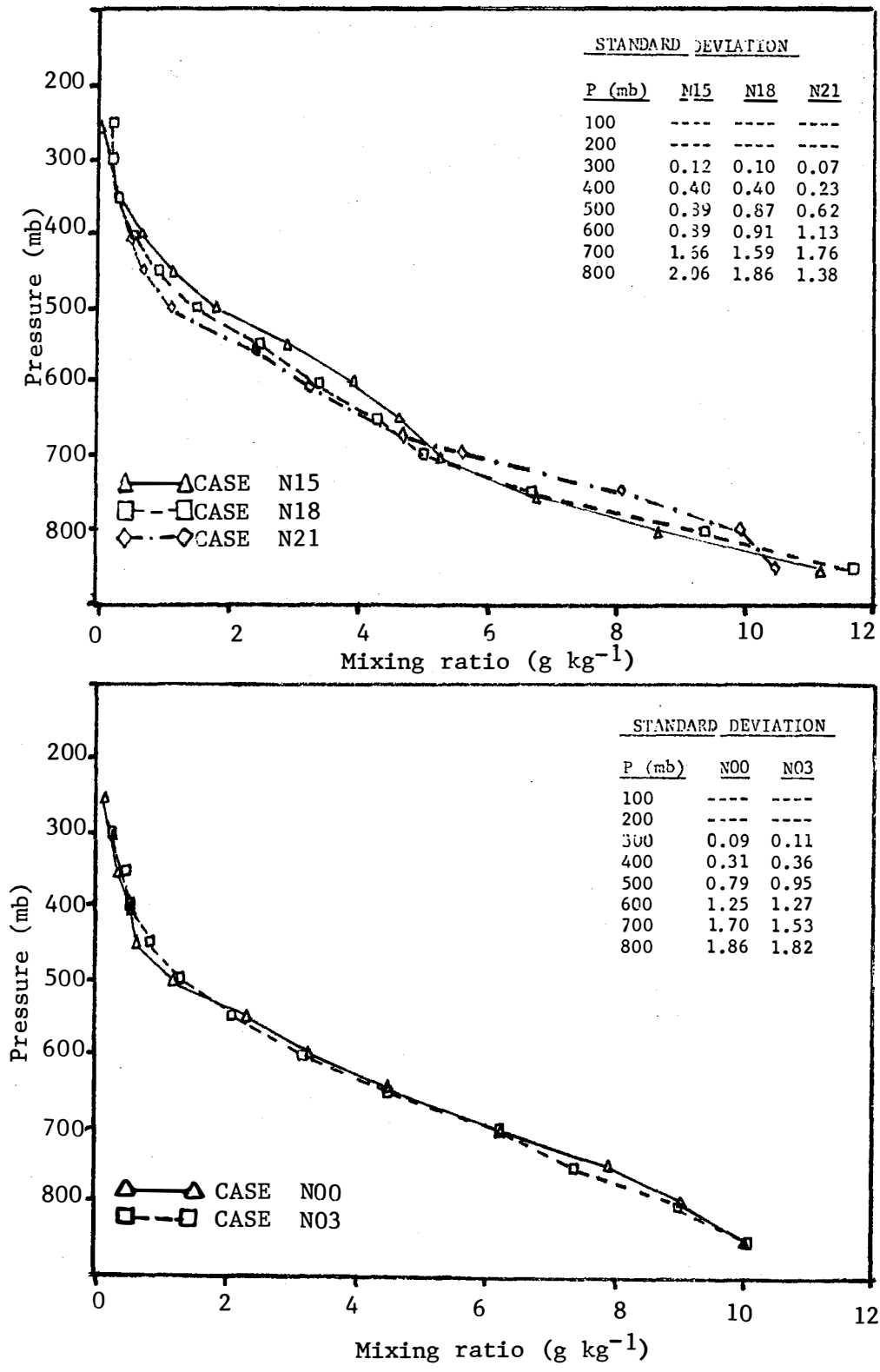


Fig. 6.2. Profiles of mixing ratio for the no-convection classification. N15 = no convection at 1500 GMT, etc.

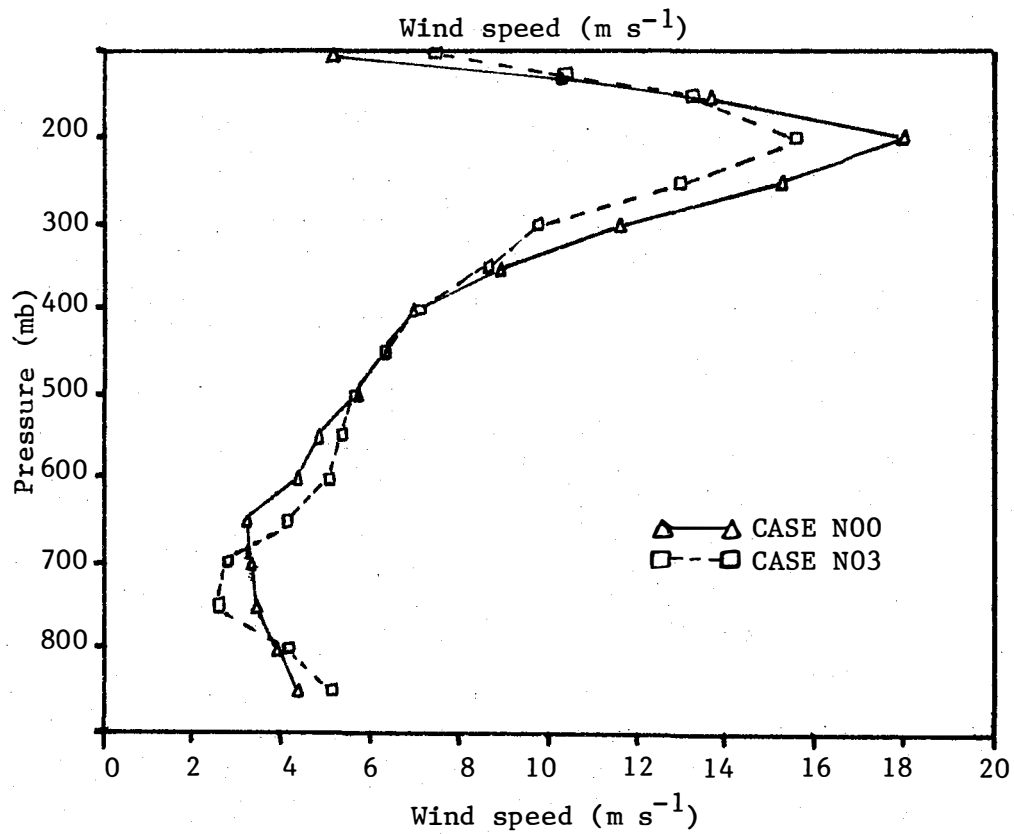
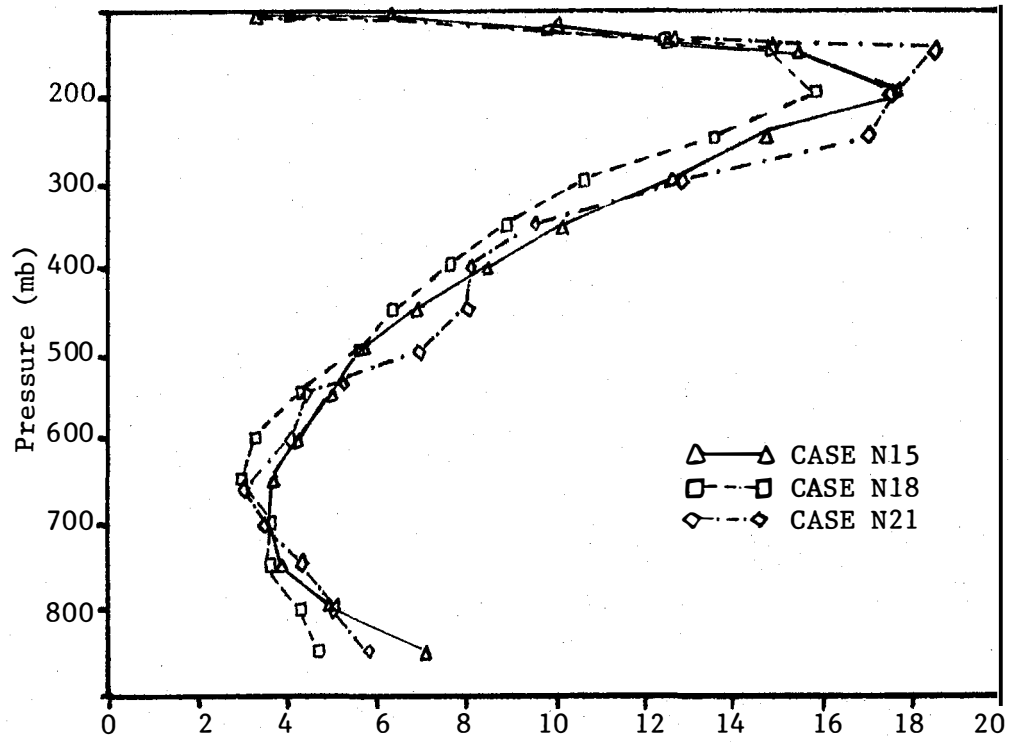


Fig. 6.3. Profiles of wind speed for the no-convective classification, N15 = no convection at 1500 GMT, etc.

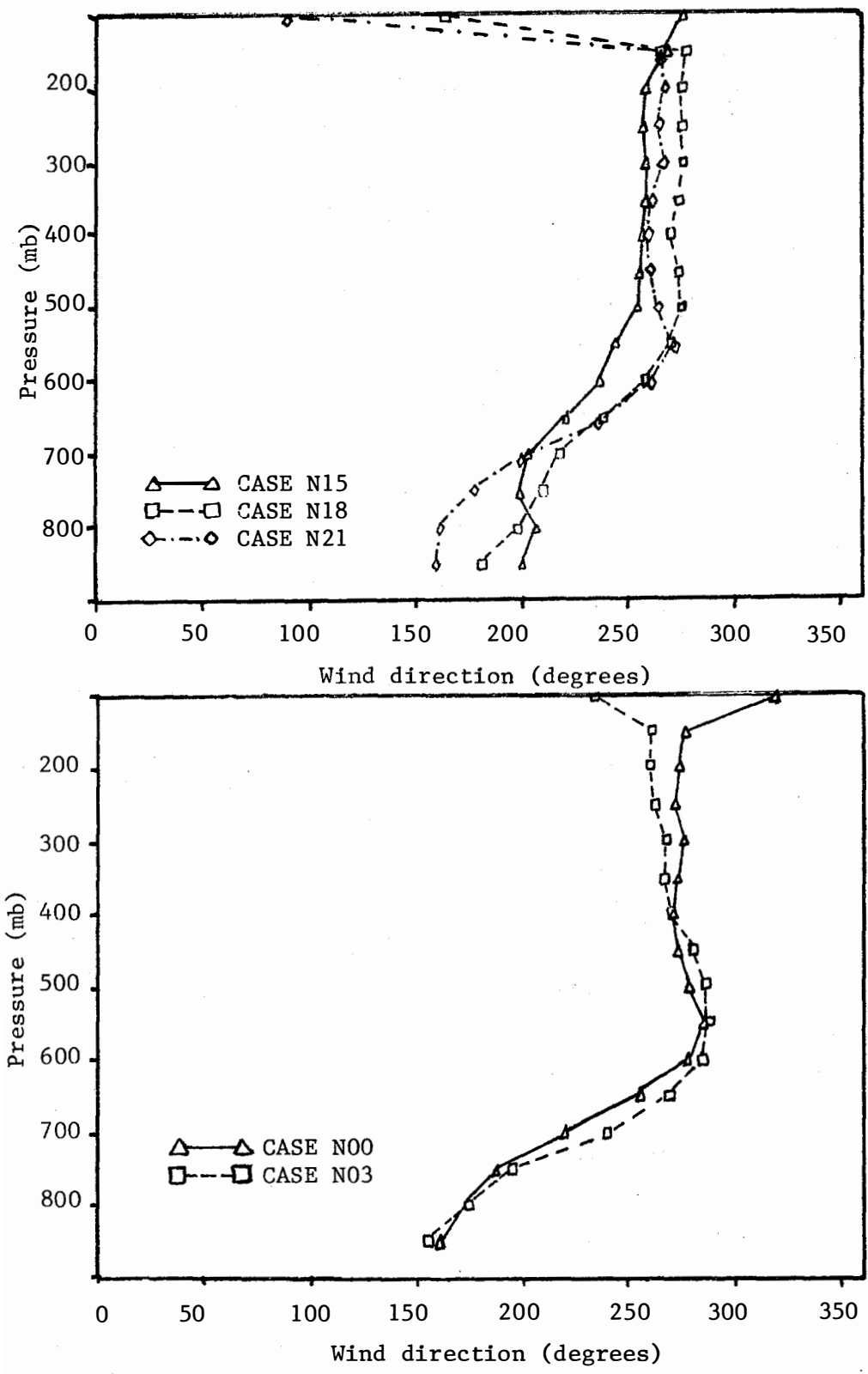


Fig. 6.4. Profiles of wind direction (from which wind is blowing) for the no-convection classification. N15 = no convection at 1500 GMT, etc.

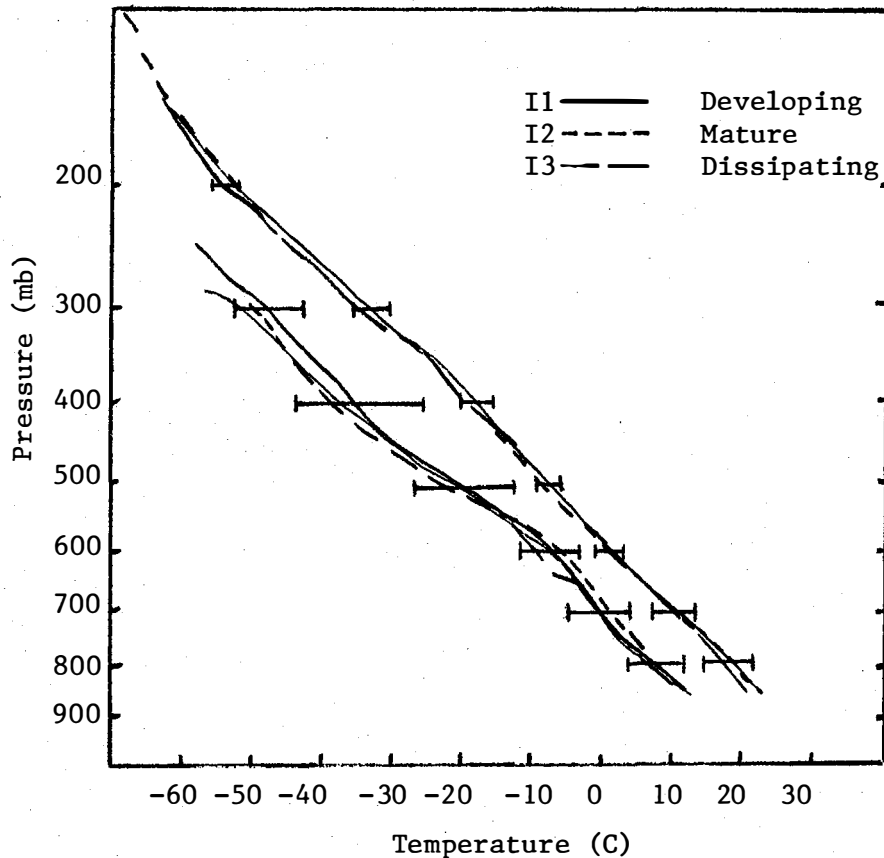


Fig. 6.5. Profiles of temperature and dewpoint temperature for the isolated convection classification. Standard deviation bars are for the I1 profile.

the isolated convection models, particularly that of the mature and dissipating models is confirmed in the mixing ratios in Figure 6.6. The moisture content for isolated convection averages 1 to 2 g kg^{-1} greater than the no-convection case throughout the troposphere.

Wind speeds for the isolated convection models are shown in Figure 6.7. There is a weak tendency for jet stream level winds to weaken as the isolated convection matures. Throughout most of the troposphere, there is no significant variation in wind speed as a function of storm maturity. On the other hand, there are important differences between the profiles of no-convection and isolated convection models. The speed minimum at 650 mb, which is observed for no-convection models, is typically observed at 850 with the winds increasing monotonically up to 200 mb. Except at the lowest layers, below 800 mb, wind speeds increase by several m s^{-1} throughout the troposphere.

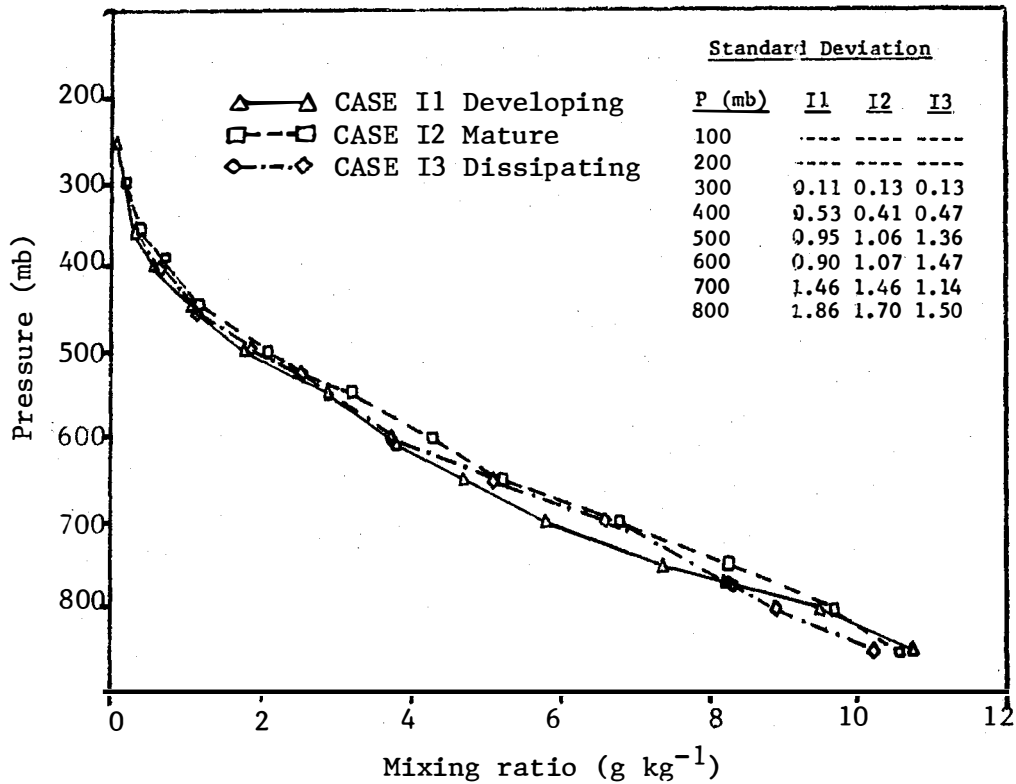


Fig. 6.6. Profiles of mixing ratio for the isolated convection classification.

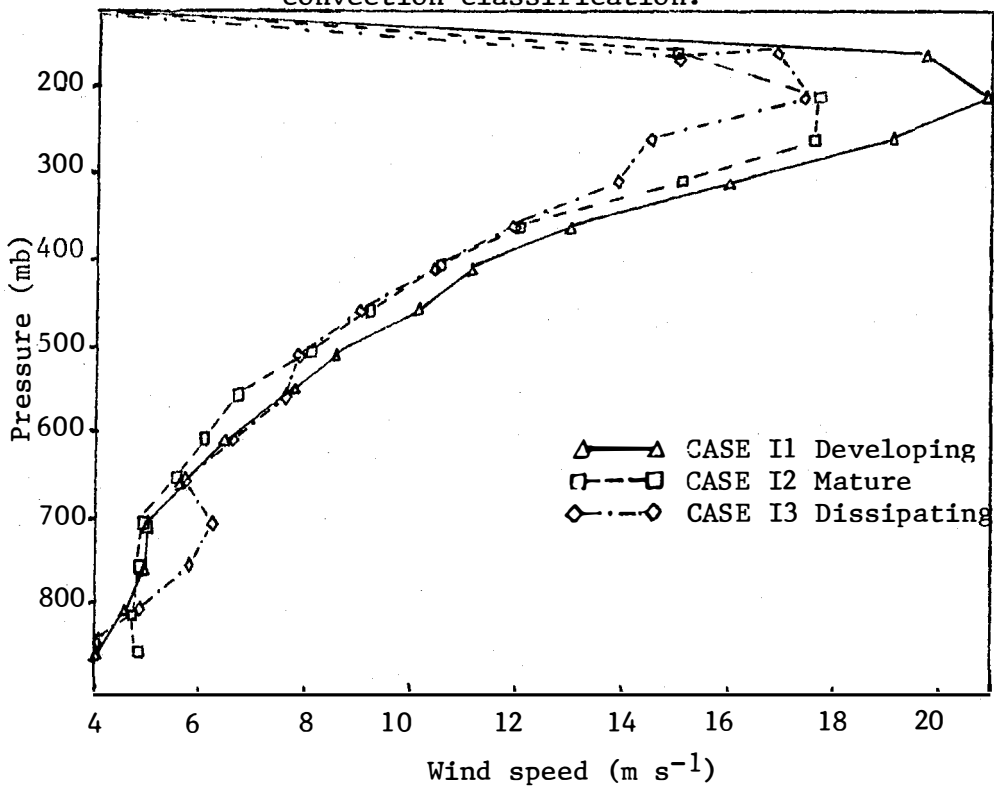


Fig. 6.7. Profiles of wind speed for the isolated convection classification.

The variation in wind direction among the isolated convection models is small (Figure 6.8), but once again the differences with respect to no-convection models is significant. For most model comparisons, wind direction differences are less than 30 degrees at a given level. However, when isolated convection is present, the winds are more south-southwesterly (less southeasterly) below 700 mb and less westerly above 700 mb than when no-convection is present. The result is that the low-to-mid tropospheric directional shear is significantly less when isolated convection is present. For example, typical directional shear between 850 and 500 mb for isolated convection is 75 degrees (veering) and 110 degrees (veering) for no convection. Clusters. Due to the importance of convective clusters with respect to the amount of precipitation they produce, several different stratifications of clusters were considered (See Section 5). The clusters were analyzed, as with isolated cases, according to developing, mature, and dissipating categories.

Figures 6.9 and 6.10 describe the temperature, dewpoint, and mixing ratio models for the convective cluster classification. On the average, the temperatures below 700 mb were slightly cooler, 1-1.5°C, when convective clusters were present compared to cases when only isolated cells were present. This cooler air would have the effect of decreasing the mid tropospheric lapse rate and thus increasing atmospheric stability. Cooler temperatures were also observed above 250 mb when convective clusters were present. At all levels below 250 mb, the moisture content is significantly higher with convective clusters present compared to situations of isolated convection, as measured both by the dewpoint temperature and the mixing ratio. Below 750 mb the developing cluster model is moister than the mature and dissipating stages. These differences are likely to be a result of the cluster convection because one of the results of extensive convection will be the drying out of the lower layers and the moistening of the mid and upper troposphere as the convective towers transport moisture upwards. Because of the increase in moisture, and also the slight decrease of temperature at lower altitudes, the relative humidity is much higher in the cluster models than in the isolated convection models. For example, comparing developing cases, the relative humidity for the cluster model varies from 60% at 850 mb to 70% at 600 mb, whereas the isolated cell model relative humidity varies between 50% and 45% at the same levels.

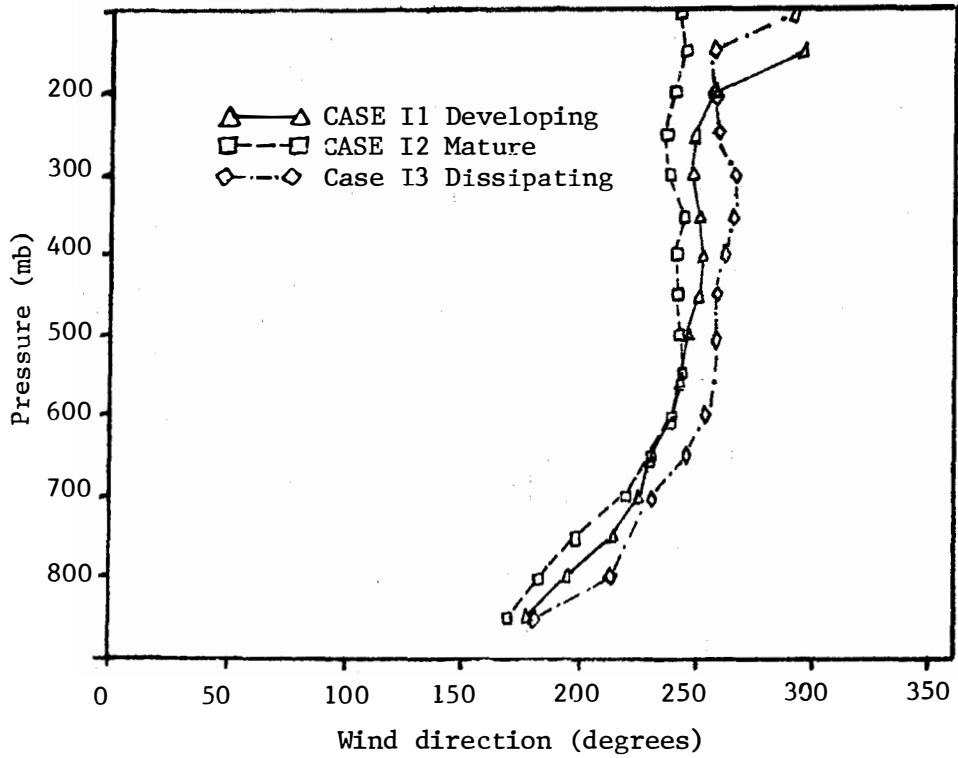


Fig. 6.8. Profiles of wind direction (from which wind is blowing) for the isolated convection classification.

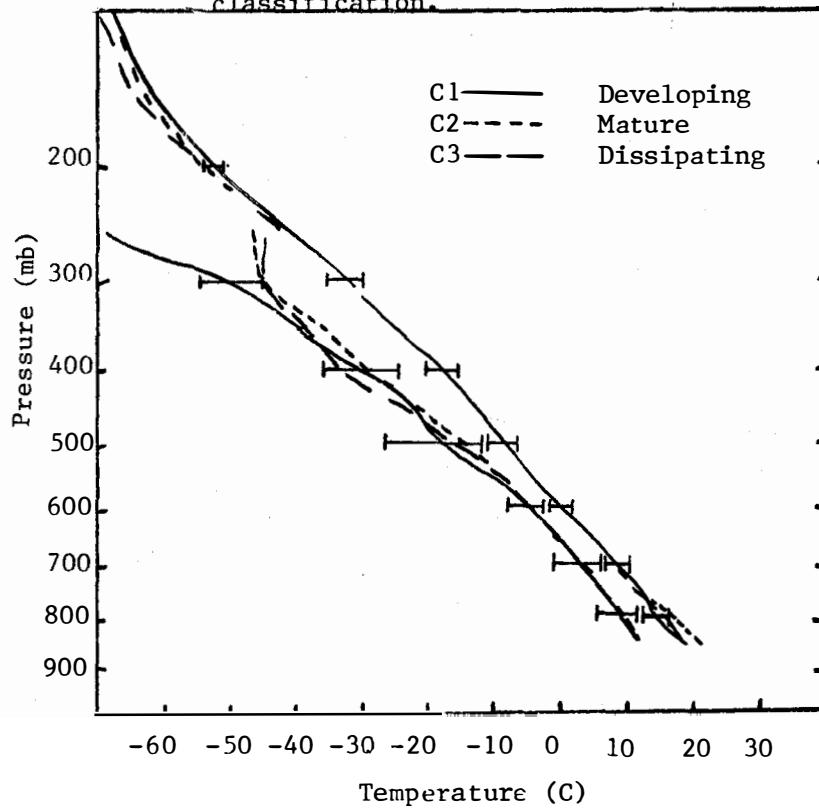


Fig. 6.9. Profiles of temperature and dewpoint temperature for the cluster classification. Standard deviation bars are for the C1 profile.

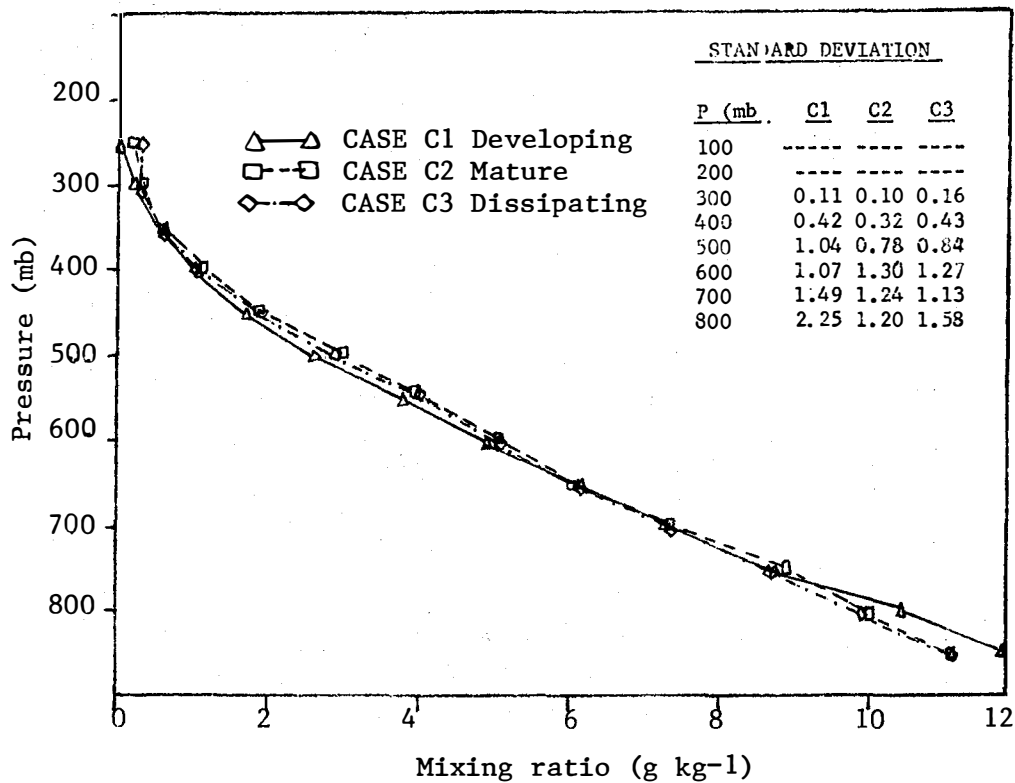


Fig. 6.10. Profiles of mixing ratio for the cluster classification.

Wind speed profiles for the cluster models appear in Figure 6.11. The speed is strongest throughout the troposphere for the developing model and decreases for the mature model and still more for the dissipating model. In fact, the profile for the dissipating model resembles that for no convection. Generally speaking, for most cases and at most elevations, the wind speed when cumulus clusters are present is slightly less than when only isolated convection is present. Thus, the weakest winds seem to be associated with no convection or clustered convection, and somewhat stronger winds are associated with isolated convection.

Profiles of wind direction associated with clusters are shown in Figure 6.12. Wind directions for dissipating clusters follow the same trend as that for no convection (just like the wind speeds): very strong directional shear (veering) in the lower troposphere, and backing above 600 mb. The developing and mature models follow the same profile as the models for isolated convection. The only difference is that the wind direction angle for the cluster models is slightly smaller throughout the troposphere than that for isolated convection. This difference

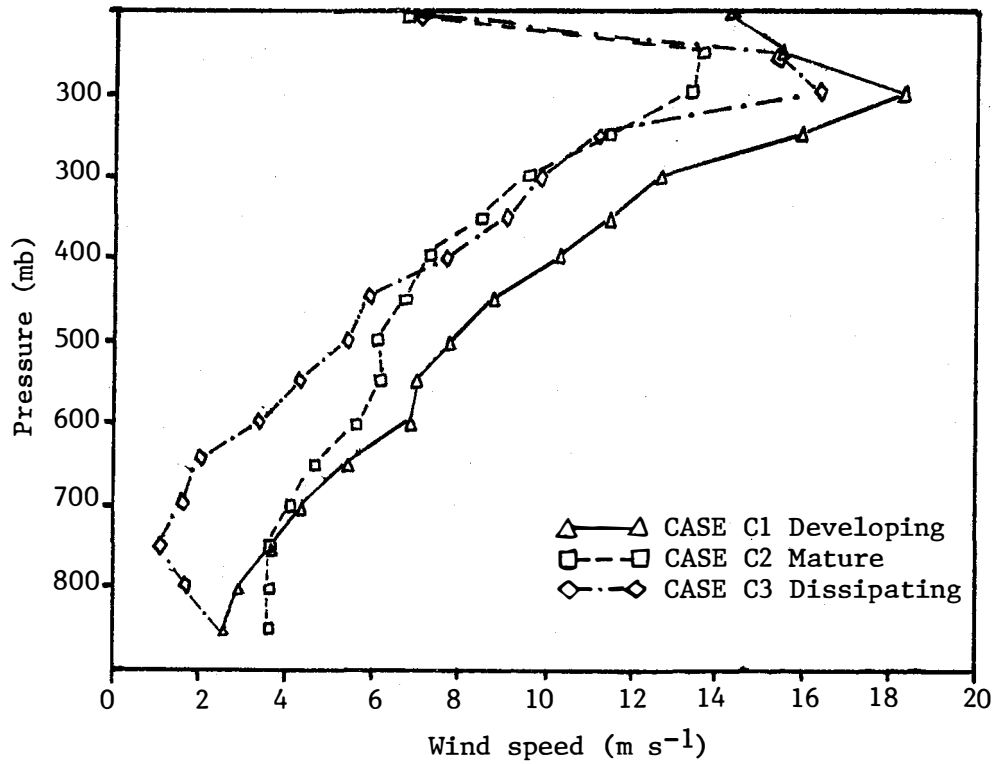


Fig. 6.11. Profiles of wind speed for the cluster classification.

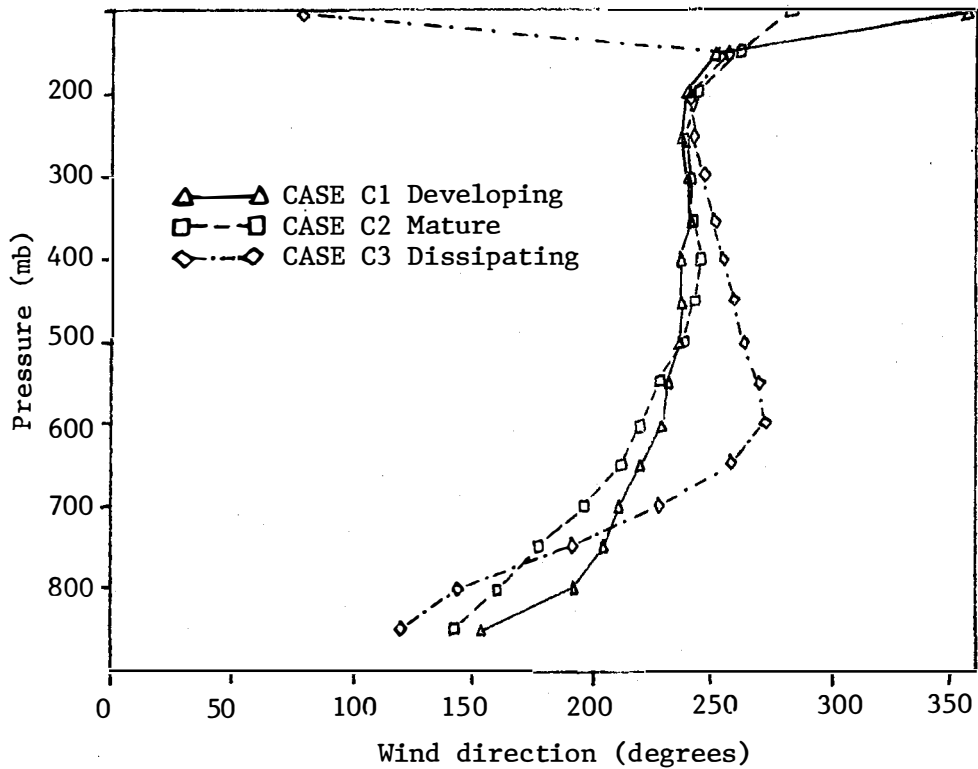


Fig. 6.12. Profiles of wind direction (from which wind is blowing) for the cluster classification.

implies a more easterly wind direction of between 15 and 40 degrees for cluster cases throughout the troposphere.

Because of the importance of large convective clusters as precipitation producers, the cluster cases were also stratified according to size, with roughly half of the cases classified as "big" and the other half classified as "small." Further, a subset of the big clusters, nine in number, were classified as "huge." It must be emphasized that, although these clusters are expected to provide a large amount of precipitation on the ground, precipitation was not analyzed, so no guarantee of their precipitation effectiveness is established.

The temperature and dewpoint soundings for the small, big, and huge cluster models appear in Figure 6.13. Only slight differences occur. Big convective clusters possess slightly higher dewpoints below 600 mb than small clusters. Between 500 and 200 mb, big clusters are drier than small clusters (both lower dewpoints and relative humidities). Around 800 mb and again around 600 mb, big clusters are slightly cooler than small clusters, but these differences are less than 1.5°C . The result of these differences leads to modest differences in the relative humidities of the two models. At 850 mb and at 600 mb the small clusters possessed about 5% less relative humidity than the big and huge clusters. It must be pointed out though the differences from case-to-case within a given model are much larger than this value. Thus, while the relative humidity provides a bias for or against more general or larger convection, it is by no means a controlling mechanism. It also must be emphasized that even though there are a large number of cluster cases, there are only 24 cluster days throughout the 3-year data set. Thus, the huge cluster model samples only nine cases over eight days.

Profiles of wind speed for the cluster classification are shown in Figure 6.14. Generally, the larger the cluster, the larger the wind speed, although the extreme differences are only about 4 m s^{-1} . The small cluster model is similar in profile to the no-convection model. An unusual result is that wind speeds for the huge cluster model are nearly as large as those for isolated convection. Wind directions are almost the same for the huge cluster and the big cluster model. The wind directions, Figure 6.15, for the small cluster model are similar to those for dissipating convection. Big clusters are biased very heavily towards the mature

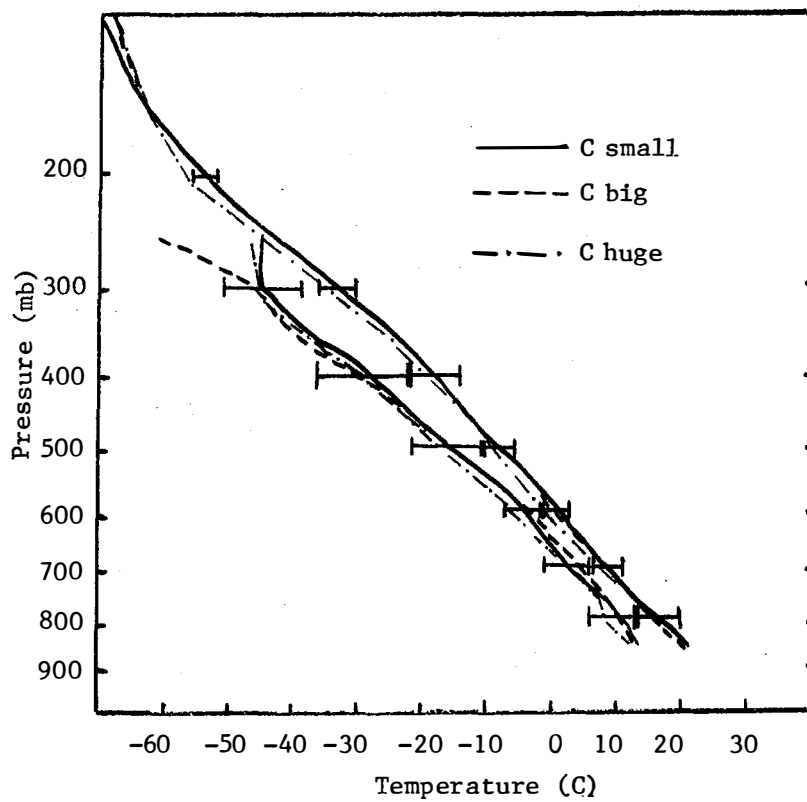


Fig. 6.13. Profiles of temperature and dewpoint temperature for the cluster classification. Standard deviation bars are for the Csmall profile.

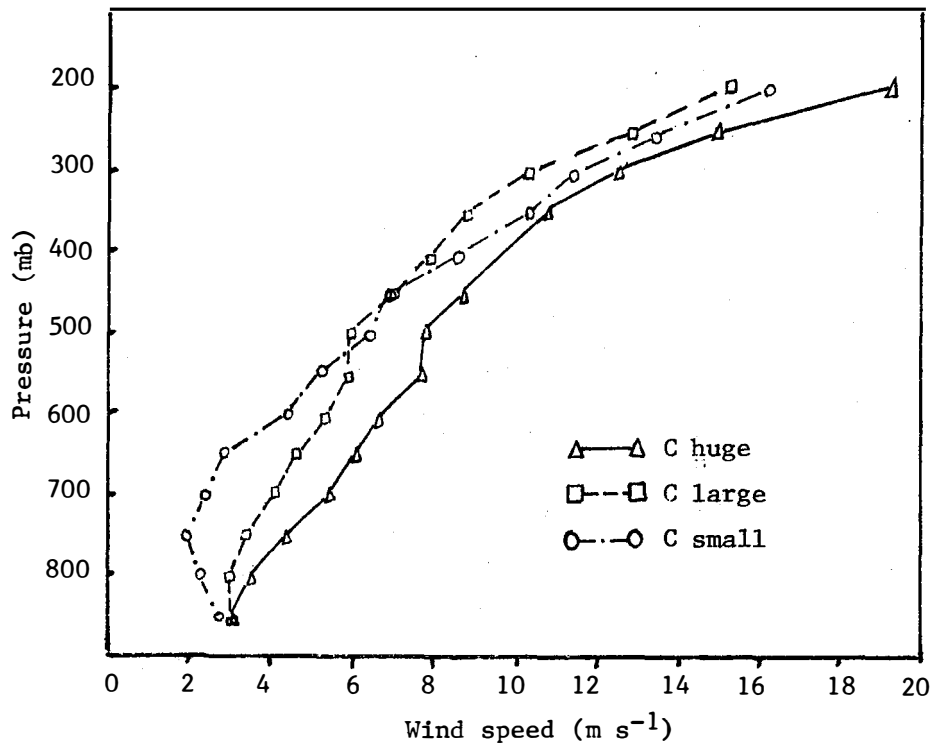


Fig. 6.14. Profiles of wind speed for the cluster classification.

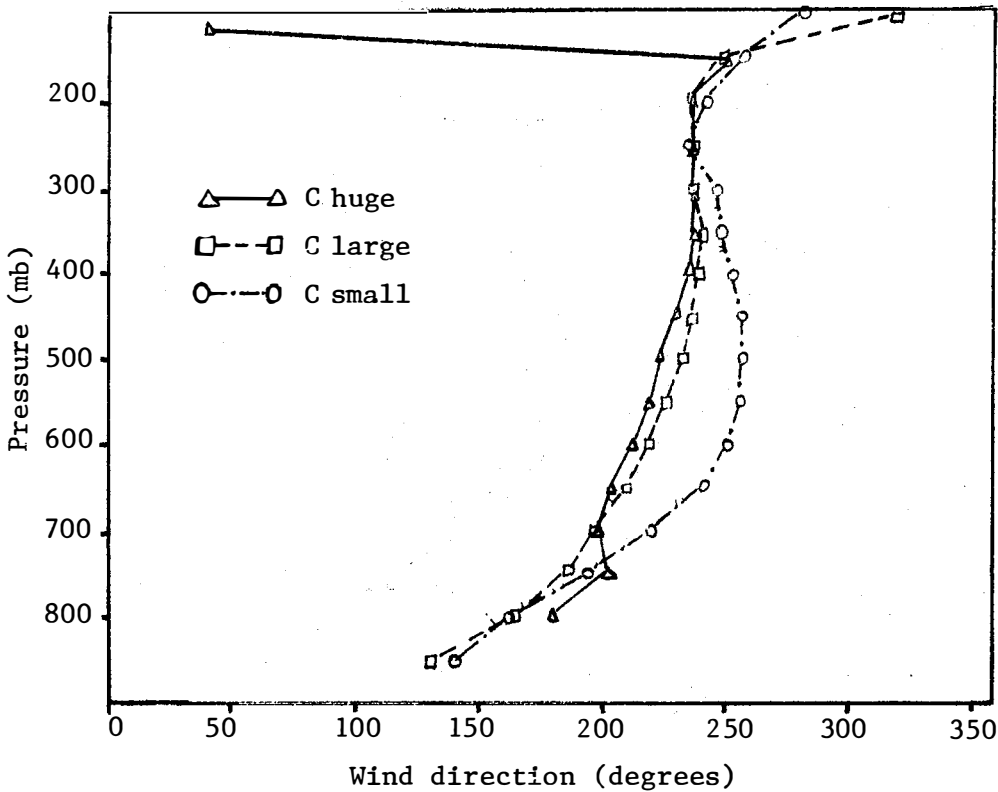


Fig. 6.15. Profiles of wind direction (from which the wind is blowing) for the cluster classification.

classification. In fact, the majority of the cases of big clusters are also mature clusters. Thus, it is not surprising that big cluster profiles should bear some resemblance to the mature model and the small convection should resemble dissipating cluster convection which, in turn, resembles the no-convection model. Two thirds of the huge cluster cases were also mature cases.

Finally, in an effort to examine the environments of big cluster cases independent of the mesoscale or thunderstorm scale circulation effects, the 1500 GMT soundings on all days in which big clusters were observed were composited. In a sense, this model describes the precursor environment preceding the development of big convective clusters. Temperature and dewpoint soundings for the precursor model are shown in Figure 6.16. Except for the weak diurnal heating below 800 mb in the precursor, the temperature profile is nearly identical to the big cluster model. At all elevations the precursor model possesses lower dewpoint temperatures. The most probable reason for the drier conditions is that the convection itself is responsible for moistening the mid troposphere, and before the

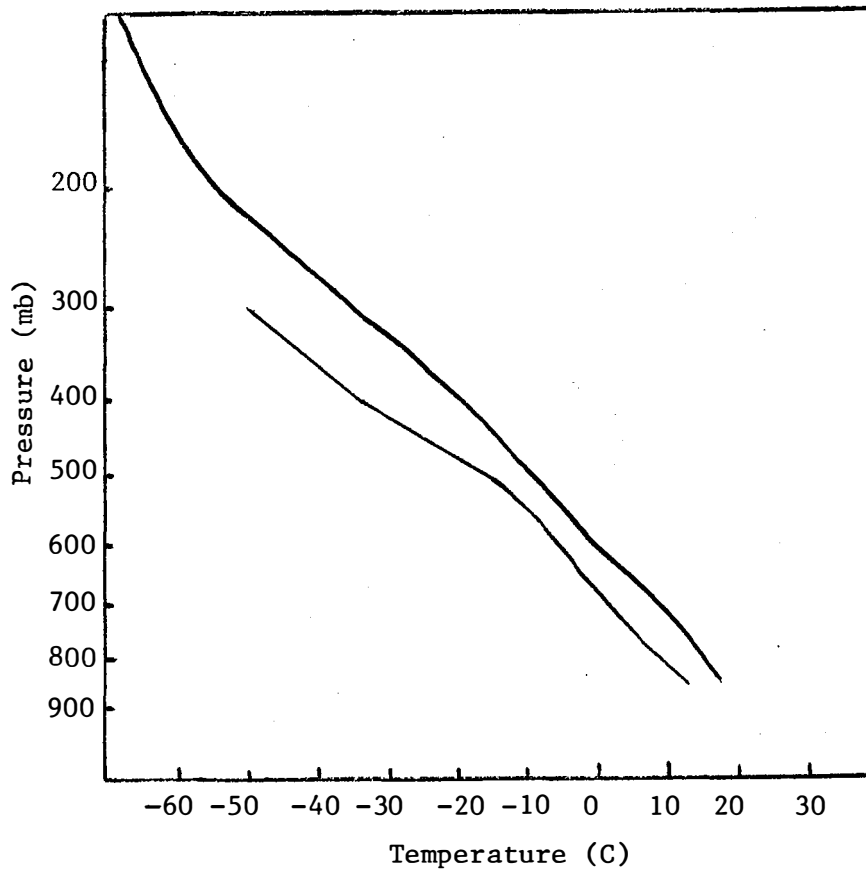


Fig. 6.16. Profiles of temperature and dewpoint temperature preceding the development of big convective clusters.

convection develops, the mid troposphere will be somewhat drier. The only differences in the precursor wind speeds is a relatively stronger wind at 850 and 800 mb; since these stronger winds are observed as diurnal variations in cases of no convection, they are assumed to be diurnally induced in this model as well. In a similar fashion, the low level wind direction is similar to the 1500 GMT no-convection case and is similar to the big cluster model at upper levels.

Line: Temperature and dewpoint profiles for the line classification are shown in Figure 6.17. Although the lapse rate is the same as that in other convective cases, temperatures are between 2 and 3.5°C colder than the less-organized convection throughout the troposphere. Major differences also occur in the dewpoint temperature as well. Below about 550 mb the dewpoint

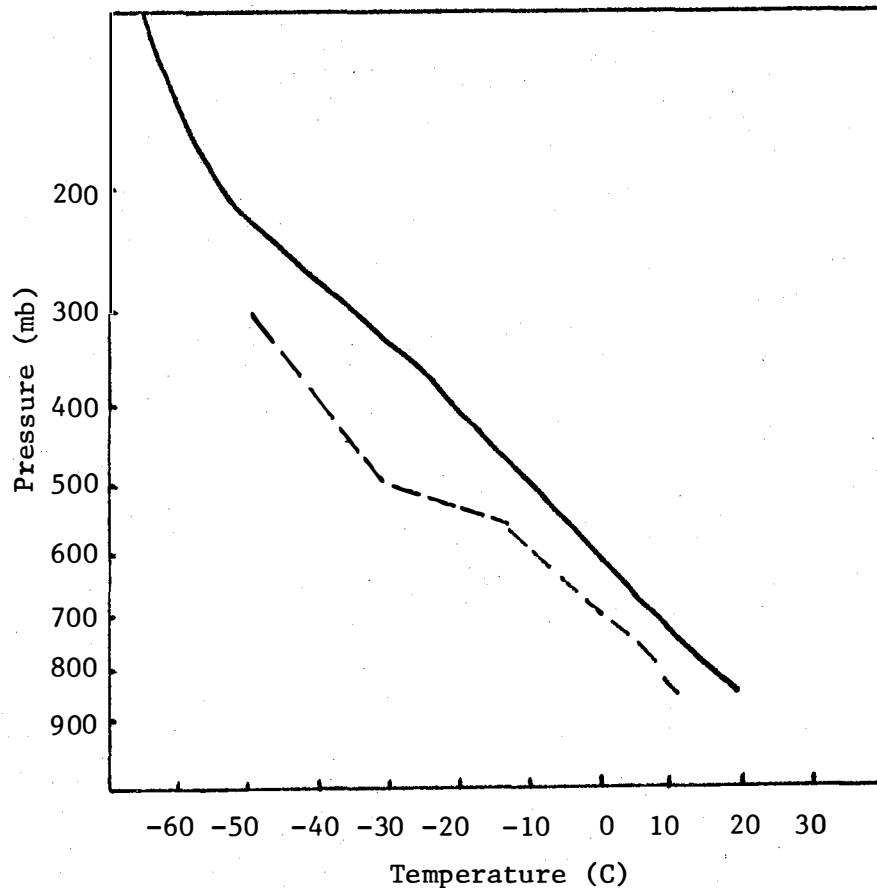


Fig. 6.17. Profiles of temperature and dewpoint temperature for the line classification.

temperatures are similar to those associated with isolated convection, thus being somewhat lower than those associated with clustered convection. However, because of the lower temperatures, the low-level relative humidity is the same as that for cluster models. Above 550 mb, however, line convection exhibits a significantly drier atmosphere. At most elevations, above 500 mb the dewpoint temperature is similar to that observed with no convection. At 500 mb, the line convection is drier than any other model. No speculation is made as to why the moisture distribution appears the way it does with line convection. However, if the convection is frontal or associated with a dry line, one might anticipate the existence of dry air somewhere in the domain.

The wind speed profiles for the line classification (Figure 6.18) also are different from other models, both in profile slope and magnitude. With line convection, two speed maxima are observed, one at 400 mb and the other between 100 and 200 mb at a level higher than the speed maxima of the other models. Below 400 mb the profile is similar to that of cluster convection, except that at most levels, the line convection speeds are much stronger. The wind direction (Figure 6.19) varies only weakly throughout the troposphere. In fact, the winds back with height slightly from 750 to 250 mb, the only model to do this. The low level winds possess a much stronger westerly component than any of the other models. These westerly winds are most likely indicative of a low-level front with more common occurrence of westerly or north-westerly winds at low levels.

6.3 Kinematic Models

One of the essential features needed for active convection, particularly intense clustered convection, seems to be upward vertical motion. Vertical motion profiles were available only for the 1978 HIPLEX season (Profiles for 1979 and 1980 are presented in Section 4 and in Appendix A). Therefore, the following results do not carry the confidence of the previously discussed models. Nevertheless, the results are essentially confirmed by the analysis of 1979 and 1980 cases. The convective classifications used are described in Section 5. Only a small random sample of cases was selected. The analysis of vertical motion incorporated 10 cases of no convection, 8 cases of isolated convection, 10 cases of small clusters, and 4 cases of large clusters. Convective lines were not analyzed.

Figures 6.21-6.24 show the calculated vertical profiles of the vertical velocity ($\mu\text{bars s}^{-1}$) stratified according to the intensity of convection as defined in Section 5. The heavy lines represent the class means; the error bars give the standard deviation within the class. Means and deviations for the large clusters (only 4 cases) were not computed. Additionally, the means and standard deviations for the small clusters were computed without using the profiles for 1800 GMT June 6 and 0000 GMT July 23. These two profiles were so different from the rest of the classification that they are probably storm-scale observations, and are thus unrepresentative of the prevailing environmental vertical motion.

These vertical motion profiles are slightly different than those computed by Sienkiewicz et al. (1980) for the same season. Their results

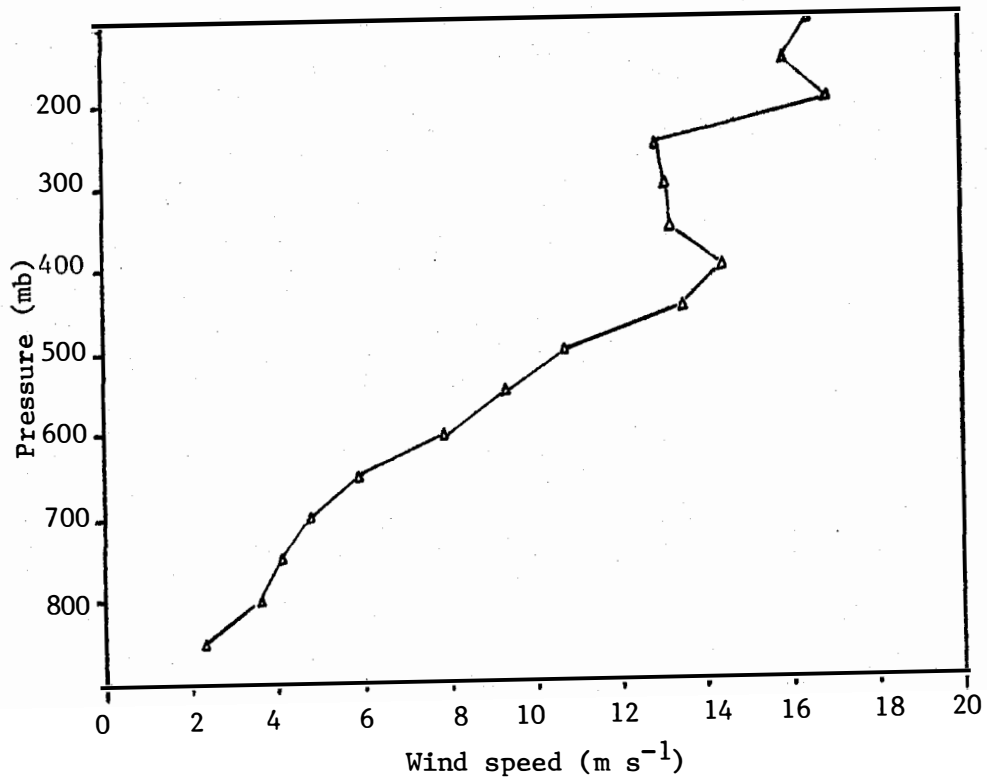


Fig. 6.18. Profile of wind speed for the line classification.

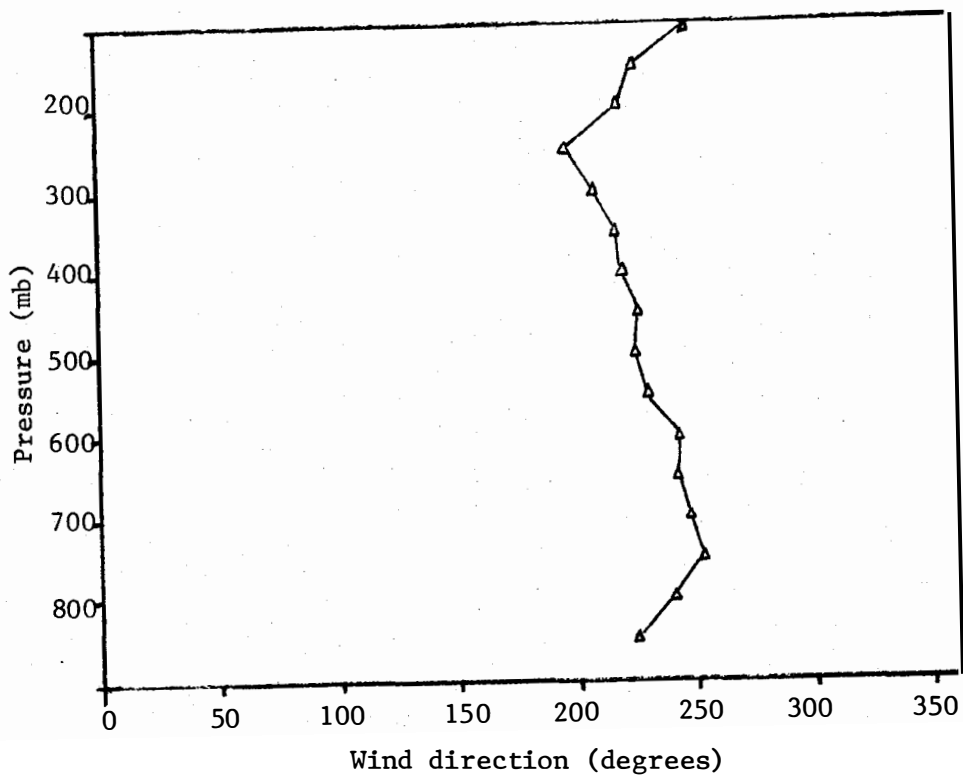


Fig. 6.19. Profile of wind direction (from which the wind is blowing) for the line classification.

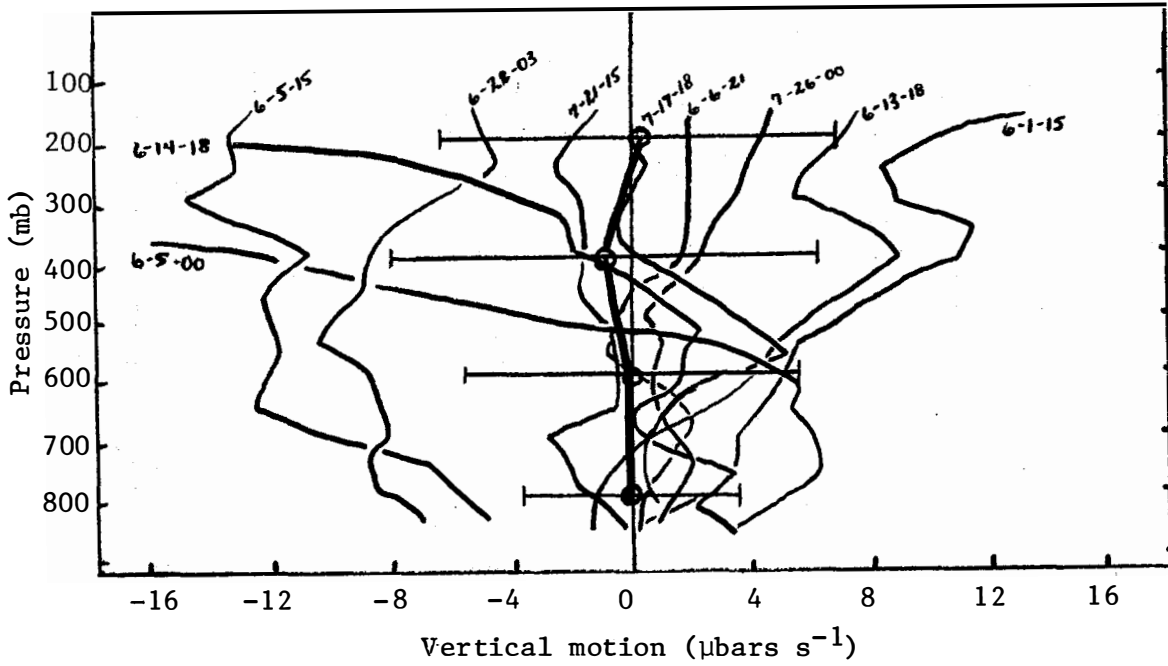


Fig. 6.21. Profiles and standard deviation of vertical motion for the no-convection classification based on 1978 data.

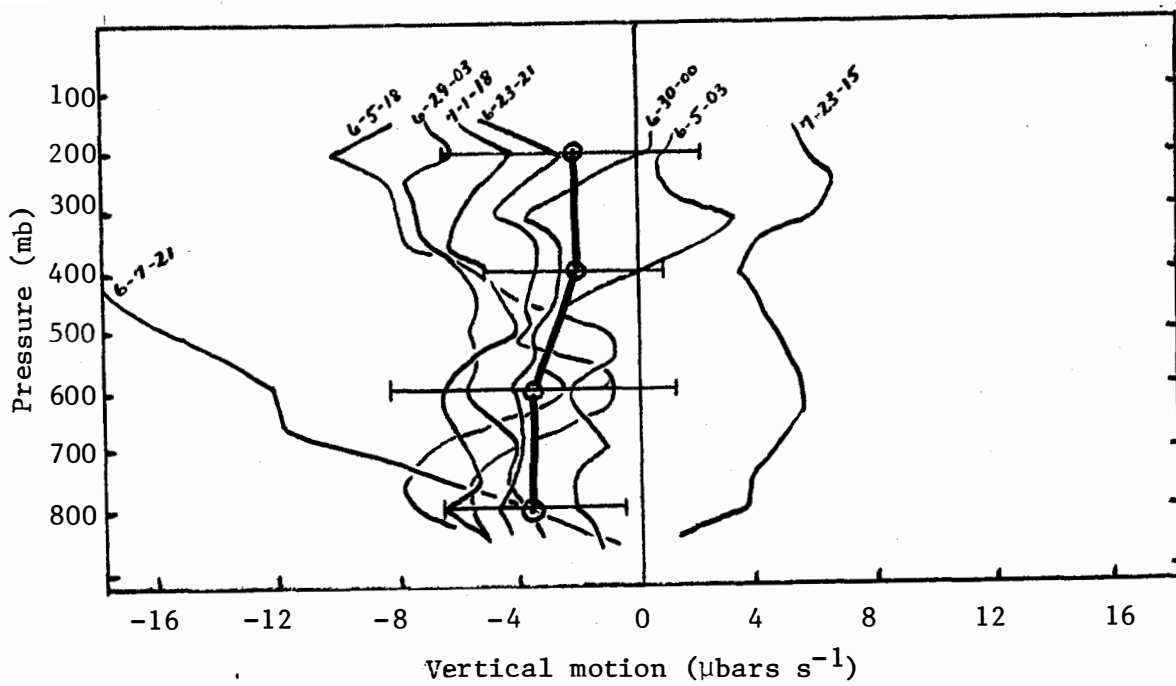


Fig. 6.22. Profiles and standard deviation of vertical motion for the isolated convection classification based on 1978 data.

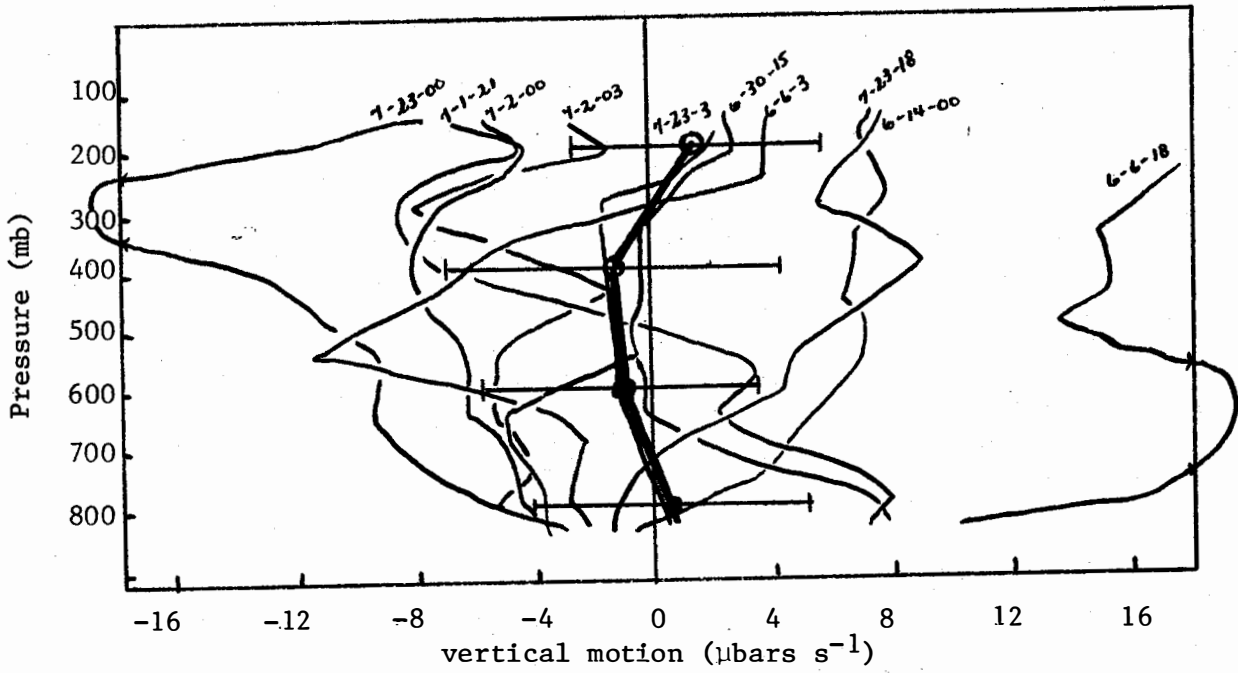


Fig. 6.23. Profiles and standard deviation of vertical motion for the small clusters classification based on 1978 data.

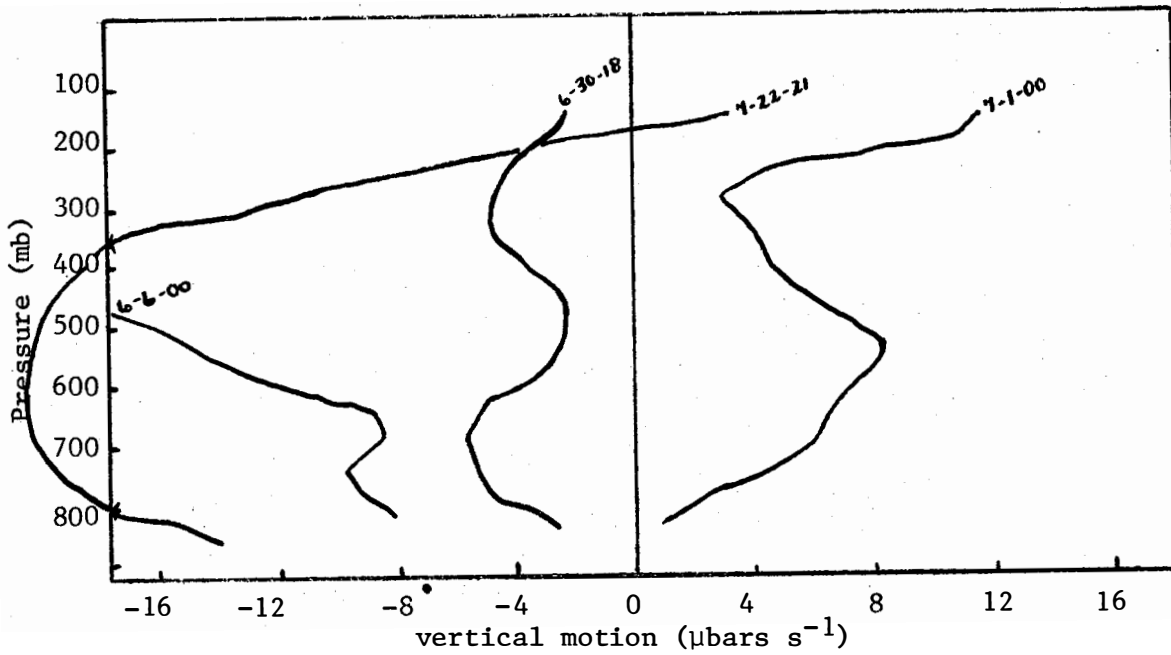


Fig. 6.24. Profiles of vertical motion for big clusters during 1978 season.

are based on all sounding times for the 1978 season. However, they did not stratify the convective cases according to type or strength of convective activity. Nevertheless, their convection case looks very similar to the isolated convection case shown in Figure 6.21. Additionally, their nonconvection class is defined somewhat differently than the no-convection class in this study. Their stratification excluded all radar echo cases, even those with echo tops which did not reach 6.1 km. These shallow convection cases were considered no-convection cases in the present study. Vertical motions for the Sienkiewicz non-convection model show weak rising motion at 850 mb (less than $2 \mu\text{bars s}^{-1}$) with decreasing rising motion up to zero values at about 250 mb. Figure 6.21 shows that non-convective vertical motions (including cases with shallow echoes) differ from those computed by Sienkiewicz *et al.* by only a small fraction of one standard deviation. On the other hand, Figure 6.21 shows that the distribution of vertical motion in the lower troposphere for individual cases is skewed, with moderate subsidence ($2-4 \mu\text{bars s}^{-1}$) normally observed below about 400 mb.

Immediately apparent in the figures is the very large standard deviation of the vertical velocity at all levels and for all classes. The spread is largest for the clustered convection, where the storm-scale circulation is more vigorous and covers a relatively large area, and also where no convection is present, representing subsiding motion or rising motion in the presence of dry or stable air masses. No-convection cases are marked by almost no average vertical motion. However, the distribution of individual cases is skewed, such that most days when no convection is occurring, weak subsidence is observed to occur below 400 mb all the way down to the boundary layer. For these cases the amplitude of the vertical motion seems to be nearly constant with height so that the atmosphere is nondivergent above the surface layer and below 400 mb. For two of the no-convection cases, large rising motion was observed. One of these cases (June 5) was an early morning sounding, and nine hours later a cluster, classified as huge, appeared over the HIPLEX area. The other case (June 28) was a situation of very dry surface air with surface mixing ratios generally below 10 gm kg^{-1} .

Isolated convection generally develops in a weakly rising air mass, with typical vertical motions of slightly less than $2 \mu\text{bars s}^{-1}$ from 800 mb all the way up to 200 mb (Figure 6.22). Only a single case of

isolated convection occurred in generally subsiding air. Also, only a single case of isolated convection was observed when tropospheric rising motion exceeded $4 \mu\text{bars s}^{-1}$. Still, with the large scatter of data in both the no convection and isolated convection models, statistical verification of the differences between the two models is weak. Based on a t-test, these two vertical motion profiles can be asserted to be different only with a confidence of about 85%.

Vertical motion for both the small and large clusters show tremendous variability (Figures 6.23 and 6.24). The class mean for small clusters is nearly zero, with several observations of both large rising and large sinking motions. Since large rising motion should be associated with extensive thunderstorm development, the incidences of subsiding vertical motion with clusters must be assumed to sample the meso-circulation associated with these storms. For some of the events, the HIPLEX region defined by the Midland-Post-Robert Lee triangle must be dominated by subsidence associated with the strong storm downdraft. For example, it seems hard to comprehend a cluster developing in an $8 \mu\text{bar s}^{-1}$ subsidence region as the one on June 6 seemingly did. The atmosphere eighteen hours earlier in this day was also experiencing a cluster case, and the atmosphere at this time was undergoing $2-4 \mu\text{bars s}^{-1}$ rising motion. The conclusion is that vertical motion profiles measured on the temporal and spatial scales of HIPLEX and in the presence of active convection represent some complicated mixture of storm and environmental vertical motions.

To examine some of these temporal and spatial scales more closely, composite profiles of the average and standard deviation of each variable for each classification described in Section 5 were prepared from the profile data presented in Section 4 and Appendix A for 1979 and 1980 data. The composite averages for four pressure levels shown in Table 6.1 and Figures 6.25-6.29 represent spatial variations across the HIPLEX area. These results reveal significant differences in both the average profiles and the deviations from these averages.

Before enumerating some of the significant differences between categories the interpretation of the information for each variable will be discussed. The average profile given by the solid line in each figure represents the average value of that variable over the Texas HIPLEX mesoscale area as a function of pressure for all cases listed in Table 6.1 for the convective category represented. The dashed lines

Table 6.1. Composite averages of the average and standard deviation of each variable for each convective classification. The averages were computed from similar data presented in the Appendix for each date and time. The average is on the left and the standard deviation on the right of the diagonal.

	<u>Divergence (10^{-5} s^{-1})</u>				<u>Moisture Divergence (10^{-7} s^{-1})</u>			
	800	700	500	300	800	700	500	300
Widespread Echoes	0.2/3.6	0.6/3.6	-0.1/3.3	-1.1/3.9	0/3.9	0.8/1.9	0.2/1.4	0/3.2
No Echoes	-0.09/3.6	1.1/3.1	0.5/3.4	0.7/3.9	0.3/3.3	0.9/2.5	0.5/1.4	0.1/0.2
Isolated	-0.4/5.1	0/5.0	1.7/6.0	2.9/5.1	0.8/5.7	0.7/3.5	1.0/2.3	0.1/0.2
Convective Complex	-1.5/6.0	1.0/6.7	1.0/5.0	1.7/4.2	-0.7/6.3	0.5/5.2	0.5/2.3	-0.3/0.3

	<u>Vertical Velocity ($\mu\text{bar s}^{-1}$)</u>				<u>Vertical Moisture Flux ($10^{-5} \text{ g cm}^{-2} \text{ s}^{-1}$)</u>			
	800	700	500	300	800	700	500	300
Widespread Echoes	0/3.2	0.5/5.3	0.7/6.1	0/6.4	-0.1/2.6	0.7/3.1	0.4/1.7	-0.1/0.4
No Echoes	-0.9/4.1	0.04/4.9	0.6/6.1	0.9/7.1	-0.9/3.2	-0.1/3.1	0.2/1.2	0.08/0.2
Isolated	-0.2/5.3	-0.5/6.0	0.6/11.6	3.9/13.4	-0.1/3.8	0/4.6	0.1/3.5	0.1/0.5
Convective Complex	-4.4/5.6	-4.6/6.6	-1.8/9.3	0.6/9.6	-4.2/5.0	-2.9/5.6	-0.7/4	0/13

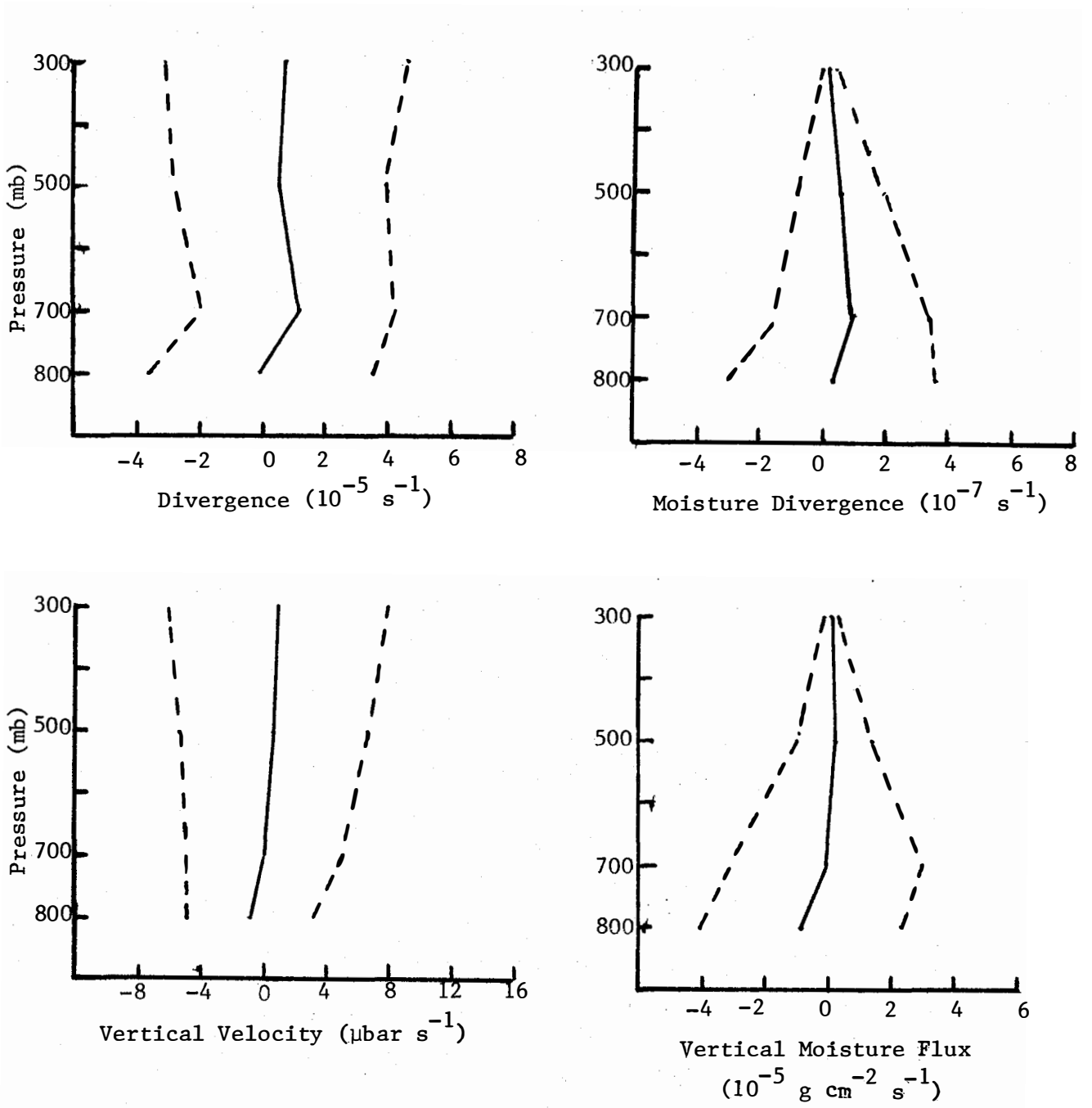


Fig. 6.25. Composite average and standard deviation profiles when no echoes were present.

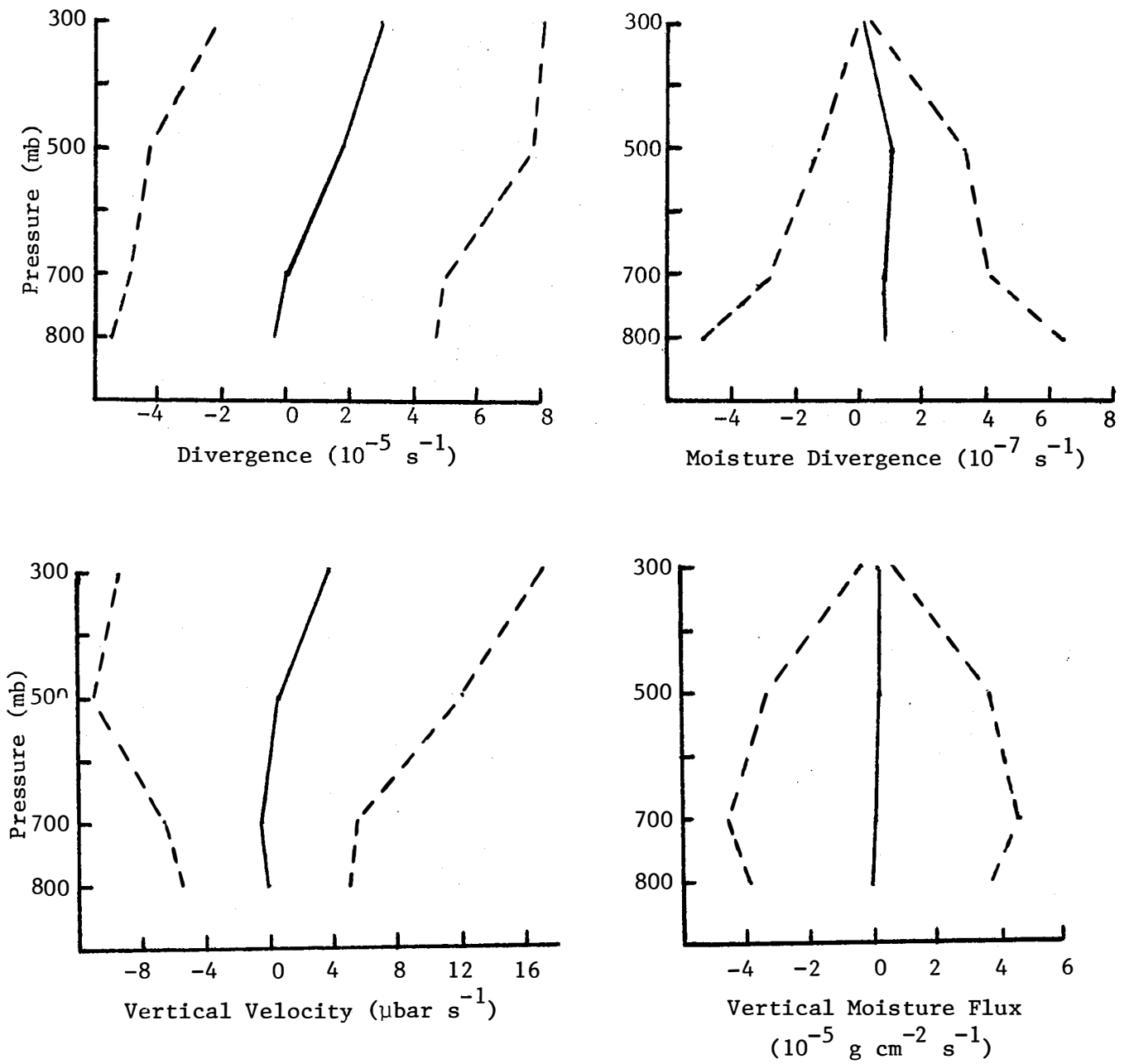


Fig. 6.26. Composite average and standard deviation profiles when isolated cells were present.

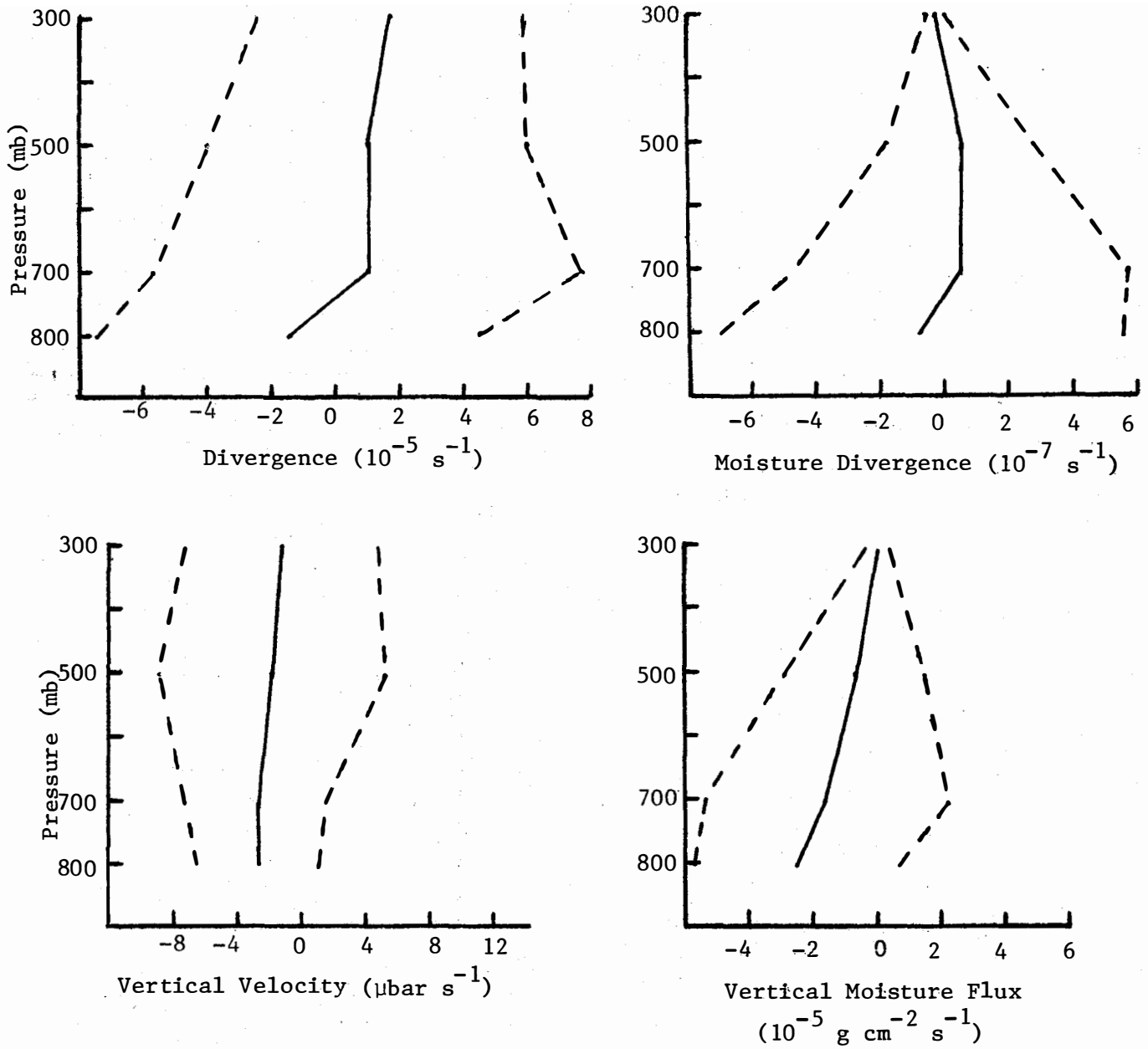


Fig. 6.27. Composite average and standard deviation profiles when clusters of convective cells were present.

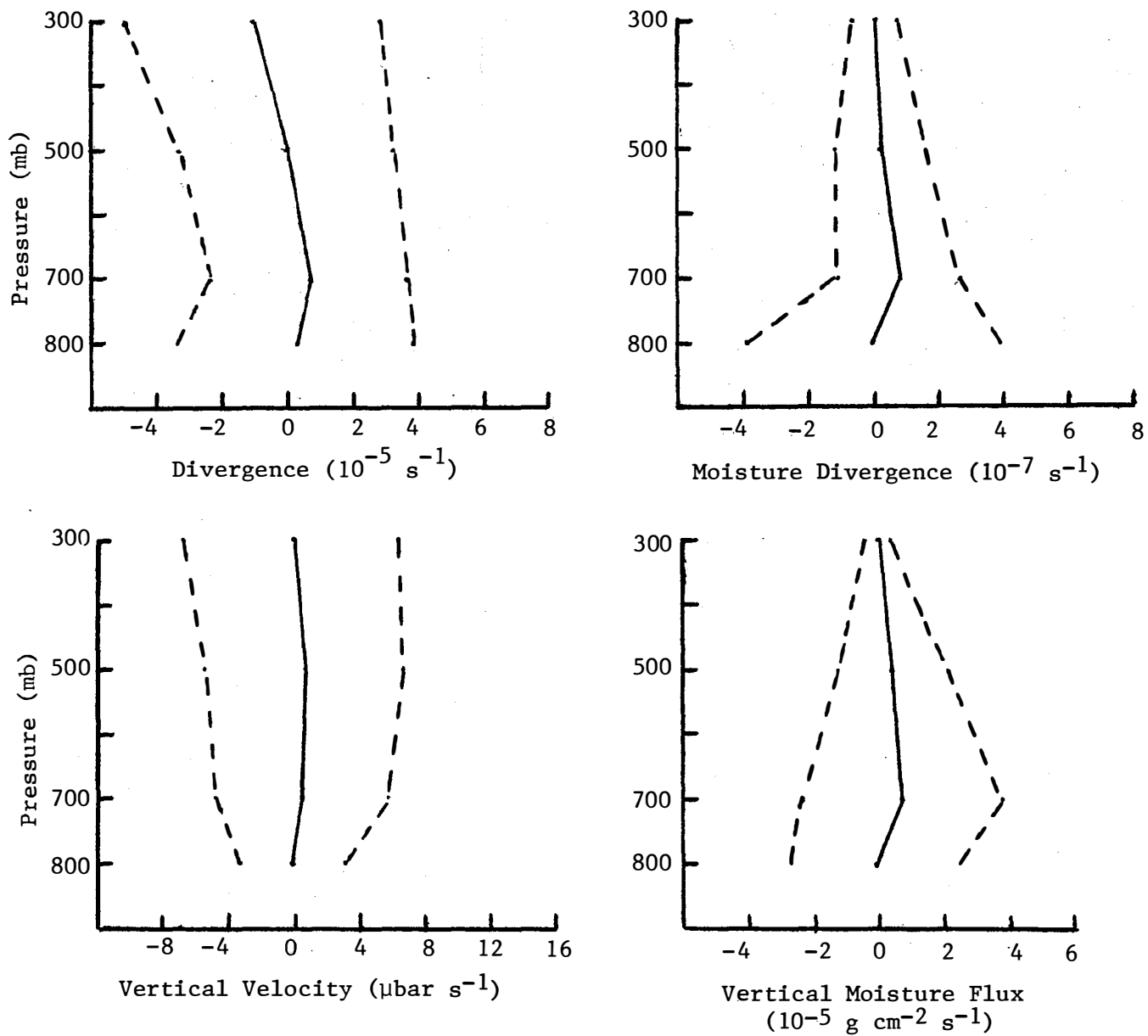


Fig. 6.28. Composite average and standard deviation profiles when widespread echoes were present.

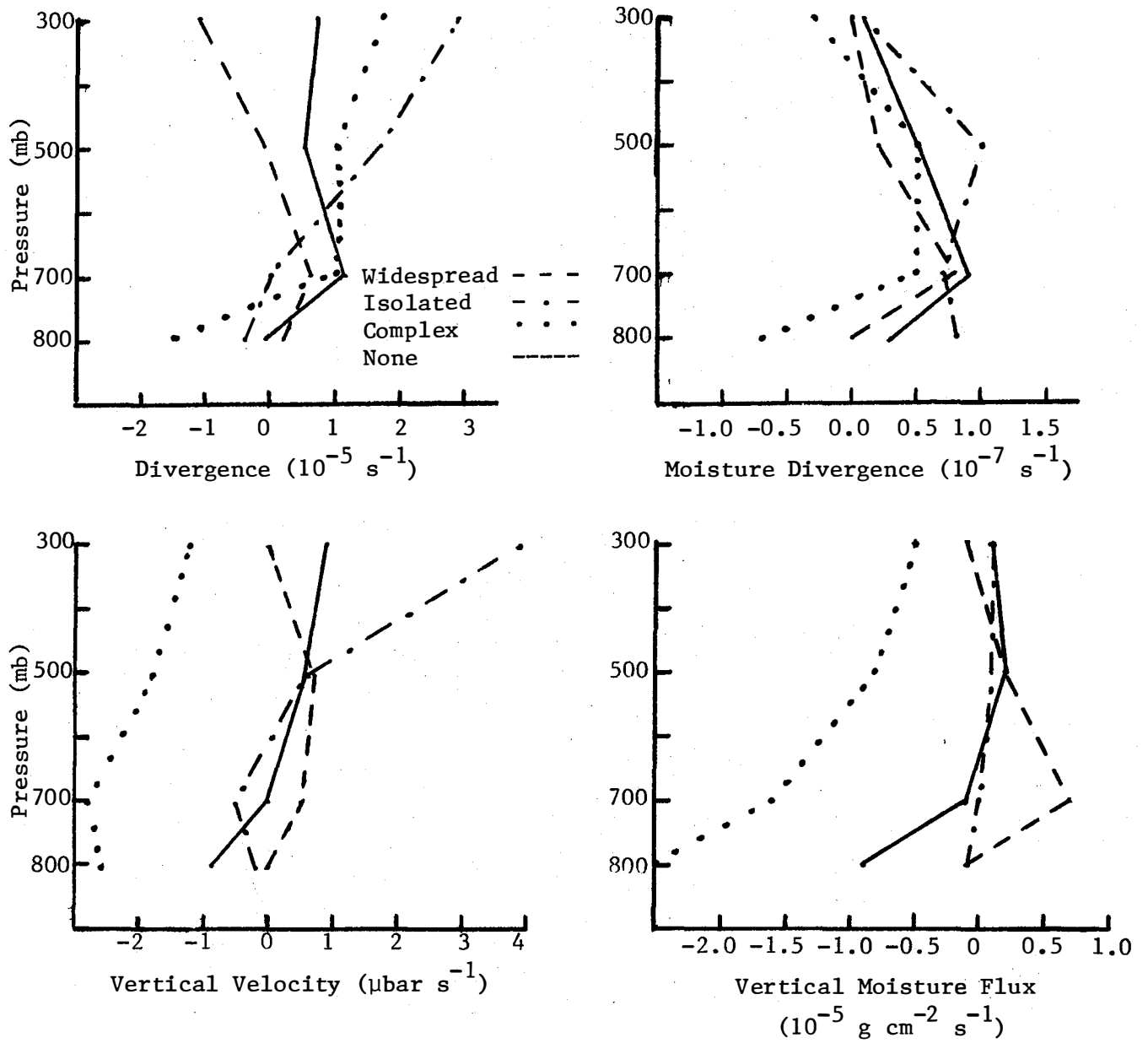


Fig. 6.29. Comparison of composite average profiles for various categories of convective activity.

represent the variation of that variable across the Texas HIPLEX mesoscale area computed from the average profiles for the defined areas presented in Appendix A. A large part of the variation results from the convective activity. Thus, the profiles presented in Figures 6.25-6.28 represent for each convective category the average values of each variable and of the standard deviation of that variable. The standard deviation is plotted on each side of the mean profile in order to give a better visual representation of the variation on each variable across the network.

No attempt will be made to describe in detail all of the differences between convective categories that are shown in the figures. However, a few of the differences are listed below.

Velocity Divergence: Average profiles of velocity divergence vary considerably with convective classification as shown in the figures. Variation with altitude is considerably greater when isolated cells or convective complexes are present than for the other classifications. The profiles indicate that across the mesoscale network rather strong divergence or convergence can occur simultaneously through virtually the entire layer below 300 mb. The average profiles in Figure 6.29 indicate that when an isolated cell or convective complex is present over the network the convergence is stronger below 700 mb, and divergence is stronger above this level than for the other convective classifications.

Moisture Divergence: Profiles of moisture divergence for no echoes and widespread echoes are similar, but the standard deviation for isolated cells and convective complex categories are much larger than for the other categories. The average profiles shown in Figure 6.29 indicate strong moisture convergence below 700 mb for the convective complex category, and slight divergence for all categories above 700 mb. However, Figures 6.25-6.28 show that within the Texas HIPLEX mesoscale area there are regions of strong moisture convergence, particularly in the lower levels, that extend through a deep layer. It is these regions which provide the energy source for the convective activity.

Vertical Velocity: The average profiles of vertical velocity presented in Figure 6.29 show very significant differences between convective categories. The convective complex category indicates average upward vertical velocity at all levels below 300 mb, while the isolated cell

category indicates slight vertical motion below approximately 600 mb. It is interesting that the no-echo category indicates slight upward vertical motion below 700 mb. In all except the convective complex category average downward vertical motion is indicated above approximately 600 mb. However, as shown in Figures 6.25-6.28, areas with strong vertical motion occur within the mesoscale network.

Vertical Moisture Flux: From Figure 6.29 it is clear that large differences in vertical moisture flux occur between categories. The average profile for convective complexes indicates a large vertical moisture flux at all levels below 300 mb, while the other categories, except for no cells below 700 mb, indicate a near zero vertical flux of moisture. Again, profiles of the standard deviation indicate strong regions of vertical moisture flux within the mesoscale area as well as strong regions with downward flux. Variations in the vertical flux of moisture across the network appear to be greater when isolated cells are present than for any other convective category.

The results presented above demonstrate the complex nature of mesoscale systems accompanying convective activity. Within the Texas HIPLEX mesoscale area quite intense mesoscale systems coexist which can either lead to the development or destruction of convective activity. With these large variations present, it is difficult to determine where and when convective activity will form, but with the results presented above one can understand and appreciate factors responsible for the formation of convective activity and the complex nature of mesoscale systems.

6.4 Comparison of Models of Vertical Motion

One of the problems encountered in the models presented above is: Given the general mesoscale variability of all atmospheric parameters, how can one examine a given day and time, and assign the convection which will soon evolve into one of the convective classifications already described? The variability of cases within a single classification is so large that a given case could equally well fit within the natural variability of more than one case.

One way to resolved this problem is an intercomparision of the temporal variability of a set of cases within a given classification with the areal variability of a "typical" case across the HIPLEX grid. The models represent snapshots of a certain type of convection without reference

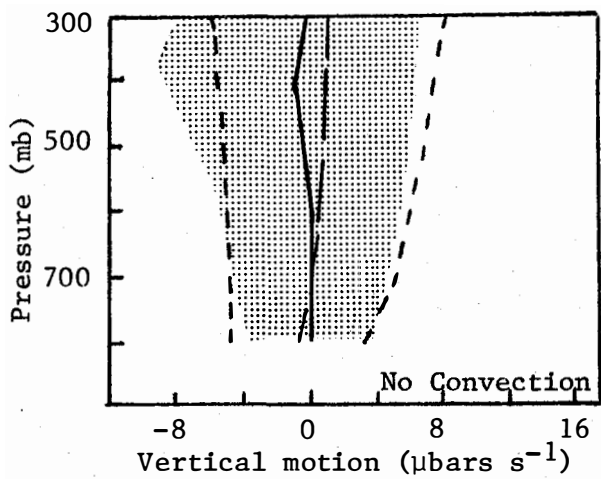
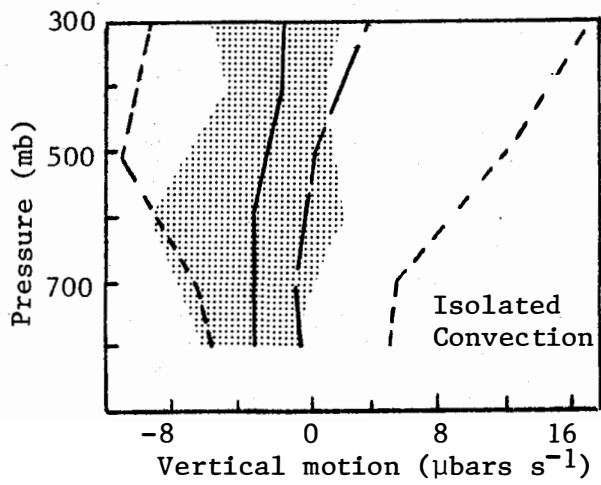
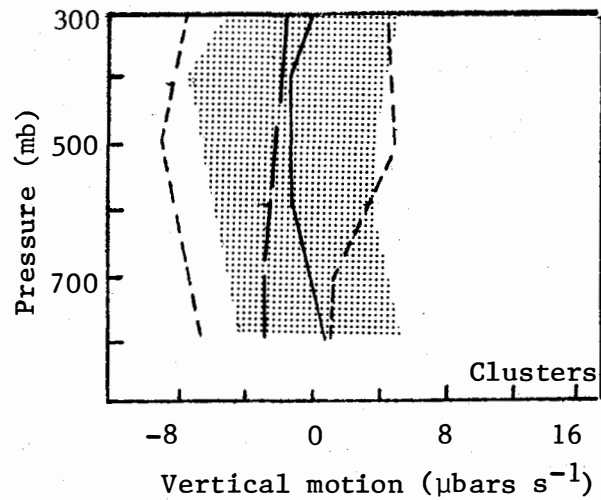
to where the active cells occur in the grid. Thus the standard deviations within these models represent a combination of the variation which may be expected from case to case (each isolated cell, for example, is slightly different from every other isolated cell), and also some component of the areal variation (in certain cases, for example, the downdraft may be located on the edge of the HIPLEX grid, whereas in other cases the downdraft may be well-centered in the grid). However, this variability is that which would most likely be detected in any verification experiment or operational program for cloud seeding.

Contrasted with this variability are the calculations presented in Section 4, in which the areal resolution was fine enough to identify variability due to the mesoscale circulation across the grid. Areas of subsidence could generally be separated and analyzed separately from areas of strong rising motion.

To facilitate the comparison of these two analyses of vertical motion, figures are redrawn in simplified form in Figure 6.30. In this figure the shaded areas represent primarily the temporal variability as depicted in Figures 6.21-6.24; the dashed lines represent the standard deviation of spatial variability within a typical convective case (Figures 6.25-6.28). This interpretation is a simplification of the actual analysis, but it should be fairly realistic. Before discussing the results, it is important to understand the differences in the separate analyses, since they are not identical.

The analysis of temporal variability is based on three soundings. The profiles of vertical motion begin with a surface network of many stations, upon which the boundary layer vertical motion and divergence is based. On the other hand, the boundary layer parameters used in the areally-differentiated computations are extrapolated downward from 850 mb. Both procedures are considered to be of equivalent accuracy and, in the case of convection to be equally representative; but they are nevertheless slightly different.

Both analyses suffer somewhat from a lack of a large number of cases. The temporal variability classifications each encompass about 10 cases. The spatial variability classifications of convection are limited to ten or less cases. Several of these cases are taken from the same day so that independence of cases is not guaranteed. Even though there are 28 cases of no convection, convection developed on the same day on all but four



Legend

- Solid line: 1978 Mean data
- Shaded area: 1978 Standard Deviation
- Large dashed line: 1979-80 Mean data
- Small dashed line: 1979-80 Standard Deviation

Fig. 6.30. Comparison of vertical motion models.

of the days. Thus, on about half of the days the observed mesoscale circulations may be representative of incipient or dissipating convective systems.

Figure 6.30 shows that mean tropospheric vertical motion increases as the level of convection increases at least insofar as the 1979 and 1980 data show. The 1978 data (heavy lines) show that small clusters average slightly weaker vertical motion than do cases of isolated convection. Based on the shaded regions, this difference could easily fall within the sampling uncertainty within the sample of cases.

The mean vertical motion when no convection is present is almost identical for 1978 and 1979-80 cases. The mean motion for isolated convection contains a systematic discrepancy of about $3 \mu\text{bars s}^{-1}$ with the 1978 data showing much stronger rising motion. There is no apparent reason besides sampling differences for the discrepancy; the difference between the two profiles is within one standard deviation below 400 mb. It is worth noting that the 1979-80 record contains observations for only five days of isolated convection and the 1978 record contains only six days. Finally, for the case of clusters, or multiple-cell convection, the 1979-80 cases average about $2 \mu\text{bars s}^{-1}$ stronger than the 1978 cases. The probable reason for this is that the 1978 stratification excludes large clusters. If the proper sampling of large clusters were incorporated into Figure 6.30, the vertical motion would most likely have been comparable to the more recent sampling.

Even more interesting than the mean vertical motion profiles are the deviations and differences of the profiles. For no convection, the dashed lines approximate the differences across the sounding network on a typical non-convective day. Thus, even when no echoes are present, there are still occurrences of vigorous mesoscale circulations. The left-hand-side dashed line represents regions of strong updraft, sometimes reaching values of $5-6 \mu\text{bars s}^{-1}$ upwards; the right-hand-side dashed line represents maximum mesoscale subsiding regions, also reaching $5-6 \mu\text{bars s}^{-1}$. In the case of no convection, these extremes in mesoscale motions closely approximate the standard deviation of vertical motion, computed as a deviation from case-to-case (the shaded area). Thus, one can conclude that, in the case of no convection, the day-to-day variability in the computed large scale vertical motion (1978 data) is largely a consequence of how the large scale grid samples the dry mesoscale circulations. If a subsiding cell is close

to one of the stations, the vertical motions will be strong and subsiding; the farther this subsiding cell is located from sounding stations, the weaker the computed large-scale subsidence. As an average, the net vertical motion on these days will be close to zero.

This consistency of data sets is not observed in the case of isolated convection. The extremes of the mesoscale motions determined from the 1979-80 data set are much larger than the temporal standard deviations. In this comparison, the intensity of the mesoscale circulation is of such a small scale that it does not normally have a large effect on the day-to-day variability of typical isolated convection days. In the vicinity of these isolated cells, however, the upward and downward motions can possess much larger amplitudes than those typically observed by the large scale network. In fact, subsidence in these systems may become three standard deviations larger than the mean large scale vertical motions. The implication of this result is that vertical motions alone may enable one to identify isolated thunderstorms and the regions in which they form. This conclusion is most accurate if the isolated cells develop close to sounding stations or if the sounding network is somewhat expanded, as it was in the 1979 and 1980 HIPLEX seasons. The importance of vertical motion in the formation of convective activity has been demonstrated by Matthews (1981).

Finally, similar conclusions can be drawn for clusters of multiple cell systems. In these systems, the extremes of vertical motion are smaller than in the case of isolated convection. The reason for this discrepancy is uncertain, although it could be related to the much larger scale of the mesoscale motions compared to those of isolated systems. Whatever the reason the regions of upward vertical motion in these systems typically average $8 \mu\text{bars s}^{-1}$ which is approximately 1.5 standard deviations more than the large-scale mean vertical motion. Thus, if these typical vertical motions are observed with a network like that of 1979-80 grid resolution, then most of these cases could be distinguished from weaker convective and non-convective days.

7. SUMMARY AND RECOMMENDATIONS

The mesoscale and environmental models presented in this report represent a first attempt to assimilate the vast amount of available information into composite forms. The approach taken was based on the concept of utilizing all available results in order to increase the sample size. The models are formulated on the basis of statistical concepts with the full realization that the data samples were too small, and that results for the years 1976, 1977, and 1978 when data from four rawinsonde stations were available is not strictly compatible with results for 1979 and 1980 when data from seven rawinsonde stations were available. However, the approach in formulating the models was designed to make maximum use of both types of data to specify variations in the mesoscale environment associated with various classifications of convective storms. The models are of two types: one represents the mesoscale environment for various classifications of convective activity, while the other represents spatial variations for each classification. The models themselves are not representative of conditions at any given time but rather show average conditions and the expected variability.

In the development of the models each variable was considered independently of every other variable. A multiple variable approach no doubt would have been better in which intervariable dependency was considered. Also, the data could have been stratified in different ways and models derived which would have been more easily interpretable in terms of seeding effects. However, the scope of the present research was limited by a lack of funds and did not include these approaches.

A summary of numerical and semi-quantitative models appearing in the literature was made for two purposes. One was to examine methods of presentation of results for use as a guide in presenting the models derived in this study, and the other was to examine results from models in an attempt to identify one model that might be considered best for the Texas HIPLEX area. Methods used by previous authors to present model results and consideration of the objectives of the Texas HIPLEX program lead the authors to formulate the methods used to present the models in this research. However, the literature survey did not reveal any specific existing model which appears to be best for the Texas HIPLEX area. It appears that mesoscale numerical models appropriate for scales between 20 and 200 kilometers (scales of interest in the Texas HIPLEX area) are inadequate.

Results of the case studies presented in this report, as well as the models for various classifications of convective activity, are listed below:

1. The mesoscale processes, as described in the seeding hypothesis chain of events, are present in West Texas convective activity.
2. The chain of events presented in the seeding hypothesis suggest that appropriate mesoscale response variables are horizontal moisture flux, subcloud convergence, vigorous downdrafts, vertical motion, and vertical transport of moisture in the mid-troposphere. This study supports this choice of mesoscale response variables. Based on both the case studies and the models, it appears that vertical motion is the response variable most likely to be measured in response to seeding from the 7-station sounding network, although the others may also be measured.
3. Because of the limitations of the models developed in this study, it is not possible to confirm that seeding a cloud with silver iodide will amplify the mesoscale processes to the extent that they will exceed the natural variability.

In summary, neither the case studies nor the models presented in this report suggest a change in the seeding hypothesis developed previously for the Texas HIPLEX area.

It could turn out that seeding effects in individual cases could be detected in all the mesoscale processes included in the seeding hypothesis. A theoretical study of dynamical seeding effects in individual convective clouds, given the natural variability presented in this report, would help to resolve this question.

8. REFERENCES

- Anthes, Richard A., 1974: Data assimilation and initialization of hurricane prediction models. J. Atmos. Sci., 31, 702-719.
- Anthes, Richard A., and Thomas T. Warner, 1978: Development of hydrodynamic models suitable for air pollution and other mesometeorological studies. Mon. Wea. Rev., 106, 1045-1078.
- Ballentine, R. J., 1980: A numerical investigation of New England coastal frontogenesis. Mon. Wea. Rev., 108, 1479-1497.
- Barnes, Stanley L., 1964: A technique for maximizing details in numerical weather map analysis. J. Appl. Meteorol., 3, 396-409.
- Bergthorsson, P., and B. Döös, 1955: Numerical weather map analysis. Tellus, 7, 329-340
- Blackadar, Alfred K., 1979: High-resolution models of the planetary boundary layer. Adv. Envir. Sci. Eng., 1, 50-85.
- Bleck, Rainer, 1975: An economical approach to the use wind data in the optimum interpolation of geo- and Montgomery potential fields. Mon. Wea. Rev., 103, 807-816.
- _____, 1978: On the use of hybrid vertical coordinates in numerical weather prediction models. Mon. Wea. Rev., 106, 1233-1244.
- Bosart, Lance F., 1981: The President's Day Snowstorm of 18-19 February 1979: a subsynoptic-scale event. Mon. Wea. Rev., 109, 1542-1566.
- Carbone, Richard E., 1982: A severe frontal rainband. Part I: Stormwide hydrodynamic structure. J. Atmos. Sci., 39, 258-279.
- Chang, C. B., D. J. Perkey and C. W. Kreitzberg, 1981: A numerical study of the squall line of 6 May 1975. J. Atmos. Sci., 38, 1601-1615.
- Cotton, W. R., R. L. George and K. R. Knupp, 1982: An intense, quasi-steady thunderstorm over mountainous terrain. Part I: evolution of storm-initiating mesoscale circulation. J. Atmos. Sci., 39, 328-342.
- Doswell, Charles A. III, 1980: Synoptic-scale environments associated with High Plains severe thunderstorms. Bull. Amer. Meteor. Soc., 61, 1388-1400.
- Friend, Arnold L., Dusan Djuric and Kenneth C. Brundidge, 1977: A combination of isentropic and sigma coordinates in numerical weather prediction. Beitr. Phys. Atmosph., 50, 290-295.
- Fritsch, J. M., and C. F. Chappell, 1980: Numerical prediction of convectively driven mesoscale pressure systems. Part II: Mesoscale model. J. Atmos. Sci., 37, 1734-1762.
- Fuelberg, Henry E., and James R. Scoggins, 1980: Kinetic energy budgets during the life cycle of intense convective activity. Mon. Wea. Rev., 106, 637-653.
- _____, and _____, 1980: Kinetic energy budget during strong jet stream activity over the eastern United States. Mon. Wea. Rev., 108, 69-77.
- Fujita, T. Theodore, and Roger M. Wakimoto, 1981: Five scales of airflow associated with a series of downbursts on 16 July 1980. Mon. Wea. Rev., 109, 1438-1456.
- Gandin, Lev S., 1963: Objective analysis of meteorological fields. Gidrometeorizdat, Leningrad,; English translation Jerusalem 1965, Program for Scientific Translations, 242 pp.
- Gerhard, Myron L. and James R. Scoggins, 1981: Potential Flow Models of Thunderstorm-Environment Interaction. TDWR Report LP-170, Texas Department of Water Resources, Austin, Texas, 68 pp. plus one Appendix.

- Haltiner, George J., and Roger T. Williams, 1980: Numerical prediction and dynamic meteorology. Second edition. New York (Wiley), 477 pp.
- Haragan, Donald R., 1978: Precipitation Climatology for the HIPLEX Southern Region. TDWR Report LP-63, Texas Department of Water Resources, Austin, Texas, 58 pp.
- Henry, W. K., 1979: Some aspects of the fate of cold fronts in the Gulf of Mexico. Mon. Wea. Rev., 107, 1078-1082.
- _____, and A. H. Thompson, 1978: On return flow in winter over the East China Sea. Mon. Wea. Rev., 106, 947-953.
- Herzogh, Paul H., and Peter V. Hobbs, 1981: The mesoscale and microscale structure and organization of clouds and precipitation in midlatitude cyclones. IV: Vertical air motions and microphysical structures of pre-frontal surge clouds and cold-frontal clouds. J. Atmos. Sci., 38, 1771-1784.
- Hobbs, Peter V., and P. Ola G. Perrson, 1982: The mesoscale and microscale structure and organization of clouds and precipitation in midlatitude cyclones. Part V: The substructure of narrow cold-frontal rainbands. J. Atmos. Sci., 39, 280-295.
- Hoke, James E., and Richard A. Anthes, 1976: The initialization of numerical models by a dynamic-initialization technique. Mon. Wea. Rev., 104, 1551-1556.
- Holliday, Charles R., and Aylmer H. Thompson, 1979: Climatological characteristics of rapidly intensifying typhoons. Mon. Wea. Rev., 107, 1022-1034.
- Hovermale, J. B., and R. E. Livezey, 1977: Three-year performance characteristics of the NMC hurricane model. Preprints, Eleventh Technical Conference on Hurricanes and Tropical Meteorology, 13-16 December 1977. Amer. Meteor. Soc., 122-124.
- Jurica, Gerald M., and Shih-Cheng Chao, 1981: A study of Clouds Using Satellite Radiance Data in Comparison with Rainage Network and Radar Observations. TDWR Report LP-140, Texas Department of Water Resources, Austin, Texas, 151 pp.
- Keyser, Daniel, Melvyn A. Shapiro and Donald J. Perkey, 1978: An examination of frontal structure in a fine-mesh primitive equation model for numerical weather prediction. Mon. Wea. Rev., 106, 1112-1124.
- Klemp, J. B., R. B. Wilhelmson and P. S. Ray, 1981: Observed and numerically simulated structure of a mature supercell thunderstorm. J. Atmos. Sci., 38, 1558-1580.
- Knupp, Kevin R., and William R. Cotton, 1982: An intense, quasi-steady thunderstorm over mountainous terrain. Part II: Doppler radar observations of the storm morphological structure. J. Atmos. Sci., 39, 343-358.
- _____, and _____, 1982: An intense, quasi-steady thunderstorm over mountainous terrain. Part III: Doppler radar observations of the turbulent structure. J. Atmos. Sci., 39, 359-368.
- Koch, Steven E., and John McCarthy, 1982: The evolution of an Oklahoma dryline. Part II: Boundary-layer forcing of mesoconvective systems. J. Atmos. Sci., 39, 237-257.
- Maddox, Robert A., 1980: An objective technique for separating macroscale and mesoscale features in meteorological data. Mon. Wea. Rev., 108, 1108-1121.
- _____, 1980a: Mesoscale convective complexes. Bull. Amer. Meteor. Soc., 61, 1374-1387.
- _____, and Charles A. Doswell III, 1982: An examination of jet stream configurations, 500 mb vorticity advection and low-level thermal advection patterns during extended periods of intense convection. Mon. Wea. Rev., 110, 184-197.

- _____, D. J. Perkey and J. M. Fritch, 1981: Evolution of upper tropospheric features during the development of a mesoscale convective complex. J. Atmos. Sci., 38, 1664-1674.
- Maher, Ytzaq, and Roger A. Pielke, 1977: The effects of topography on sea and land breezes in a two-dimensional numerical model. Mon. Wea. Rev., 105, 1151-1162.
- _____, and _____, 1978: A test of an upstream spline interpolation technique for the advective terms in a numerical mesoscale model. Mon. Wea. Rev., 106, 818-830.
- Matthews, David A., 1981: Natural variability of thermodynamic features affecting convective cloud growth and dynamic seeding: A comparative summary of three High Plains sites from 1975 to 1977. J. Appl. Meteor., 20, 971-996.
- McCarthy, John, and Steven E. Koch, 1982: The evolution of an Oklahoma dry-line. Part I: A meso- and subsynoptic-scale analysis. J. Atmos. Sci., 39, 225-236.
- Mesinger, Fedor, and Akio Arakawa, 1976: Numerical methods used in atmospheric models. GARP Publication Series No. 17. World Meteorological Organization, 64 pp.
- Morel, P., 1973: Space and time meteorological data analysis and initialization. In: Dynamic Meteorology, Edited by Morel, Dordrecht and Boston (Reidel), 469-512.
- Nickerson, E. C., 1979: On the numerical simulation of airflow and clouds over mountainous terrain. Contrib. Atmos. Phys., 53, 161-177.
- Orlanski, Isidoro, 1973: Trapeze instability as a source of internal gravity waves. Part I. J. Atmos. Sci., 30, 1007-1016.
- _____, 1975: A rational subdivision of scales for atmospheric processes. Bull. Amer. Meteor. Soc., 56, 527-530.
- _____, 1981: The quasi-hydrostatic approximation. J. Atmos. Sci., 38, 572-582.
- Perkey, Donald J., 1976: A description and preliminary results from a fine-mesh model for forecasting quantitative precipitation. Mon. Wea. Rev., 104, 1513-1526.
- _____, and Carl W. Kreitzberg, 1976: A time-dependent lateral boundary scheme for limited area primitive equation models. Mon. Wea. Rev., 104, 744-755.
- Pielke, Roger A., 1981: Mesoscale numerical modeling. Advanced Geophys., 23, 185-344.
- Ray, P. S., B. C. Johnson, K. W. Johnson, J. S. Bradberry, J. J. Stephens, K. K. Wagner, R. B. Wilhelmson and J. B. Klemp. The morphology of several tornadic storms on 20 May 1977. J. Atmos. Sci., 38, 1643-1663.
- Reynolds, P. G., M. L. Gerhard, G. S. Wilson, and J. R. Scoggins, 1979: Texas HIPLEX Mesoscale Experiment-Summer 1978 Data Tabulations. TDWR Report LP-80, Texas Department of Water Resources, Austin, Texas, 9 pp. plus 4 Appendices.
- Rosenthal, Stanley., 1978: Numerical simulation of tropical cyclone development with latent heat release by the resolvable scales I: model description and preliminary results. J. Atmos. Sci., 35, 258-271.
- _____, 1979: The sensitivity of simulated hurricane development to cumulus parameterization details. Mon. Wea. Rev., 107, 193-197.
- Ross, Bruce B., and Isidoro Orlanski, 1982: The evolution of an observed cold front. Part I: numerical simulation. J. Atmos. Sci., 39, 296-327.
- Rotunno, Richard, and Joseph B. Klemp, 1982: The influence of the shear-induced pressure gradient on thunderstorm motion. Mon. Wea. Rev., 110, 136-151.

- Scoggins, James R., and Gregory S. Wilson, 1976: Texas HIPLEX Mesoscale Experiment-Summer 1976 Data Tabulations. TWDB 76-12, Texas Water Development Board, Austin, Texas, 33 pp. plus 3 Appendices.
- _____, 1977: Texas HIPLEX Mesoscale Experiment-Summer 1977 Data Tabulations. TDWR Report LP-10, Texas Department of Water Resources, Austin, Texas, 9 pp. plus 4 Appendices.
- _____, Henry E. Fuelberg, Steven F. Williams, and Mark E. Humbert, 1978: Mesoscale Characteristics of the Texas HIPLEX Area During Summer 1976. TDWR Report LP-65, Texas Department of Water Resources, Austin, Texas, 343 pp.
- _____, Gregory S. Wilson, and Steven F. Williams, 1979: Mesoscale Characteristics of the Texas HIPLEX Area During Summer 1977. TDWR Report LP-99, Texas Department of Water Resources, Austin, Texas, 433 pp.
- _____, Dusan Djuric, Phanindramohan Das, George L. Huebner, and Alexis B. Long, 1982: TAMU Texas HIPLEX Studies for 1979. TDWR Report LP-181, Texas Department of Water Resources, Austin, Texas, 301 pp.
- Shapiro, M. A., 1981: Frontogenesis and geostrophically forced secondary circulations in the vicinity of jet stream-frontal zone systems. J. Atmos. Sci., 38, 954-973.
- Sienkiewicz, Meta E., and Myron L. Gerhard, 1981: Texas HIPLEX Mesoscale Experiment-Summer 1980 Data Tabulations. TDWR Report LP-147. Texas Department of Water Resources, Austin, Texas, 21 pp. plus 3 Appendices.
- _____, James R. Scoggins, Steven F. Williams, and Myron L. Gerhard, 1980: Mesoscale Characteristics of the Texas HIPLEX Area During Summer 1978. TDWR Report LP-123, Texas Department of Water Resources, Austin, Texas, 609 pp.
- Stephens, Graeme L., and Peter J. Webster, 1981: Clouds and climate: Sensitivity of simple systems. J. Atmos. Sci., 38, 235-247.
- Sun, Wen-Yih, and Isidoro Orlanski, 1981: Large mesoscale convection and sea breeze circulation. Part II: Nonlinear numerical model. J. Atmos. Sci., 38, 1694-1706.
- _____, and _____, 1981a: Large mesoscale convection and sea breeze circulation. Part I: Linear stability analysis. J. Atmos. Sci., 38, 1657-1693.
- Tapp, M. C., and P. W. White, 1976: A non-hydrostatic mesoscale model. Quart. J. Roy. Meteor. Soc., 102, 277-296.
- UCAR, 1982: National STORM Program. Draft. Boulder.
- Uccellini, Louis W., Donald R. Johnson, and Robert E. Schlesinger, 1979: An isentropic and sigma coordinate hybrid numerical model: model development and some initial tests. J. Atmos. Sci., 36, 390-414.
- Warner, Thomas T., Richard A. Anthes and Alan L. McNab, 1978: Numerical simulations with a three-dimensional mesoscale model. Mon. Wea. Rev., 106, 1079-1099.
- Williams, Steven F. and James R. Scoggins, 1980: Models of Atmospheric Water Vapor Budget for the Texas HIPLEX Area. TDWR Report LP-117, Texas Department of Water Resources, Austin, Texas, 50 pp.
- _____, Myron L. Gerhard, and James R. Scoggins, 1980: Texas HIPLEX Mesoscale Experiment-Summer 1979 Data Tabulations. TDWR Report LP-118, Texas Department of Water Resources, Austin, Texas, 16 pp. plus 3 Appendices.
- Wilhelmson, Robert B., and Joseph B. Klemp, 1981: A three-dimensional numerical simulation of splitting severe storms on 3 April 1964. J. Atmos. Sci., 38, 1581-1600.

- Wilson, Gregory S., and J. R. Scoggins, 1976: Atmospheric structure and variability in areas of convective storms determined from 3-h rawinsonde data. NASA Contractor Report, NASA CR-2678, 118 pp.
- Wippermann, F., 1981: The applicability of several approximations in meso-scale modelling - a linear approach. Beitr. Phys. Atmosph., 54, 298-308.
- Woodley, William L., Jill Jordan, Anthony Barnston, Joanne Simpson, Ron Biondini, and John Flueck, 1982: Rainfall Results of the Florida Area Cumulus Experiment, 1970-76. J. Appl. Meteor., 21, 139, 164.
- Zawadzki, L., E. Torlaschi and R. Sauvageau, 1981: The relationship between mesoscale thermodynamic variables and convective precipitation. J. Atmos. Sci., 38, 1535-1540.
- Zipser, E. J., 1977: Mesoscale and convective-scale downdrafts as distinct components of squall-line structure. Mon. Wea. Rev., 105, 1568-1589.

